Stockholm University

Master Thesis

Degree Project in
Geochemistry 60 hp

A temporal and spatial study of CH_4 sea-to-air fluxes from shallow bays in the archipelago of Stockholm and Trosa

Thea Bisander

Stockholm 2021

Department of Geological Sciences
Stockholm University
SE-106 91 Stockholm

A temporal and spatial study of CH_4 sea-to-air fluxes from shallow bays in the archipelago of Stockholm and Trosa

FRONT PAGE: *Left: The chamber, anchored in a bay on Ingarö. Right: The eddy covariance mast on Askö.*

Abstract

Coastal areas have been suggested to contribute the majority of the methane emissions from the ocean to the atmosphere, yet there are still many uncertainties connected to the global budget. The uncertainties mainly arise from the relatively limited amount of empirical data in comparison to other gases. In this study, methane fluxes from shallow bays in the archipelago around Stockholm and Trosa have been sampled, to both spatially and temporally map the methane flux in an attempt to determine both environmental-, as well as method specific- factors controlling it. The period for the sampling campaign reached from late August, 2020, to May, 2021. The floating chamber (FC) method, the eddy covariance (EC) method and the boundary layer (BL) method from Wanninkhof (2014) have been used to determine the flux. Here, we present 263 repeated FC flux measurements with corresponding BL calculations, and 3013 EC 30-minute flux periods. The results showed that vegetation density and sediment type were poor predictors for F_{CH4} during the period that the study was carried out, while there were possible indications that eutrophication influenced the outcome of the study. U_{10} and temperature have commonly been used to predict F_{CH4}. Our results showed that U_{10} was influential for the more exposed bays, while temperature did not appear to have a direct relationship with F_{CH4}. Water depth and distance to shore were not found statistically significant when determining F_{CH4}, but the time of day when the sampling was carried out influenced the results. The three methods showed a relatively good agreement, but it was concluded that the FC method was the most suitable. The BL method underestimated the gas transfer at low wind speeds and the EC tower did show a large signal to noise ratio, where the majority of the F_{CH4} was under the detection limit. Finally, we discuss the implications of the results in terms of upscaling.

Table of contents:

1. INTRODUCTION

The trace gas methane (CH_4) is, after carbon dioxide (CO_2), the most abundant greenhouse gas in the atmosphere, with an approximate concentration of 1.875 ppm reported in 2019 (Dlugokencky, 2020). Since pre-industrial times, the CH_4 concentrations have almost tripled in the atmosphere (Nisbet *et al.,* 2019; Schaefer *et al.,* 2016). CH_4 is about 20 times, per molecule, more efficient at absorbing radiation than CO_2 (Schiermeier, 2020), which makes it a very potent greenhouse gas. To study the sources and processes contributing CH_4 to the atmosphere is an important part in understanding the dynamics of today's, as well as future, climate change. There are still great uncertainties in the budgeting of CH_4 sources, mostly due to large differences between top-down and bottom-up approaches (Nisbet & Weiss, 2010). All sources considered; marine contributions are estimated to only 2-4 % (Bange *et al.*, 1994), up to 10 % (Grunwald *et al.,* 2009), of yearly emissions of CH_4 to the atmosphere. However, the contribution is not homogeneous, and even though coastal regions hold only a small portion of the oceans area, they could stand for about 75% of those emissions (Weber *et al.,* 2019; Borges *et al.,* 2016; Bange *et al.*, 1994).

Gas exchange over the sea-air interface have been subject to numerous studies trying to understand the factors controlling it (Reeburgh, 2007; Bange *et al*., 1994; Wanninkhof, 1992; Liss & Merlivat, 1986, etc.), yet there are still many uncertainties in the global oceanic emissions of CH_4 due to limited amount of data, if you compare to other greenhouse gases such as CO_2 and nitrous oxide (N_2O) (Bakker *et al.,* 2014). The lacking coverage on temporal and spatial data for CH_4 sea-to-air fluxes, as well as the heterogeneous distribution of these fluxes between coastal regions and the open ocean, makes the variability on regional scale hard to predict (Gutiérrez-Loza *et al.,* 2019; Gülzow *et al.,* 2013). To make global upscaling reliable and, with more precision, being able to determine the factors controlling the CH_4 flux, the variability in inshore marine environments need to be investigated further.

There are four recognized pathways from which CH_4 can be emitted to the atmosphere from the ocean or freshwater bodies: Diffusive flux, ebullition flux, vegetation-mediated flux and storage flux, see Figure 1 (Jeffrey *et al.,* 2019; Carmichael *et al.,* 2014; Bastviken *et al.,* 2004; Fendinger *et al.,* 1992; Chanton & Dacey, 1991). In the sediment column, CH_4 is formed via methanogenesis, which is the last step in the degradation of organic matter, and requires anoxic and reducing conditions (Cicerone & Oremland, 1988; Zehnder, 1978). Methanogenesis is preformed solely by archaea, and its main pathways are by splitting acetate ($CH_3COO^- + H^+ \rightarrow CH_4 + CO_2$) or reducing CO_2 ($CO_2 + 4H_2 \rightarrow CH_4 + 2H_2O$). These reactions only take place in the absence of other oxidants such as oxygen, nitrate, manganese (4+), ferric iron, or sulfate. For this reason, methanogenesis commonly occur at a depth of one to several meters down in the sediment column, below the sulfate zone (Barker Jørgensen & Kasten, 2006). Methanogenesis is favored by a high input of labile organic matter, where the other electron acceptors have time to be exhausted, before the organic carbon is (Kelley *et al.,* 1990). Other sources of CH_4 can be groundwater or riverine input (Grinham *et al.,* 2017; Lechter *et al.,* 2015), as well as *in situ* production in the water column by zooplankton (de Angelies & Lee, 1994), decomposition of methylphosphonate (Karl *et al.,* 2008) or associated with sinking fecal pellets or particles (Karl & Tilbrook, 1994).

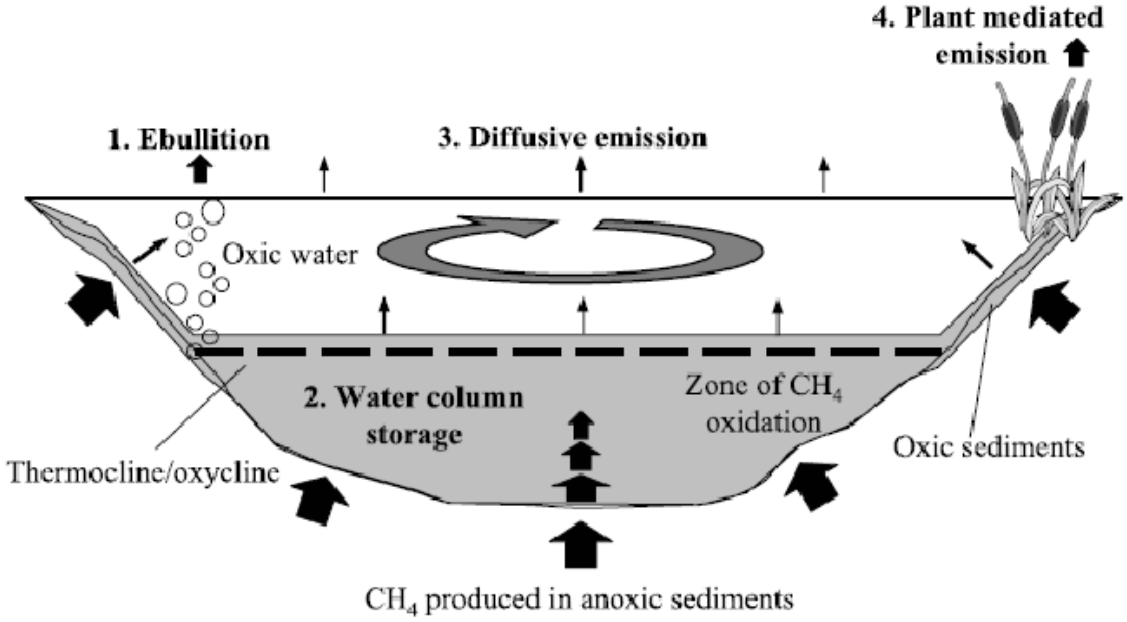

FIGURE 1: *Illustrative picture of CH_4 emission pathways from a water body. Source: Bastviken et al. (2004).*

CH_4 becomes oxidized when seeping up into the sulfate zone and only a small percentage of what is being produced reaches the water column. When in the water column, the CH_4 is subject to further anaerobic and aerobic oxidation (Reeburgh, 2007). If the water column has density stratification it can limit the upward diffusion of CH_4 even more (Gentz *et al.,* 2014). The water depth also has an effect on the CH_4 concentrations in the surface waters, since deeper waters mean longer time in the water column, which allows for more oxidation, and therefore favoring higher CH_4 concentrations in shallower waters (Humborg *et al.,* 2019; Reeburgh, 2007). The diversity of dissolved CH_4 in coastal marine environment is controlled by factors such as temperature in the water and the sediment, availability of labile organic carbon, presence of other electron acceptors, and salinity (Jeffrey *et al.,* 2019; Aaujo *et al.,* 2018; Borges & Abril, 2011).

In large, CH_4 fluxes over the sea-to-air interface are driven by the physical properties governing gas transfer, as well as the balance between its production and oxidation in the water-, as well as sediment- columns, which controls the concentration gradient between the water and the atmosphere (Borges & Abril, 2011). At both sides of the water-air interface there exists a viscous boundary layer that suppresses the gas transfer (Herlina & Jirka, 2008). Away from this boundary layer, gas transfer is governed by turbulent diffusion or advective transport, but through the boundary layer, the dominant way of gas transfer is by molecular diffusion. CH_4 is an insoluble gas, and as such the aqueous boundary layer represents a bigger limitation for the gas transfer than the atmospheric boundary layer (Jähne *et al.,* 1987). Because of this property, CH_4 flux across the water-air boundary layer is controlled by variations in molecular diffusivity and the turbulence at the interface, which affects the thickness of the aqueous boundary layer (Zappa *et al.,* 2003).

Surface water turbulence is controlled by varying factors dependent on the kind of environment. For the open ocean, or other areas with large fetch, the turbulence, and hence

the gas transfer, is strongly related to wind speed (Ho *et al.,* 2011; Wanninkhof, 1992). Microbubbles and temperature driven convection can have a large additional influence on turbulence in areas with smaller fetch, like lakes or inshore environments (McGinnis *et al.,* 2015; Podgrajsek *et al.,* 2014), while surface turbulence at locations with moving water is, to a great extent, controlled by current velocity (Zappa *et al.,* 2003). Further, surfactants can have an additional effect on gas transfer by either suppressing or enhancing it (Garbe *et al.,* 2014; Liss, 1983; Liss & Martinelli, 1978).

Since the surface turbulence can be difficult to estimate, a lot of effort has been put into making a flux equation that depends on the wind speed as the turbulence predictor (Wanninkhof, 2014, 1992; Ho *et al.,* 2011, 2006; Nightingale *et al.,* 2000; Wanninkhof & McGillis, 1999; Liss & Merlivat, 1986; Liss & Slater, 1974, etc.). Based on Fick's first law, the equation (1) for the flux through the boundary layer is:

1) $F = k\Delta C$

Where F is the flux, k is the transfer velocity and ΔC is the concentration gradient across the boundary layer.

Gas transfer velocity, k, is dominantly the product of the turbulence and the chemical reactivity of the gas in question (Liss & Slater, 1974). However, the wind based equations have been suggested to underestimate the flux for lower winds, and in coastal regions (Lundevall-Zara *et al.,* 2021; Erkkilä *et al.,* 2018; Duchemin *et al.,* 1999), indicating a need for more specific models for these habitats.

Marine inshore zones are, to a greater extent than the open ocean, affected by human activities such as eutrophication, coastal engineering and exposure. Estuaries have one of the highest productivity rates of the aquatic systems, since they are loaded with nutrients from wastewater runoff, agriculture and industries, and then transport these to the open ocean (Bianchi, 2007). The primary production leads to more organic material being buried, as well as possible depletion of oxygen, and in turn more CH_4 is produced in the sediment (Naqvi *et al*., 2010). This *in situ* production, together with allochthonous and autochthonous CH_4 contributions from riverine input, can potentially make estuaries hot spots for CH_4 emissions (Borges & Abril, 2011; Upstill-Goddard *et al*., 2000). The Baltic Sea is a suitable location for investigating the CH_4 fluxes from such an environment. The archipelago around Stockholm represents a densely populated area that can be used to, in part; predict a future, where even more people are expected to live within 100 km of the coast (Kummu *et al*., 2016).

The Baltic Sea is one of the world's largest basins with brackish water and functioning as an estuary, connected to the north Atlantic only via Kattegat and Skagerrak. Total annual riverine input to the Baltic is 450 km^2, a big volume made possible by its extensive catchment area (Andersen at al., 2017; Dargahi et al., 2017). The episodic saline water inflow from the Atlantic has stratified the Baltic water mass with a warmer, fresher top layer and a colder, saltier bottom layer (Dargahi et al., 2017). The stratification has led to a density difference which makes vertical mixing limited (Gülzow et al., 2013), and has made some of the deeper basins in the Baltic hypoxic, or even anoxic (Conley et al., 2011). The salinity for the surface waters goes from 3 ‰ in the northeast to 17 ‰ in the west (Feistel et al., 2008).

CH_4 in the Baltic Sea is mainly produced via methanogenesis in the organic-rich sediments: clay- and mud layers (Thießen *et al.,* 2006). Emissions of CH_4 in the Baltic have been observed to vary with the seasons. However, different suggestions have been made for when maximum emissions occur; either in the summer months (Lundevall-Zara *et al.,* 2021; Heyer & Berger, 2000; Bange *et al.,* 1994) as an effect of the elevated productivity and higher temperatures, or in the winter months (Gülzow *et al.*, 2013), due to a deepening of the mixed layer and higher wind velocities. A more temporally homogeneous distribution has also been suggested (Gutiérrez-Loza *et al.,* 2019). Emission rates for the Baltic Sea open water have been reported to have monthly averages between 0.001 and 3.110 mmol m^{-2} d^{-1}, varying between time of year, as well as between different studies, where the lower range is more common (Gutiérrez-Loza *et al.,* 2019; Gülzow *et al.*, 2013; Bange *et al.,* 1994). Coastal regions have a generally higher range of suggested fluxes. Values of 0.019 – 10.20 mmol m^{-2} d^{-1} were reported for a study in the archipelago of Trosa, where the highest fluxes were found in densely vegetated habitats (Lundevall-Zara *et al.,* 2021). Fluxes between 0.450 – 156.0 mmol m^{-2} d^{-1} were reported for a coastal wetland in the southern Baltic (Heyer & Berger, 2000). Connected to very warm conditions and a storm event fluxes between 1.0 and 3.3 mmol m^{-2} d^{-1} were reported for a coastal region in Finland (Humborg *et al.,* 2019).

The difference in reported fluxes highlights the need for deeper understanding of the spatial variance of CH_4 emissions in the Baltic, especially for coastal regions. The studies mentioned have used a variety of methods, including the floating chamber (FC) method (Lundevall-Zara *et al.,* 2021; Heyer & Berger, 2000), the eddy covariance (EC) method (Gutiérrez-Loza *et al.,* 2019) and the boundary layer (BL) method (Humborg *et al.,* 2019; Gülzow *et al.*, 2013; Bange *et al.,* 1994). These methods all have advantages and disadvantages. The FC method is a very direct method, and requires little data processing; however, it only represents the flux from a restricted area, and is very labor intensive. It has also been discussed to disturb the boundary layer, and therefore influence the flux (Mannich *et al.,* 2019). The EC method is a micrometeorological method that is less labor intensive and does not disturb the boundary layer, but it requires a lot of data processing, as well as knowledge of the site specific atmospheric conditions (Blomquist, 2012, 2010). The BL method is an indirect method that is convenient for upscaling, and is more efficient than the FC method, and requires less data processing than the EC method. However, it is very dependent on the predictors put into k and might not represent the actual flux (Wanninkhof, 2014, 1992; Ho *et al.,* 2011, 2006; Nightingale *et al.,* 2000; Wanninkhof & McGillis, 1999; Liss & Merlivat, 1986; Liss & Slater, 1974, etc.)

In an attempt to increase the understanding of the CH_4 emissions in the coastal regions of the Baltic Sea, this study will focus on shallow marine environments in the archipelago around Stockholm, using all three methods mentioned above.

1.1 Aim and objectives of the study

This study aims to identify environmental- and site specific- factors controlling CH_4 flux over the sea-air interface in shallow bays, in the archipelago of Stockholm during the period late August, 2020 – May, 2021. With the use of the FC method, the EC method and a BL method it strived to, both spatially and temporally, map CH_4 fluxes in order to quantify the effects from location-, habitat-, method- and season-specific factors.

The study posed the following specific questions:

- Can vegetation density and sediment type be used to predict the CH_4 flux from an inshore environment, and does the answer to this question change with time of year?

- Wind speed and temperature are common environmental factors used as predictors for CH_4 sea-to-air flux, how well can they explain the variation in flux data collected from various, heterogeneous inshore environments?

- What factors, imposed on the flux measurements by the execution of the FC method, such as water depth, distance to shore or time of day, influences the CH_4 flux?

- How well does the EC method work in a spatially, and temporally, highly heterogeneous inshore environment?

- How well does the FC, EC, and BL methods correlate? Can EC flux data be used to interpolate FC flux data that does not have the same temporal resolution?

2. MATERIALS AND METHODS

2.1 Study sites

2.1.1 Classification

The bays were classified based on vegetation density and sediment type. The sediment classification was done in accordance to the EUNIS-classification from the Swedish Geological Survey (Naturvårdsverket, 2009). The classification was only based on visual examination of the bays. Four bay types have been distinguished: Type 1, unfortunately only represented by one bay in this study, was the most densely vegetated type and had fine sand, to soft mud bottom substrate, K5 and K8 in the EUNIS-classification. Type 2 was represented by bays that were not as densely vegetated as type 1, still these bays were partly covered by reed beds and quite a lot of seaweed was growing during the late spring. The sediments varied between soft mud (K8), fine sand (K5) and coarser sand (K3). Type 3 included bays where coarser sand (K3) was the main sediment type and water-vegetation was limited but present. Type 4, which was represented by only one bay in this study, had fine sand, with occasional exposed bedrock, as bottom substrate (K3 and K1), and had no to only very sparse vegetation during the periods measured in this study.

2.1.2 Locations

Location:	ID:	Bay type:
Embayment north of Norra Kalvholmen	A-1	2
Östernäs	I-1	3
Södersved	I-2	2
Björkvik	I-3	4
Björnö	I-4	2
Mörtviken	I-5	3
Ingarö Channel	I-6	1

TABLE 1: Locations, their ID, and to what bay type they belong.

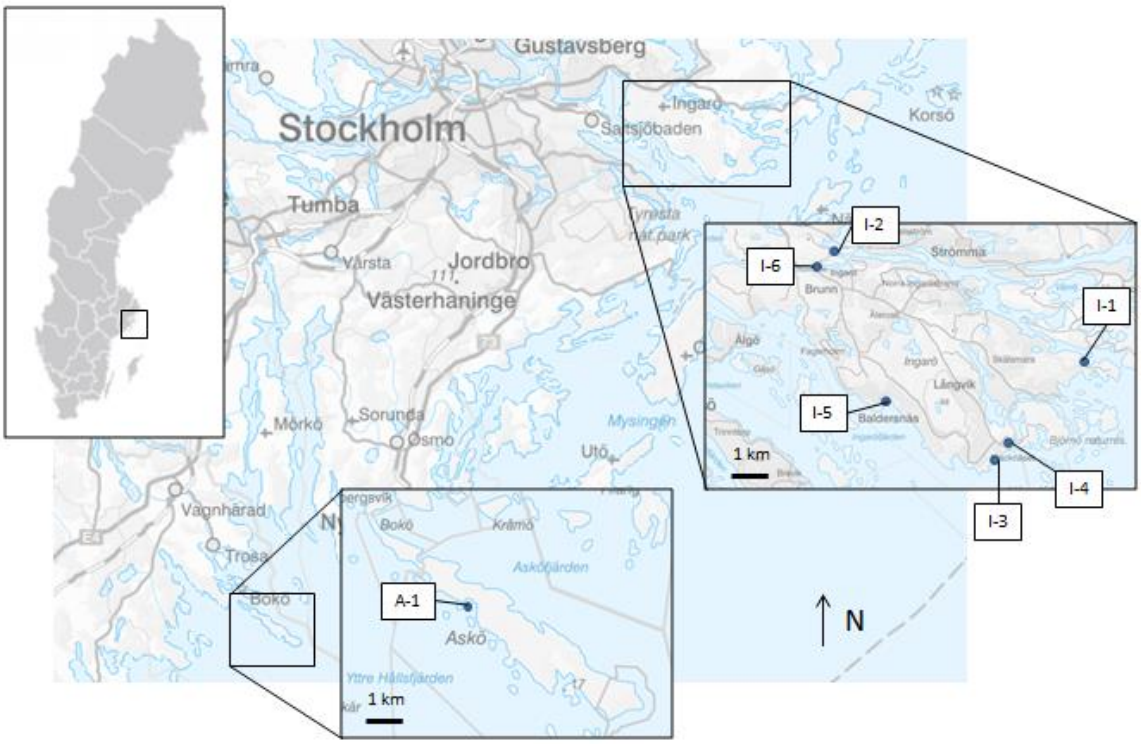

FIGURE 2: Map showing the locations. (Base map obtained from SGU, 2021).

Askö: Embayment north of Norra Kalvholmen (A-1) – Type 2

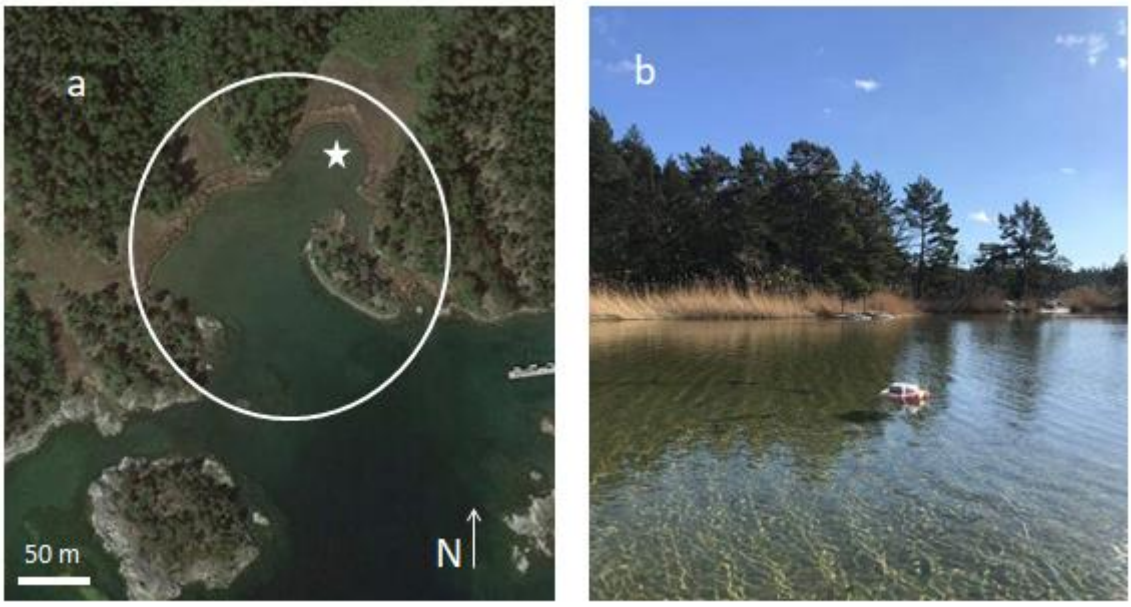

FIGURE 3: Embayment north of Norra Kalvholmen, location A-1. Satellite picture (a) (Google maps, 2021) showing the location of where the picture (b) is taken (star). The circle shows from where in the bay samples have been taken. Picture (b) is taken in May 2021.

A-1 (Fig. 3) is located on the island of Askö, Trosa, on the southern side by the research station, 58.8237458 N 017.6325973 E. The bay is partly covered by reeds, have a varying sediment bottom between soft mud and some sand, during the warmer periods a lot of seagrass was growing. The shoreline is varying between exposed bedrock and vegetation. The southern side of the island is very exposed to wind and waves, but the bay is relatively protected by two smaller islands located in front of the research station. The bay is affected by boat traffic and from activities at the laboratory. The depth is exceeding two meters at places.

Ingarö: Östernäs (I-1) – Type 3

I-1 (Fig. 4) is located on the northeastern tip of Ingarö, 59.2500139 N 018.5983860 E. The sediment consists of coarse sand. The beach is boarded by steep cliffs on one side and grass shore with very sparse reed vegetation on the other side. There was some seaweed growing during warmer seasons. A few houses are built close to the waterline in the bay and have belonging docks. The bay is located on the northern side of a narrow land crossing to a half-island, and is protected from southerly winds. The water depth is up to two meters within the range of the sampling locations.

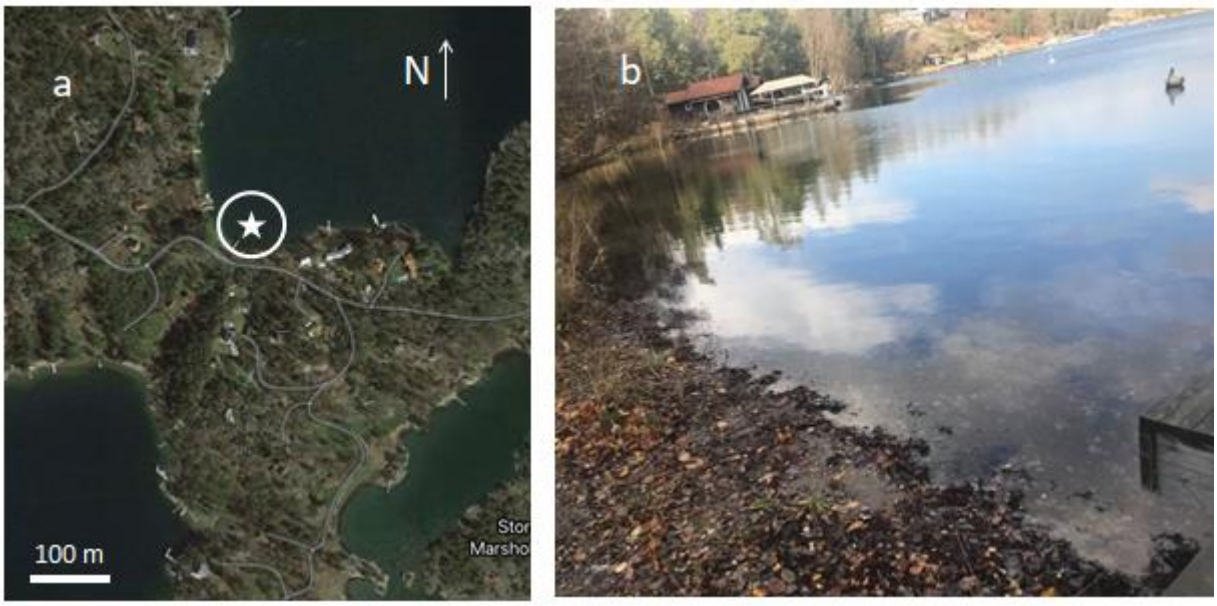

FIGURE 4: Östernäs, location I-1. Satellite picture (a) (Google maps, 2021) showing the location of where the picture (b) is taken (star). The circle shows from where in the bay samples have been taken. Picture (b) is taken in November 2020.

Ingarö: Södersved (I-2) – Type 2

I-2 (Fig. 5) is located in the water passage between Ingarö and Värmdö where the channel is expanding and there are no currents, 59.2953280 N 018.4235533 E. The bay has a grassy shoreline with reeds and seagrass growing quite dense during warmer months. At places the shoreline is reinforced with rocks. The bottom substrate is mud varying with coarser sand. In close proximity to the bay there is a sand beach that during the summer is a popular bathing

location. The bay is relatively protected against waves. The depth is reaching two meters within the range of the sampling locations.

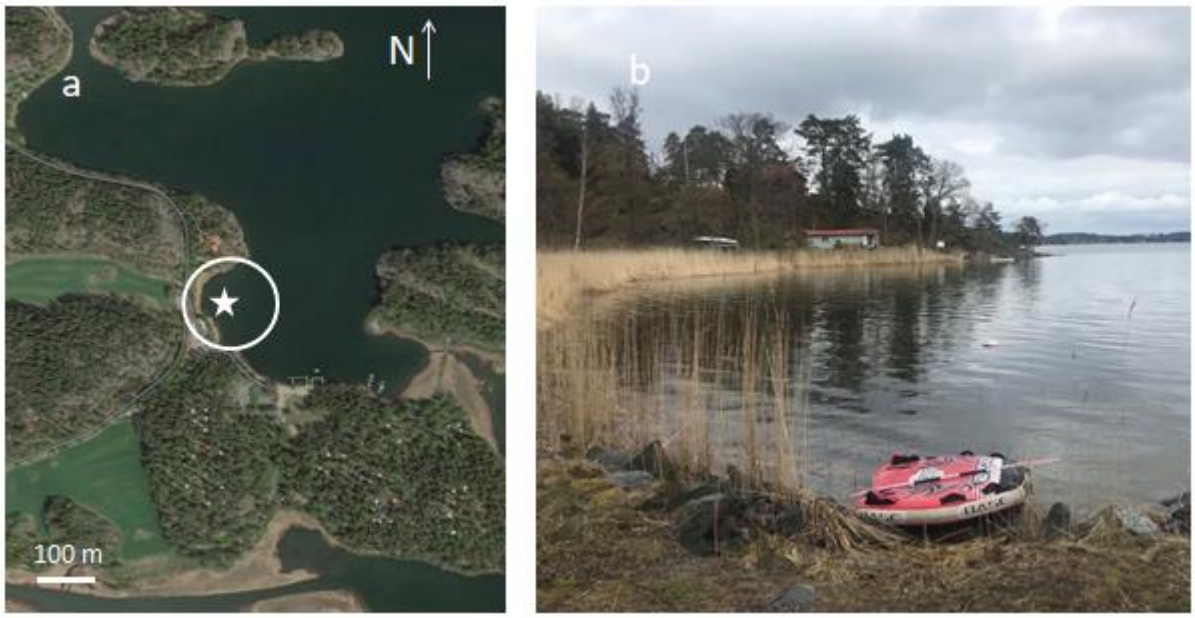

FIGURE 5: Södersved, location I-2. Satellite picture (a) (Google maps, 2021) showing the location of where the picture (b) is taken (star). The circle shows from where in the bay samples have been taken. Picture (b) is taken in May 2021.

Ingarö: Björkvik (I-3) – Type 4

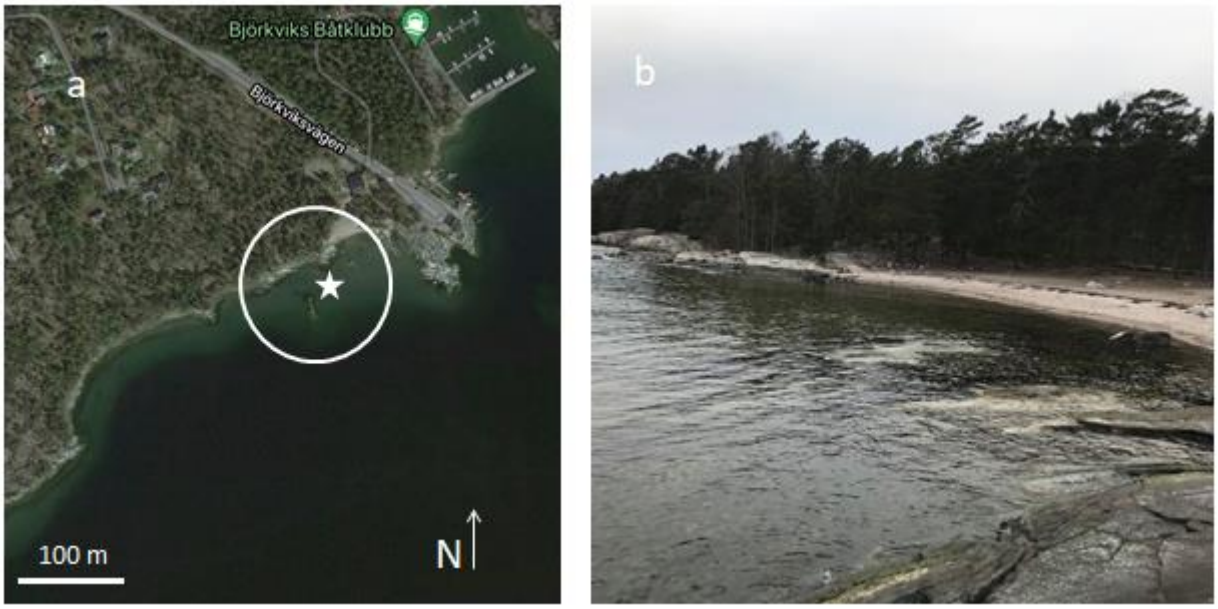

FIGURE 6: Björkvik, location I-3. Satellite picture (a) (Google maps, 2021) showing the location of where the picture (b) is taken (star). The circle shows from where in the bay samples have been taken. Picture (b) is taken in April 2021.

I-3 (Fig. 6) is located on the southeastern tip of Ingarö, 59.2191560 N 018.5350738 E. The shoreline consists of cliffs and sand, and is very shallow, <1 meters, at least 40 meters from

the shore. The bight is facing the open ocean and is exposed to waves and southerly winds. Almost no vegetation grew in the bay during the time of sampling. In proximity to I-3 there is a ferry stop and large boat traffic is frequent.

Ingarö: Björnö (I-4) – Type 2

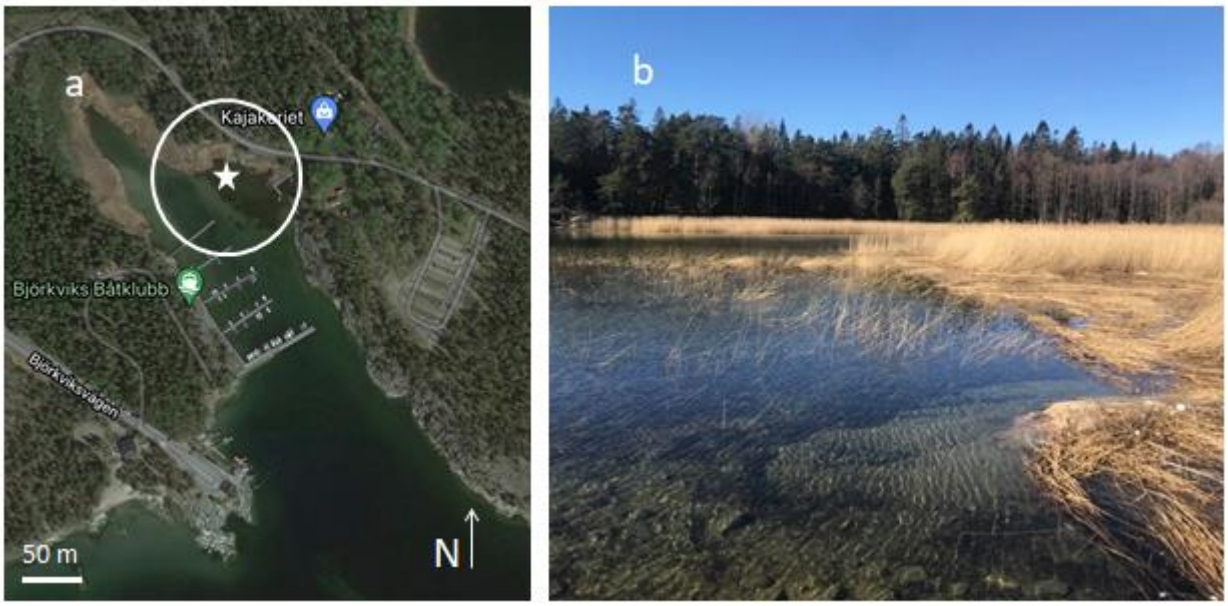

FIGURE 7: Björnö, location I-4. Satellite picture (a) (Google maps, 2021) showing the location of where the picture (b) is taken (star). The circle shows from where in the bay samples have been taken. Picture (b) is taken in April 2021.

I-4 (Fig. 7) is also located on the southeastern tip of Ingarö, 59.223708 N 018.5401278 E. The bay is narrow with dense reed beds along the shoreline. The shoreline is varying between exposed bedrock and vegetation, and the sediment is fine sand or mud. The opening to the ocean is partly blocked by a boat dock and along one of the sides there are two more boats docks. The bay is, for this reason, rarely exposed to bigger waves.

Ingarö: Mörtviken (I-5) – Type 3

I-5 (Fig. 8) is located on the southern side of Ingarö, 59.2171535 N 018.5012247 E. The bay is a coarse sand beach with a bathymetry that is shallow the first ten meters and thereafter has a very steep slope reaching depths over three meters, within a two meters range. The bay is very exposed to wind and waves. The shoreline is disturbed by docks and residences. There were some seaweeds growing in the sand during warmer periods.

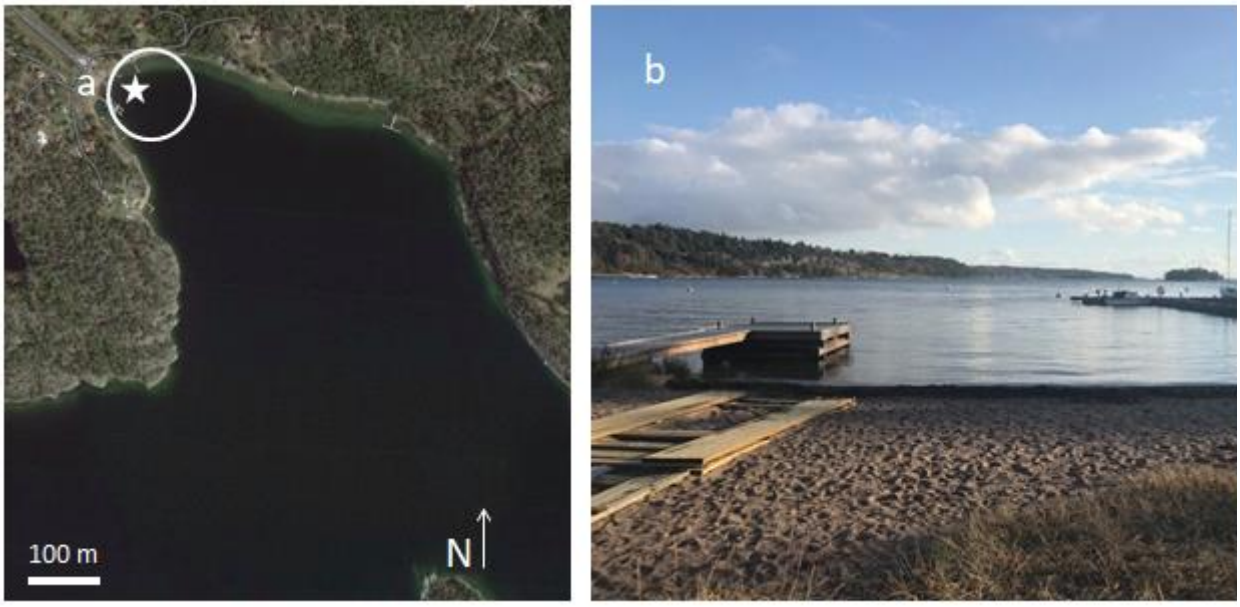

FIGURE 8: Mörtviken, location I-5. Satellite picture (a) (Google maps, 2021) showing the location of where the picture (b) is taken (star). The circle shows from where in the bay samples have been taken. Picture (b) is taken in November 2020.

Ingarö: Ingarö channel (I-6) – Type 1

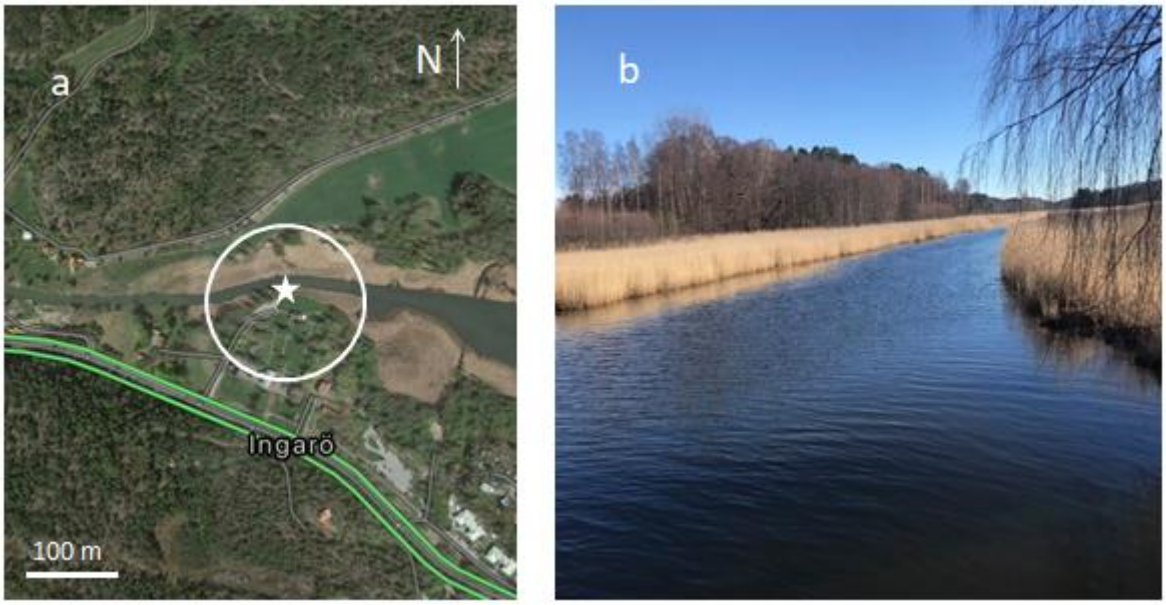

FIGURE 9: Ingarö channel, location I-5. Satellite picture (a) (Google maps, 2021) showing the location of where the picture (b) is taken (star). The circle shows from where in the bay samples have been taken. Picture (b) is taken in Mars 2020.

The narrow channel running between Ingarö and Värmdö, I-6, (Fig. 9) is another measurement location, 59.2896733 N 018.4073614 E. The channel is five to ten meters wide and bordered by dense reed beds. It is a passage for the water from more central parts of Stockholm, out towards the open ocean. The channel is at the place of the sample locations two meters deep.

2.2 Field methods

2.2.3 The floating chamber (FC) method

The flux measurements with the FC method were performed continuously together with a greenhouse gas analyzer (Elder *et al.,* 2020). The analyzer used was a cavity ring down spectrometer from Los Gatos Research: Greenhouse DLT-100 GGA gas analyzer, from now on referred to as LGR-1. The chamber had a plastic material, and was covered with aluminum foil to reduce heating in the chamber. Foam was attached on the down facing sides for floating and adjusted so it did not lift the chamber out of the water. The chamber was connected to the LGR-1 via two plastic tubs, one to the inlet and the other to the outlet. The tube transporting air to the LGR-1 ran through two 100 ml Winkler bottles and an Acro® 50 vent filter to reduce the risk of water entering the LGR-1. The chamber was anchored to the seafloor to be able to measure the flux at different depths, as well as distances, from shore. The LGR-1 was set to the LO setting, only using the internal pump, and to a frequency of 20 seconds. The setup had an aspect ratio (volume/area) of 10.38 $x10^{-3}$ m. The total volume of the chamber, tubing system, and LGR-1 cavity added up to 7574.13 ml and the area that the chamber took up on the water surface was 73.02 $x10^{-3}$ m^2. The chamber walls reached approximately 1.5-2 cm down into the water.

At each study site, measurements were taken at certain distances from shore at various places in the bay. One measurement spanned approximately 20 minutes, from that the chamber was launched, to that it was lifted from the water surface. The time interval was chosen to minimize the risk for, at high fluxes, the concentration increase in the chamber-LGR-1 system to affect the gas transfer velocity (Mannich *et al.,* 2019), and at the same time making sure that the system measured real fluxes and not just an equilibration of the gases within the system. Each measurement was repeated one time after allowing the gas in the system to equilibrate with the air. The flux was calculated based on the mean of the two measurement duplicates.

The sampling was done two days at each location, for each period, in an attempt to capture different weather conditions within the same time of year. These two days were within a week from each other. The periods were September 2020, November/December 2020, January/February 2021, March/April 2021 and May 2021. During Jan - Feb, only a few locations were possible to sample due to ice cover. For September, only location A-1 was sampled due to instrumental problems that needed a month to be repaired.

Anchored vs. not anchored

An experiment testing the effect of an anchored chamber versus a non-anchored chamber on the CH_4 flux was carried out at location I-1. Since an anchor disturbs the sediment, both when it is launched, but also during a measurement if the chamber is being pulled by winds or currents, since the anchor could cause sediment resuspension and an increased release of CH_4 from the sediment to the water column. Further, if the chamber is fixed in relation to

the waters movement it could cause an enhanced turbulence; this is especially true for higher wind velocities or strong currents (Mannich *et al.,* 2019).

For the experiment, the launching of the chambers was done from two distances from shore, one at 5 meters and one at 20 meters. At each distance, the chamber was launched 12 times, 6 times with the anchor and 6 times without the anchor. Wind velocities and air temperature were recorded simultaneously to exclude that any changes in the flux depended on that. The results are shown in Table 2.

Test:	1st flux:	2nd flux:	3rd flux:	4th flux:	5th flux:	6th flux:	Mean:	Wind/Temp:
Anchored 5 m	0.029	0.024	0.024	0.036	0.031	0.030	0.029± 0.005	0.4 m s^{-1}, 5.3 °C
Non-anchored 5 m	0.022	0.020	0.023	0.024	0.020	0.020	0.021± 0.002	0.8 m s^{-1}, 5.6 °C
Anchored 20 m	0.009	0.010	0.012	0.008	0.009	0.009	0.010± 0.001	1.3 m s^{-1}, 6.2 °C
Non-anchored 20 m	0.010	0.012	0.012	0.009	0.007	0.011	0.010± 0.002	1.3 m s^{-1}, 6.7 °C

TABLE 2: *Data for the anchored vs. non-anchored tests. F_{CH4} is given in mmol m^{-2} d^{-1}. Uncertainty of the mean is given as the standard deviation.*

The non-anchored, 5 meters distance to shore F_{CH4} mean was 0.029 ± 0.005 mmol m^{-2} d^{-1}, and for the same distance but with an anchor the F_{CH4} mean was 0.021 ± 0.002 mmol m^{-2} d^{-1}, no significant change in wind or temperature. For the 20 meters distance, non-anchored test, the F_{CH4} mean was 0.010 ± 0.001 mmol m^{-2} d^{-1}, and for the same distance but anchored the F_{CH4} mean was 0.010 ± 0.002 mmol m^{-2} d^{-1} and no significant change in wind or temperature either. The F_{CH4} are not differing more than in the third decimal digit, no statically significant difference was found (Wilcoxon-Mann-Whitney U-test, $p > 0.05$). There seems to be no obvious effect on the F_{CH4} from the anchor, and therefore the advantage of being able to position the chamber at a certain distance have been the ground for choosing to anchor the chamber in this study.

1.1.1 Physical properties

Salinity and water temperature were measured with a handheld conductivity WTW 340i. Air temperature, wind speed, wind direction, precipitation and pressure were measured with an Eurochron wireless weather station, ECWCC1080, that was measuring at a height of 1.5 meters. Water depth was measured with a measuring tape.

1.1.2 Water samples: CH_4 concentrations

3-4 water samples were collected at each study site, for each measurement day to determine dissolved CH_4 concentrations. The samples were collected in 20 ml serum vials that had been pre-flushed with sample water three times. The vials were then sealed with butyl rubber stoppers, with a needle inserted to allow excess water to escape, and crimped with aluminum crimp rings.

1.1.3 Eddy covariance tower

FIGURE 10: *Left: Meteorology mast on location A-1. Right: Overview of the bay, the star marks the location of the mast (Google Maps, 2021).*

Eddy covariance measurements were performed in location A-1, at Askö, Trosa. A meteorological mast (Fig 10, left), reaching 1.55 m height, was positioned on the southeastern side of the bay, on a cliff adjacent to the water (location seen in Fig. 10, right). On top of the mast, a METEK uSonic-3 heated sonic anemometer was mounted, measuring a 3D wind vector, as well as the sonic temperature. The sonic was measuring at 40 Hz.

CH_4, CO_2 and H_2O atmospheric mixing ratios were measured by a cavity ring-down laser spectrometer: Los Gatos Research Fast Greenhouse Gas Analyzer (LGR-2). The LGR-2 was placed in a waterproof box a few meters away from the mast and connected to the mast via a tube measuring 10 mm diameter for inner dimensions and a length of 10 m. The inlet for the LGR-2 was attached on the mast at 1 m height. An external Edwards X35 scroll pump was used to increase the flowrate and maintain the measurement cell pressure at 140 torr. A Nafion membrane drier was installed inline on the tubing in 'reflux' configuration to reduce both mean water vapor concentration and fluctuations. Transit time through the tubing was measured as 2.2 sec using a CO_2 'puff' test. Air pressure and density of CO_2 and H_2O was also measured by an open-path infrared gas analyzer (IRGA), LI-COR 7500, mounted at 1.5 m on the mast. Both gas analyzers measured at 20 Hz.

An infrared thermometer, Heitronics KT-15 Series IIP, was also mounted on the tower, facing the water surface and measuring the water skin temperature, as well as a Vaisala HMP temperature and relative humidity sensor. Both the KT-15 and the HMP measured at 1 Hz.

2.2 Laboratory methods

2.2.1 Gas chromatography for CH4 water samples

For the CH_4 water concentration analyses an SRI 8610 Greenhouse Gas Chromatograph with FID detector, and methanizer for the reduction of CO_2 to CH_4, was used. The methanizer was operated at 350°C. The samples were analyzed at an oven temperature of 80°C, with N_2 as a carrier gas at 60 ml/min, and only the FID detector on. 3 ml of sample volume was loaded on a 1 ml sample loops in load position and transported though a Hayesep D column (1.5 m), with a 1.5-long Hayesep D pre-column and a solenoid valve through which unwanted gases could elude in the first 1.5 min of a sample run.

For the January and Mar – Apr periods water samples, a Shimadzu gas chromatograph GC-8A was used since the SRI was away for reparation during that period. The Shimadzu operated with a FID detector and N_2 as the carrier gas, with a set outlet pressure of 5.6 bars. In the Shimadzu the samples were analyzed at a column oven temperature of 60°C, and a sample injection port- and detector oven- temperature of 150°C. The initial temperature of the program was set to 65°C. 1.5 ml of sample volume was loaded on a 500 µl sample loops. Similar to the SRI the sample was transported through a Hayesep D column (1.5 m), but without the pre-column.

Standards of 10 ppm_m and 100 ppm_m CH_4 were used for the calibration of the samples. Only calibrations with a R^2 above 0.95 from the linear regression analysis were used.

The water samples were analyzed with a method similar to Magen *et al.* (2014). First 6 ml of helium gas was transferred into the serum vials through the rubber stoppers while allowing excess water to escape via a needle. The CH_4 exchange between the water and the 6 ml headspace was then allowed to reach equilibrium before analysis (24h). When the samples were ready for analysis, air from the headspace was drawn out by a needle and a 5 ml syringe through the rubber stoppers. At the same time, saturated salt solution was transferred into the vials, also via a needle and a 5 ml syringe, at the same rate as air was pulled out. 3 ml of sample was then injected into the gas chromatograph.

2.2 Data processing and calculations

The program used for handling the data collected in the field, as well as produced by the EC tower, was MATLAB R2020b.

2.2.1 Flux from the chamber data

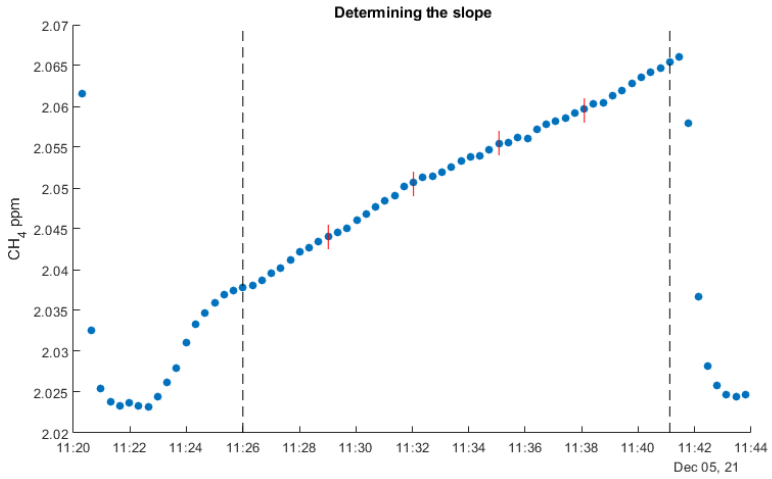

FIGURE 11: *Example of raw data from the LGR-1. The dotted black lines marks what part of the raw data was used for the F_{CH4} calculations. The red markers mark where the slope was divided for the separate linear regression analyses.*

For the F_{CH4} calculations, the slope from the raw data, see Figure 11, was analyzed to obtain the concentration increase in $ppm_m\ d^{-1}$ (Eq. 2). The measurement was analyzed if the initial CH_4 mole fraction was similar to the other measurements the same day, at the same location. In the example (Fig. 11), that mole fraction is between 2.02 and 2.025 ppm_m. 150 sec from the beginning of launching was removed from the slope analysis since that time was considered to be sufficient for the system to equilibrate with the CH_4 concentrations at the water surface. A divided linear regression analysis was applied to obtain the concentration increase: The 15 minutes chosen for analysis was divided into five equally large parts and each of these parts were analyzed for linear regression. If R^2 exceeded 0.7, the regression was included in the total analysis of the slope, this to avoid including concentration increases that were due to ebullition. If a measurement included more than two parts that had a R^2 below 0.7, the measurement was not accepted for further analysis.

$$2)\quad S_{total} = \frac{86400(S_1+S_2+S_3\ldots+S_n)}{n}$$

Where S_{total} is the mean increase in mixing ratio of the measurement in $ppm_m\ d^{-1}$, S_n is the divided part's regressions that passed $R^2 > 0.7$ and n is the number of those parts.

The F_{CH4} was then calculated following equation 3:

$$3)\quad F_{CH_4} = \frac{(N_{CH_4}+L)}{A}$$

Where F_{CH4} is the dynamic flux in mmol $m^{-2}\ d^{-1}$, N_{CH4} is the flux of CH_4 in mmol d^{-1} within the system, L is a leakage correction in mmol d^{-1} calculated for the system (see 'Leakage correction') and A is the area that the chamber was taking up on the water surface in m^3.

Eq. 3 was solved from the ideal gas law:

$$4)\quad N_{CH_4} = \frac{1000(pCH_4*V)}{R*T}$$

5) $pCH_4 = \frac{S_{total} * P_A}{1000000}$

Where pCH_4 is the change in partial pressure of CH_4 in the system in Pa d^{-1}, V is the volume of the system in m^3, R is the gas constant in m^3 Pa K^{-1} mol^{-1}, T is the air temperature in K and P_A is the atmospheric pressure in Pa.

The F_{CH4} was calculated for both of the duplicate measurements and the mean of the two then represented the flux for that measurement spot. The two variances produced by the divided linear regression method were then averaged and the square root was taken to get the standard deviation of the calculated mean F_{CH4}.

Leakage correction

A test to see the integrity of the tubing system was performed after the sampling in Mar – Apr and May. The integrity was also tested each sampling day by a simple 'puff' test on the tubes and connections, to see if it gave any reaction in CO_2, if it did; the leakage was taken care of. The more thorough test was done to check for diffusion through the tubes or very small leakages through connections that was not detectable by the 'puff' test.

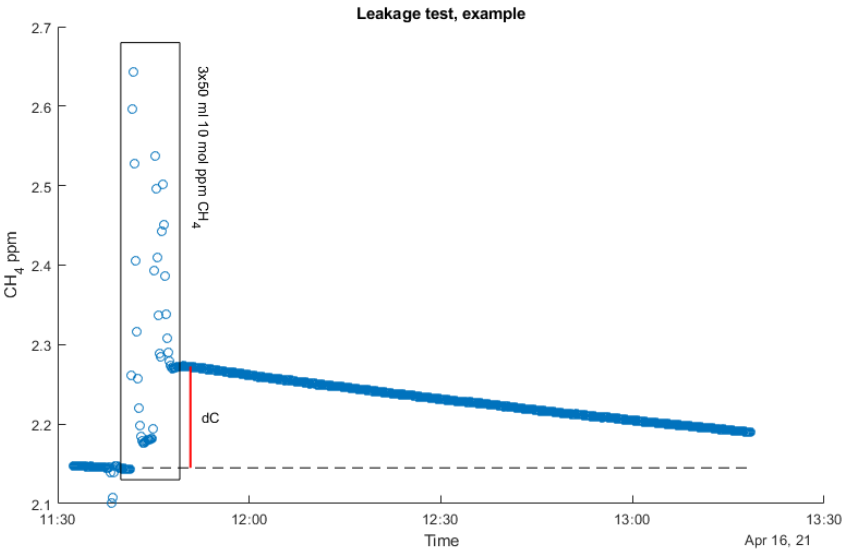

FIGURE 12: *The raw data from one of the tests.*

The test was set up with the chamber launched in a bucket of oil, after the system had been allowed to equilibrate with the air in the room. The LGR-1 was left for a while to make sure that the signal was stable and then 3x50 ml of 10 ppm_m CH_4-standard was injected in one of the three-way-cranes. The LGR-1 was again left to run for a couple of hours. The signal showed a decrease in concentration with time, and the slope was used to calculate an exchange in mmol d^{-1} in the same way as eq. 3-4 (eq. 3 without L), see Figure 12. For simplification it was assumed that the leakage was homogenous over the whole tube/chamber system, so with the area of the system the exchange could then be considered a dynamic flux. From Fick's first law, a leakage coefficient 'D' was derived:

6) $D = D_{25} + s(T - 298.15)$

7) $D_{25} = {F_{leakage,test}}/{\Delta C_{test}}$

Where D is the coefficient adjusted for the temperature T at the time of the measurement in K, D_{25} is the calculated coefficient for 25°C, s is a gradient derived from the diffusion coefficients for CH_4 for different temperatures in units per K (Winn, 1950), $F_{leakage,\ test}$ is the calculated F_{CH4} from the leakage test in mmol d^{-1} and dC_{test} is the concentration gradient in the test in ppm_m.

D was then used to calculate the leakage correction:

8) $F_{leakage} = D * \Delta C$

Where $F_{leakage}$ is the specific leakage for the temperature during the measurement and dC is the mean concentration difference between the slope of the measurement and the initial CH_4 concentration.

2.2.2 CH_4 concentrations in the water

The concentration of CH_4 in the water samples were calculated from the calibration of the gas chromatograph and resulting slopes as follows:

9) $C_T = \frac{N_{HS}+N_W}{V_W}$

Where C_T is the original concentration in the water sample before exchange with the headspace in nM, N_{HS} is the amount of moles in the headspace in nmol, N_W is the amount of moles in the water in nmol and V_W is the water volume in L.

Eq. 9 was solved from eq. 10, 11 and 12:

10) $N_W = C_{W,eq} * V_W$

11) $N_{HS} = C_{HS} * V_{HS}$

12) $C_{W,eq} = \frac{\beta * C_{HS}}{R * T}$

Where $C_{W,eq}$ is the concentration for the water in nM, C_{HS} is the concentration in the headspace calculated from the coefficients from the gas chromatograph calibration in nM, V_{HS} is the volume of the headspace in L and β is the Bunsen solubility coefficient (calculated from coefficients from Wiesenburg & Guinasso (1979).

2.2.3 BL model flux and gas transfer velocity

The flux from the BL model was calculated from the CH_4 concentration gradient and the gas transfer velocity, a version of Fick's first law (Wanninkhof, 1992; Liss & Merlivat, 1986; Liss & Slater, 1974, etc.):

13) $F_{CH_4} = 0.24k(C_W - \alpha C_A)$

Where k is the gas transfer velocity in cm h^{-1}, 0.24 is a conversion factor between cm h^{-1} to m d^{-1}, C_W is the average CH_4 concentration in the water for that location and day, α is the Oswald solubility coefficient (Eq. 17) and C_A is the concentration of CH_4 in the air (NOAA Research, 2021).

The gas transfer velocity, k, is calculated based on Wanninkhof (2014):

$$14)\ k = 0.251{U_{10}}^2 \left(\frac{Sc_{baltic}}{660}\right)^{-0.5}$$

Where U_{10} is the wind velocity at 10 m height in m s^{-1}, Sc_{baltic} is the Schmidt number for brackish water (Salinity ~ 6‰) normalized to 660 and raised to the power of -0.5.

$$15)\ U_{10} = \frac{U}{1-\left(\frac{\sqrt{c_{10}}}{\kappa}\right)} ln\left(\frac{10}{z}\right)$$

Where U is the wind velocity at the height of measurement in m s^{-1}, c_{10} is the surface drag coefficient for shallow water depth (Amorocho and DeVries, 1980), κ is the von Kármán constant (here set to 0.4) and z is the height of measurement in m.

$$16)\ Sc_{baltic} = \frac{Sal(Sc_s - Sc_f)}{35} + Sc_f$$

Where Sc_s is the Schmidt number for seawater (Salinity ~ 35‰), Sc_f is the Schimdt number for freschwater (Salinity ~ 0‰) and Sal is the salinity (‰), calculated from Gülzow et al. (2013) and Jähne et al. (1987).

The Oswald solubility coefficient (α) is calculated in accordance with Battino (1984):

$$17)\ \alpha = \frac{\beta * T_w}{273.15}$$

Where T_w is the water temperature.

2.2.4 Eddy data processing

The EC system was working and stored data correctly during the periods:

2020:
The 21st of August to the 21st of October.
The 30th of October to the 2nd of November.
The 24rd of November to the 27th of December.

2021:
The 7th of February to the 12th of Mars.
The 6th of April to the 14th of May.

Initial data processing: Meteorology and fluxes

All data from the EC tower have been averaged into 30-minute periods. The sonic temperature was side-wind corrected according to van Dijk *et al.* (2004). The wind and temperature data from the sonic were also averaged from 40 Hz down to 20 Hz frequency.

The LI-COR data, as well as the LGR-2 data, were time matched to the sonic data. The LGR-2 had a time delay of 2.2 seconds due to the time it took for the air to go through the tube; this was corrected for and assumed to be constant.

The wind components from the sonic anemometer were rotated into a mean streamline coordinate system using a double rotation method, this to avoid errors associated with the tilt of the sonic (Wilczak *et al.,* 2001). The wind components from the sonic were used to calculate the energy- as well as the mass- fluxes.

The mean wind speed was adjusted to 10 m height for the EC data using a log profile (Eq. 18), without a stability adjustment due to an error in the KT-15 thermometer which gave unreliable skin temperatures for the water.

$$18)\ U_{10} = U + u_* \log\left(\frac{10}{z_u}\right)/\kappa$$

Where $u_*$is the friction velocity in m s^{-1} and z_u the measuring height of the sonic anemometer in m.

From the cross- and vertical- wind components, the friction velocity and the momentum flux were calculated (eq. 19).

$$19)\ u_* = \left(\frac{\tau}{\rho}\right)^{1/2} = \left(\overline{u'w'}^2 + \overline{v'w'}^2\right)^{1/4}$$

Where τ is the momentum flux N m^{-2}, ρ is the mean air density in kg m^{-3} and u and v are the cross-wind components and w is the vertical wind component of the stream wise rotated wind, ' indicates the fluctuation from the mean and an overbar indicates the mean.

The sensible heat flux was calculated from the sonic temperature and corrected for humidity based on a bulk estimate of the latent heat flux (Persson *et al.,* 2005; Smith, 1988). The latent heat flux was determined from the H_2O mixing ratio from the open-path LI-COR.

$$20)\ F_H = c_p * \rho_a * (\overline{T_s'w'} - 0.51T_a * FL_{bulk})$$

Where F_H is the sensible heat flux in W m^{-2}, c_p is the specific heat capacity of the water in J K^{-1} kg^{-1}, $\rho_a$is the dry air density in kg m^{-3}, T_s is the sonic temperature in K, T_a is the air temperature in K, and FL_{bulk} is the bulk latent heat flux in W m^{-2} determined following Smith (1988).

$$21)\ F_L = L * \rho_a * \overline{r'w'}$$

Where F_L is the latent heat flux in W m^{-2}, L is the latent heat of vaporization in J kg^{-1}, and r is the humidity mixing ratio in kg kg^{-1}.

The mass fluxes for CH_4 were calculated from the dry mole fraction reported by the LGR-2:

$$22)\ F_{CH_4} = \frac{1000}{M_w} * \rho_a * \overline{c'w'}$$

Where F_{CH4} is the flux of CH_4 in mol m^{-2} s^{-1}, M_w is the molecular weight of CH_4 in g mol^{-1}, c is the dimensionless dry mole fraction. 1000 is a conversion factor used to get mol m^{-2} s^{-1}. Gas fluxes were subsequently converted to units of mmol m^{-2} d^{-1}.

The fluxes were corrected for high frequency attenuation by the tubes in the closed path system according to Bariteau *et al.* (2010). The sonic anemometer vertical wind data, as well as the mixing ratios, went through a quality control where periods when the LGR-2 sensors were not working properly or when the cell pressure changed rapidly were flagged. Further, the distributions of the 30-minute periods were checked for skewness and kurtosis (Vickers & Mahrt, 1997).

pCH_4 was determined from the LGR-2 mixing ratios, temperature, pressure and humidity measured by the mast:

$$23)\ pCH_4 = n_{fraction}(P_a - P_v)$$

Where pCH_4 is the partial pressure of CH_4 in µatm, $n_{fraction}$ is the dry mole fraction in ppm_m, P_a is the atmospheric pressure in atm and P_v is the vapor pressure calculated from the temperature and humidity in atm.

Dimensions of the bay, flux footprint and over water fraction

The dimensions of the bay were determined at the beginning of the experiment (December, 2019) with a hand-held laser range finder (Naturalife PF4). Distances across the bay were determined at approximately 15 degree intervals and used to construct a map of the bay.

For each flux period, a footprint of the measured F_{CH4} was estimated. The footprint of the F_{CH4} is the spatial dimension from where the F_{CH4} is derived, as well as how much F_{CH4} the different areas within those dimensions contribute to the total F_{CH4}. The footprint was calculated based on a two-dimensional parameterization model (Kljun *et al.,* 2015), and rotated to be in the mean wind direction.

Based on the dimensions of the bay, as well as the footprint, an over-water fraction (owf) was estimated for each 30-minute flux period (Prytherch and Yelland, 2021). The owf is an estimate of how much of the F_{CH4} is derived from the water, and how much is derived from land, and is a number between 0-1, with a value of 1 representing a F_{CH4} that is exclusively contributed by the water surface. The relationship between the measured F_{CH4} and the F_{CH4} through water and land surfaces is shown in eq. 24 (Prytherch *et al.,* 2017 cited in Prytherch and Yelland, 2021; Loose *et al.,* 2014):

$$24)\ F_{CH_4} = (1 - owf)F_{land} + owf\,F_{water}$$

Where F_{CH4} is the total measured flux and F_{land} and F_{water} is the flux through the land and water surfaces, respectively.

Note that Eq. 24 was originally derived for use in water-ice environments, where F_{water} could be determined by neglecting F_{land} or assuming it was small and constant. In environments like the enclosed embayment at A-1 on Askö, this relationship may be challenging to use because of the potentially large and varying size of F_{land}. In section 3.5.1 the relationship will be tested.

Determining the background noise of the EC system

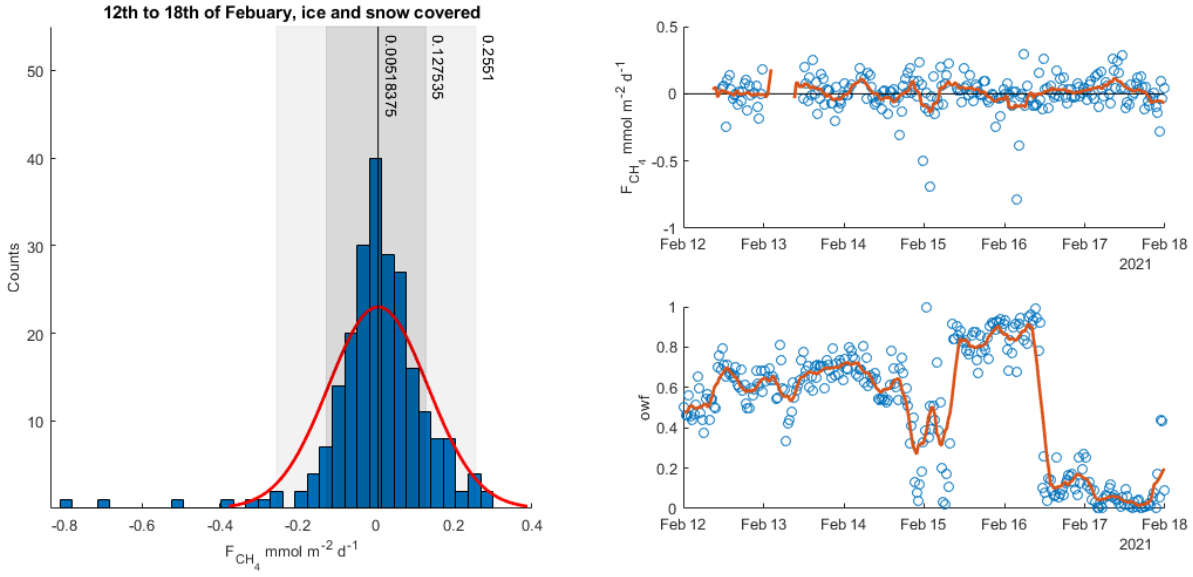

FIGURE 13: *All F_{CH4} data from the 12th to the 18th of February when the bay (A-1) was ice-covered. The histogram shows the distribution of the 30-minute flux periods, with a mean of 0.005 mmol m^{-2} d^{-1}, 1σ at 0.128 mmol m^{-2} d^{-1} and 2σ at 0.255 mmol m^{-2} d^{-1}.*

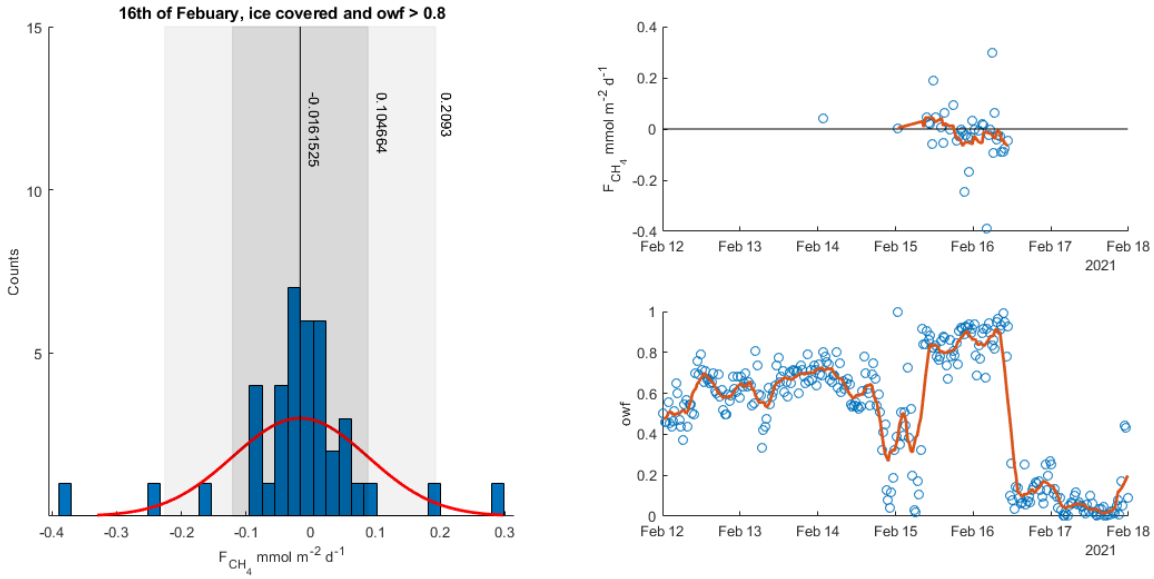

FIGURE 14: *F_{CH4} data from the 12th to the 18th of February when the bay (A-1) was ice-covered, meeting the criteria of owf > 0.8. The histogram shows the distribution of the 30-minute flux periods, with a mean of -0.016 mmol m^{-2} d^{-1}, 1σ at 0.105 mmol m^{-2} d^{-1} and 2σ at 0.209 mmol m^{-2} d^{-1}.*

A noise analysis of the F_{CH4} measurements by the EC system was performed in accordance with Thornton *et al.* (2020). A period was chosen when the bay was ice-covered (12th to 18th of February, 2021), to represent close to zero, if not zero, water-to-air F_{CH4}. The data from that period is shown in Figure 13, containing all F_{CH4} data from that period, and Figure 14, showing only the F_{CH4} data that met the requirement of owf > 0.8 to exclude most of the land derived F_{CH4}. Without the owf limit, the mean F_{CH4} was 0.006 mmol m^{-2} d^{-1} with a 1σ of

0.128 mmol m^{-2} d^{-1} and a 2σ of 0.256 mmol m^{-2} d^{-1}. With the limit of owf > 0.8 the mean F_{CH4} was -0.016 mmol m^{-2} d^{-1} with a 1σ of 0.105 mmol m^{-2} d^{-1} and a 2σ of 0.209 mmol m^{-2} d^{-1}. The two mean values could represent the actual average F_{CH4} for that period. However, they can be interpreted as a result of random distribution of the noise with a sample size that is too small to show the true mean. It would have been preferable to have a larger sample size that met the owf limit, as the histogram analysis for owf > 0.8 may not be statistically reliable on its own. For the data set including all owf-values (Fig. 13) it cannot be disregarded that the analysis might be affected by land derived F_{CH4}, even if snow-covered, and this histogram is therefore not optimal either. However, given that both data sets (Fig. 13 and 14) have similar standard deviations they will be used for estimating the noise level in this study. The mean of the two different 2σ gives 0.233 mmol m^{-2} d^{-1} and in this study this is regarded as the noise level for one 30-minute flux period. When averaging 30-minute flux periods together, the noise of that mean is calculated as two standards errors of the mean (2SEM):

$$25)\ 2\sigma_{\bar{X}} = \frac{2\sigma}{\sqrt{n}}$$

Where $\sigma_{\bar{X}}$ is the standard error of the mean, σ is the standard deviation for one 30-minute flux period, and n is the number of 30-minute flux periods being averaged.

For the 6-hour running mean which will be used for a clearer presentation of the result (6RM; each 30-minute flux period was averaged with 6 adjacent periods on each side, creating a data point averaged over 6 hours), the 2SEM is ± 0.067 mmol m^{-2} d^{-1}.

2.2.5 Statistical tools

For some analyses of the results it was necessary to test if two groups of data were sampled from continuous data with equal means (for normally distributed) or equal distributions (for non-normal distribution). This was tested with either a two-sampled t-test, for normally distributed data, or a Wilcoxon-Mann-Whitney U-test, for non-normally distributed data (Fay & Proschan, 2010). Testing for normality was done with a Shapiro-Wilk parametric hypothesis test (BenSaïda, 2021; Şahintürk & Özcan, 2017). When more means needed to be tested a Kruskal-Wallis test was performed, which does not assume normal-distribution in the data (Green & Salkind, 2008). The Kruskal-Wallis test was complemented with a Bonferroni Multiple Comparison test (Francis & Thunell, 2021), which corrects for type I errors. For all statistical tests, a significance level of 5 % was set, meaning that *p*-values under 0.05 rejected the null hypothesis. For linear regression analysis, a least squares method has been applied (Holland & Welsch, 1977). When multiple-linear regression has been applied, the variance inflation factor (VIF) has been analyzed to check for collinearity between the independent variables (Belsley, 1980).

3. RESULTS

3.1 F_{CH4} from the FC method

This section will present the data collected, with the FC and BL methods, during the field campaigns. It will go through data for all locations, both on Askö and Ingarö. This result will lay ground for the analysis of how well the classification applies to the F_{CH4} from the different bay types. The result further aims to identify site specific environmental-, and physical- properties, as well as method specific factors, that have an effect on the F_{CH4}.

3.1.1 Environmental and meteorological data

During all sampling periods the environmental and meteorological conditions were generally characterized by cold temperatures and low wind speeds. This section will only report data for days when sampling was carried out. For all periods air temperature ranged between -2 to 17 °C, water temperatures between 2 and 15 °C, while U_{10} has been measured between 0 and 5.5 m s^{-1}.

For the sampling days in September, air temperature was around 16-17 °C with just slightly colder water temperatures of 15 °C and very calm conditions with U_{10} up to 1 m s^{-1}.

In Nov – Dec the temperatures got colder with air temperatures of just under 0 up to 9 °C and water temperatures between 2 and 5 °C, this was accompanied by a higher U_{10} of up to 5.5 m s^{-1}.

In January, the few sampling days had cold air temperatures of -2 to 0 °C and water temperatures around 2 °C. In January most of the bays were ice-covered and only two bays (I-2 and I-6) were possible to sample. U_{10} was between 0 and 2 m s^{-1}.

Mar - Apr were accompanied by ice break-up and a few bays were ice-covered all the way in to April. I-2 was ice-covered the longest and was sampled one day when the bay was still partly ice-covered. Air and water temperatures showed large ranges between 0 and 16 °C and between 1 and 6 °C respectively. U_{10} reached up to 4 m s^{-1}.

In May air temperatures were between 4 and 16 °C and water temperatures between 7 and 16 °C. U_{10} was similar to Mar - Apr and reached up to 4 m s^{-1}.

3.1.2 Dissolved CH_4 concentrations

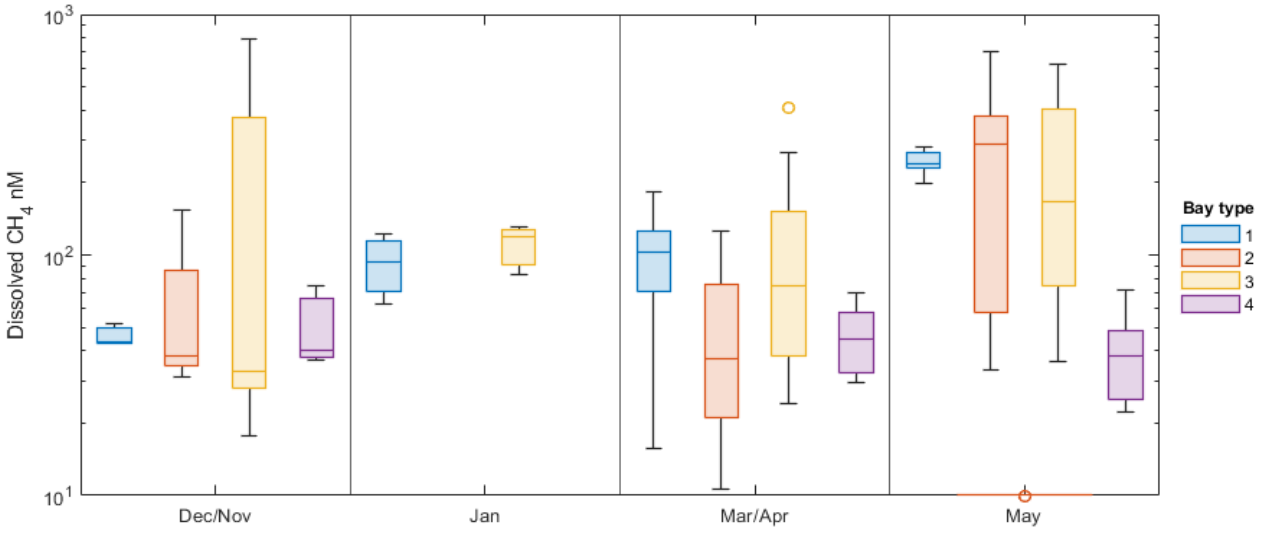

FIGURE 15: *Dissolved CH_4 for each sampling period, colored based on bay type. Sample sizes: from type 1 – type 4 starting in Dec/Nov: n = 4, 13, 8 and 4, Jan: n = 3 and 4, Mar/Apr: n = 8, 21, 16 and 8, May: n = 7, 19, 10 and 6.*

BAY TYPE:	LOCATION:	INTERQUARTILE RANGE OF DISSOLVED CH_4 nmol L^{-1}:			
		Dec/Nov:	Jan:	Mar/Apr:	May:
1	I-6	43.0 – 49.6	70.4 – 114.6	70.2 – 125.9	230.4 – 266.4
2	A-1	34.7 – 37.4		20.2 – 29.0	36.1 – 56.9
	I-2	76.5 – 141.8		16.25 – 68.3	281.8 – 527.9
	I-4	32.8 – 39.7		66.1 – 111.1	323.9 – 382.8
3	I-1	23.8 – 32.8	91.6 – 128.1	31.4 – 58.9	44.2 – 130.5
	I-5	325.8 – 708.3		92.4 – 245.8	143.9 – 466.8
4	I-3	37.3 – 66.1		32.2 – 57.9	25.2 – 48.7

TABLE 3: *The different locations dissolved CH_4 concentrations, shown as the 25th percentile to the 75th percentile.*

CH_4 water surface concentrations collected in the field are visualized and shown in Figure 15 and Table 3. The concentrations ranged from 10.7 to 787.5 nmol L^{-1} for all sampling periods and bay types. However, the median was 70.6 nmol L^{-1} with the 25th and 75th percentiles ranging between 36.0 and 168.9 nmol L^{-1}. Excluding outliers, the concentrations reached 368.3 nmol L^{-1}. Nov - Dec and Mar – Apr both had concentration distributions that were significantly lower than May, while January did not show a significant difference compared to any of the other periods.

There were large differences in CH_4 concentrations between the bays within type 2 and 3. Within type 2, significant concentration differences were found in Mar – Apr and in May. Within type 3, significant differences were found in all periods where both bays were sampled. Figure 16 visualizes the relationship between the bays, for all periods, where I-5 showed the overall highest concentration followed by I-6, I-4, I-2, I-1, I-3 and A-1. Figure 16 also displays between what bays a statistically significant difference was found.

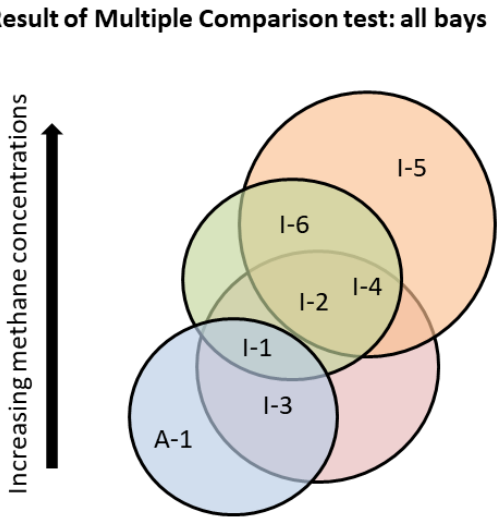

FIGURE 16: The figure helps visualize the Multiple Comparison test for the locations and dissolved CH_4. The locations that are within the same circle did not show a significant difference in CH_4 concentrations. Important note: this figure is for clarity purposes only; it is not in scale when it comes to concentration differences.

3.1.3 CH_4 sea-air fluxes with the FC method

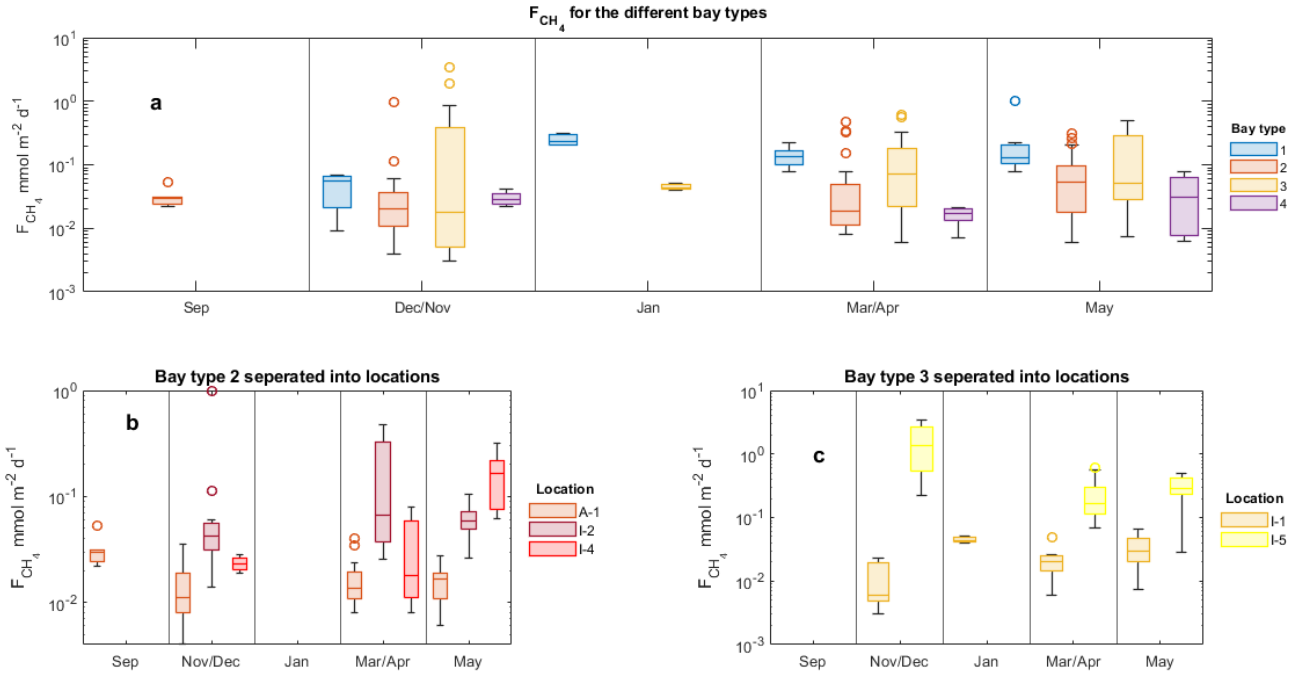

FIGURE 17: A: *F_{CH4} for all periods, color-marked for the different bay types. B: Bay type 2 separated into the locations. C: Bay type 3 separated into the locations. Note the logarithmic scale. Sample sizes (increasing type number): Sep: n =7, 5, 33, 15 and 4, Jan: n = 5 and 5, Mar/Apr: n = 8, 37, 25 and 9, May: n = 9, 32, 22 and 8.*

The F_{CH4} is visualized in Figure 17. For all periods, the F_{CH4} ranged between 0.003 and 3.125 mmol m^{-2} d^{-1}. However, the median F_{CH4} was 0.030 mmol m^{-2} d^{-1} with the 75th and 25th

percentiles ranging between 0.016 and 0.097 mmol m^{-2} d^{-1}. Excluding outliers the F_{CH4} reached 0.230 mmol m^{-2} d^{-1}. The Kruskal-Wallis test showed a difference in the F_{CH4} between Nov – Dec and May ($p < 0.05$), where May had significantly higher F_{CH4}. The other periods could not be shown to deviate from any other period.

Similar to the CH_4 concentrations, the F_{CH4} was not homogeneous within the types; see Table 4. The variation within the types was consistent during all periods. Differences within the types were more common than differences between the types.

Multiple-comparison test between the bay types and the locations:

Bay type	Location	September	Nov/Dec	January	Mar/Apr	May	All periods
1	I-6	-	-	-	-	-	See Fig. 19
2	A-1 I-2 I-4	-	I-2 ≠ *A-1*	-	I-2 ≠ A-1	I-2 and I-4 ≠ A-1	See Fig. 19
3	I-1 I-5	-	I-5 ≠ I-1	-	I-5 ≠ I-1	I-5 ≠ I-1	See Fig. 19
4	I-3	-	-	-	-	-	See Fig. 19
All types:		-	No difference	No difference	1 ≠ 2 and 4 3 ≠ 4	1 ≠ 2 and 4	1 ≠ 3 ≠ 2 and 4

TABLE 4: *The results of the Kruskal-Wallis and Bonferroni multiple comparison tests. The ≠ indicates that a significant difference was found (p-value < 0.05) between either the bay types or between the locations within the bay types. The bay/bay type on the left side of the ≠ had the largest F_{CH4}.*

When all periods were analyzed together, see Table 4; Bay type 1 had the highest F_{CH4}, followed by type 3. Type 2 and 4 had the lowest F_{CH4} but could not be distinguished from each other.

Figure 18 shows the distribution of the F_{CH4} between the bays, and where significant difference could be found between the F_{CH4} in the bays.

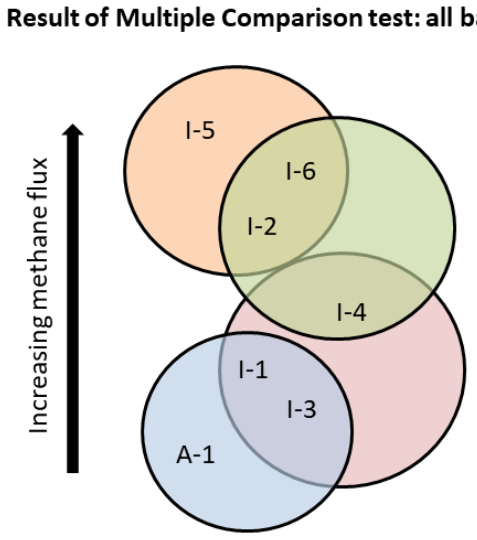

FIGURE 18: The figure helps visualize the Multiple Comparison test for the bays and their F_{CH4}. The locations that are within the same circle did not show a significant difference in F_{CH4}. Important note: this figure is for clarity purposes only; it is not in scale when it comes to concentration differences.

3.2 U_{10} and temperature as predictors for F_{CH4}

3.2.1 How the F_{CH4} change with wind speed

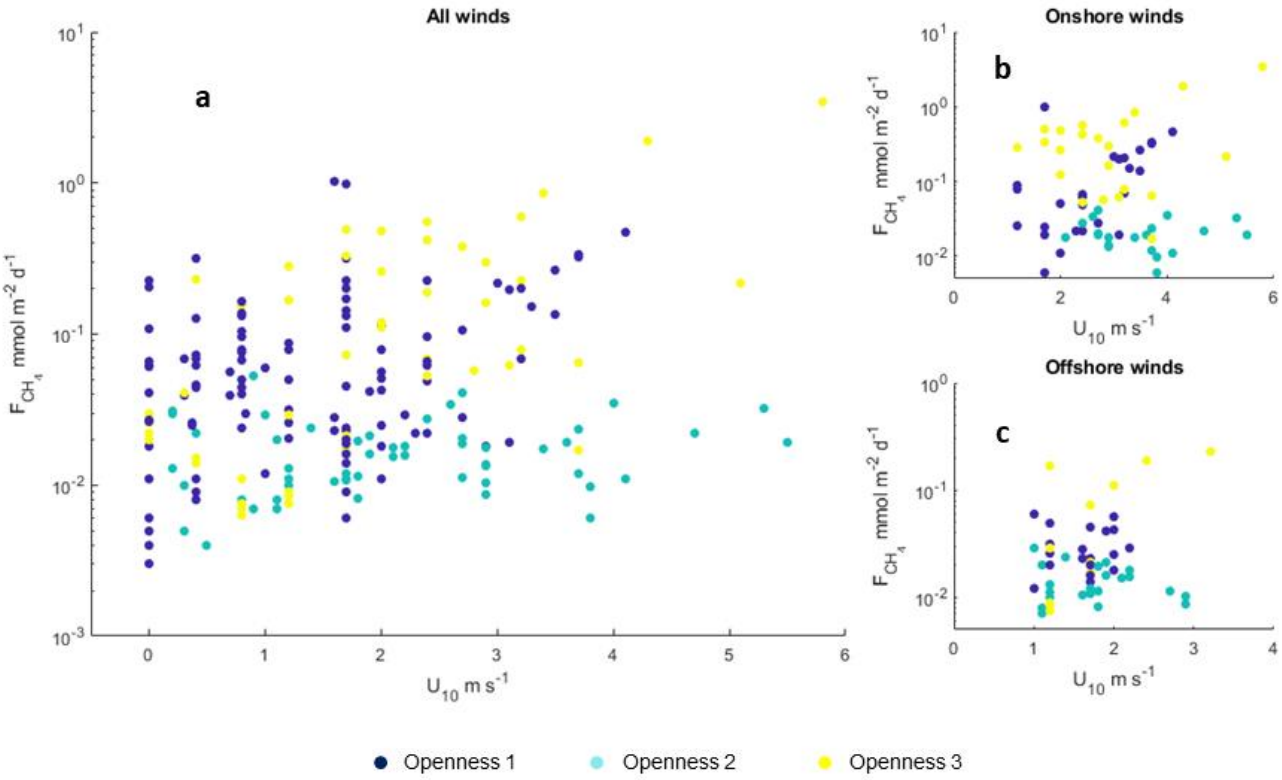

FIGURE 19: *F_{CH4} plotted against U_{10}, a: for all winds, b: onshore winds, and c: offshore winds. Since I-6 is a channel, it is not included in b and c. Further, only winds reaching above 1 m s^{-1} are included in b and c. The standard deviations for each measurement are not included in the figure for clarity purposes. However, the average standard deviation is 25% of the F_{CH4} value.*

Each bay was given a relative evaluation of how exposed or sheltered it was from wind or waves. Openness 1 represented the least exposed and includes I-1, I-2, I-4 and I-6. These bays had a blocked access by a narrow inlet and/or were oriented towards the north and were therefore protected against southerly winds. Openness 2 was only represented by A-1. A-1 faced south and was therefore on occasions relatively exposed to wind and waves. However, Norra Kalvholmen, a small island, was located in front of A-1, giving the bay some shelter. Openness 3 included I-3 and I-5; two bays who faced southeast and were fully exposed to wind and waves.

Exposure:	Openness 1	Openness 2	Openness 3
All winds	Slope = 0.04, *p* = 0.05	No relationship	Slope = 0.25, *p* = 9e-06
Onshore	No relationship	No relationship	Slope = 0.42, *p* = 0.003
Offshore	No relationship	No relationship	Slope = 0.10, *p* = 0.007

TABLE 5: *The results of the linear least squared regression analysis performed on the data in Figure 23.*

Table 5 shows the regression data for Figure 19. Openness 3 consistently showed a relationship with U_{10}. However, that relationship was stronger for onshore winds. Openness 1 only showed a relationship with U_{10} when both onshore and offshore winds were included.

3.2.2 F_{CH4} dependence on temperature

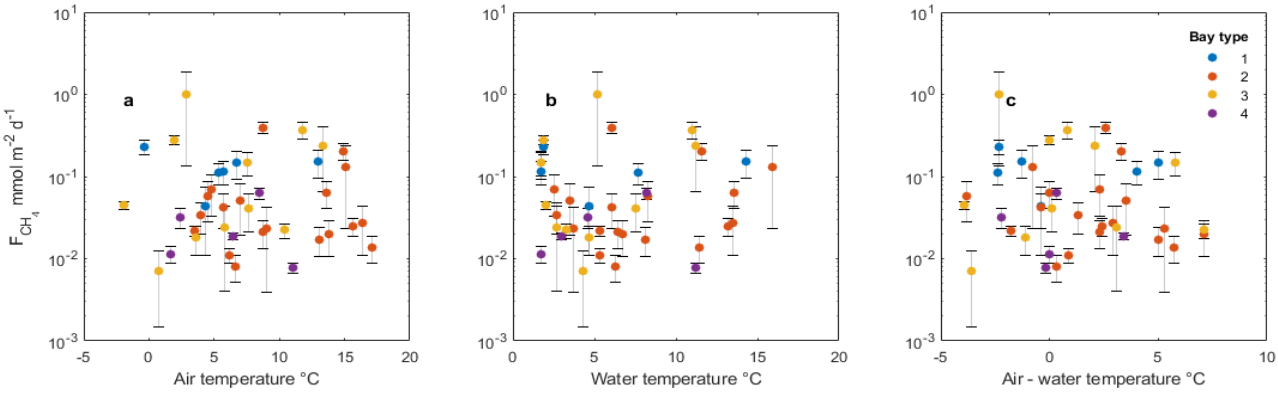

FIGURE 20: Daily averages of F_{CH4}, divided into bay types, plotted against a: air temperature, b: water temperature, and c: difference between air and water temperature. The black whiskers are standard deviations of the daily average.

F_{CH4}, and how it behaved when air and water temperature was changed, is visualized in Figure 20. No statistically reliable relationship between F_{CH4} and any of the temperature predictors was found. The analysis was performed both separately for all the bay types, as well as all bay types together. Further, these two analyses were repeated for each period, as well as including all periods.

When the bays were analyzed separately and without the daily average, only A-1 and I-4 had a relationship with water temperature, see Table 6.

Bay:	**A-1**	**I-1**	**I-2**	**I-3**	**I-4**	**I-5**	**I-6**
Slope:	0.001	-	-	-	0.011	-	-
***p*-value:**	0.001	>0.05	>0.05	>0.05	4e-04	>0.05	>0.05

TABLE 6: *Relationship between F_{CH4} and water temperature for each bay separately.*

3.3 The influence from depth, distance to shore and time of day on F_{CH4}

3.3.1 The effect of water depth and distance to shore on the F_{CH4}

Figure 21 – 26 visualizes the F_{CH4} for different water depths, divided into one figure for each bay. As I-6 had relatively homogeneous water depths where the measurements were done, it will not be included in this part of the results. Therefore, only type 2, 3 and 4 will be presented.

Type 2:

Figure 21 shows how the F_{CH4} was distributed between the water depths and distance to shore in A-1. A-1 has shoreline with both reed beds as well as more cliffs/rock dominated.

Therefore, the F_{CH4} measurements preformed on 50 cm depth have been split up between the two shoreline types. The Kruskal-Wallis test did not show any significant difference between the distributions of F_{CH4} between the depths. The test read F_{CH4} measured in reed beds and F_{CH4} measured above less vegetated (rocky) sea floor as two different sample groups, but did still not find any significant difference. However, the highest F_{CH4} in A-1 was measured in the reed beds even though the high F_{CH4} was not consistent. The same applied to distance to shore, no significant difference was found between the distances with the Kruskal-Wallis test and no relationship was found when analyzed for linear regression.

Figure 22 visualizes the F_{CH4} at different water depths and distances to shore at I-2. Similar to A-1, there was no statistically significant difference found between the distributions of F_{CH4} between the water depths. However, the highest F_{CH4} measured in I-2 was in the shallowest waters. But, looking at the 'distance to shore'-plot, where the day when the bay was partly ice-covered has been marked, the high fluxes close to shore were measured on that day. Excluding that day, no difference was found for the different distances either.

Figure 23 shows I-4. The F_{CH4} measured at 25 cm depth are over rocks/cliffs, while the rest are adjacent to, or in reed beds. There was a significant difference found between the F_{CH4} at 25 cm and the F_{CH4} at 1 m ($p < 0.05$), while the distribution of the F_{CH4} at 50 cm could not be distinguished from the other two depth groups. No difference was found for F_{CH4} for the different distance to shore.

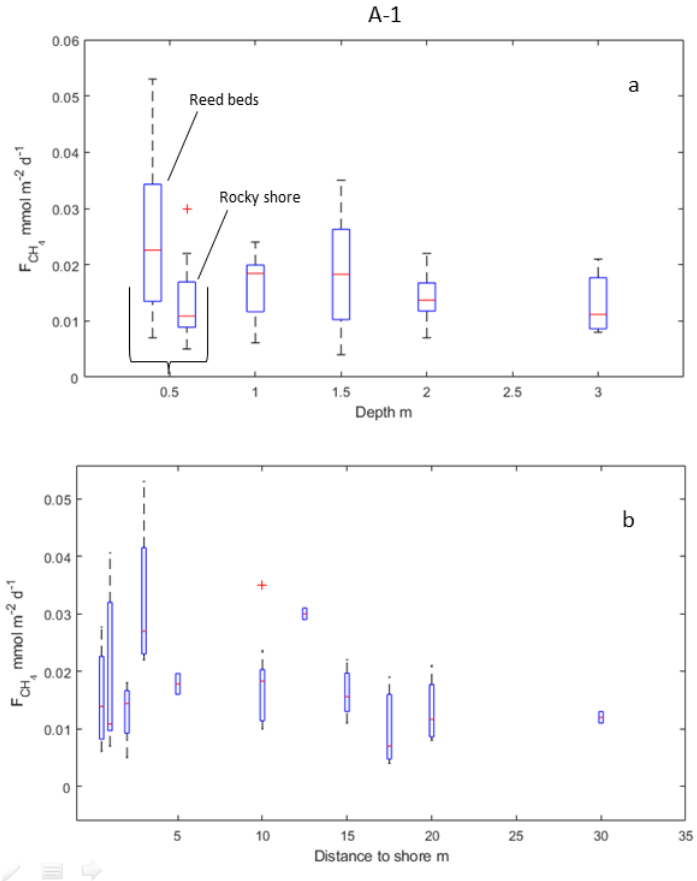

FIGURE 21: Boxplot of F_{CH4} for a) different water depths and b) distance to shore, at A-1. The red lines are the medians, the blue boxes are the 25th and 25th percentiles, the black dashed lines reaches the most extreme values not considered outliers and the red crosses are outliers. 3 m includes all measurements that reached 3 m and deeper. Two groups for 0.5 m depth are distinguished. The sample sizes for a, starting from the left, are: n = 10, 8, 8, 12, 9 and 6. For b, starting from the left, n = 4, 10, 4, 4, 2, 10, 2, 5, 3, 6 and 2.

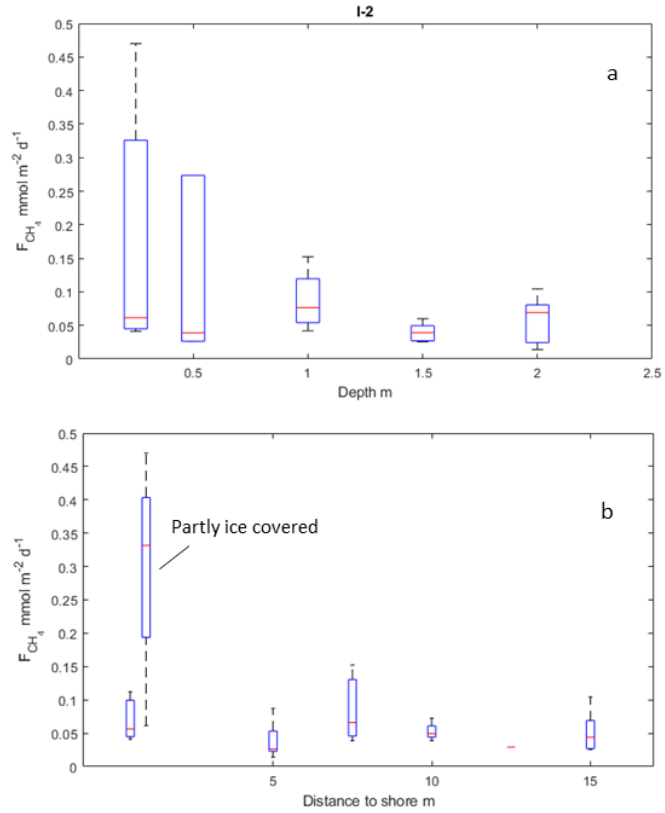

FIGURE 22: Boxplot of F_{CH4} for a) different water depths and b) distance to shore at I-2. The red lines are the medians, the blue boxes are the 25th and 25th percentiles, the black dashed lines reaches the most extreme values not considered outliers and the red crosses are outliers. 3 m includes all measurements that reached 3 m and deeper. The sample sizes for a, starting from the left, are: n = 10, 5, 6, 6 and 8. For b, starting from the left, n = 8, 5, 6, 4, 5, 1 and 6. The distributions of the measurements from the distance of 1 m are positively affected by the day that the bay was partly ice-covered.

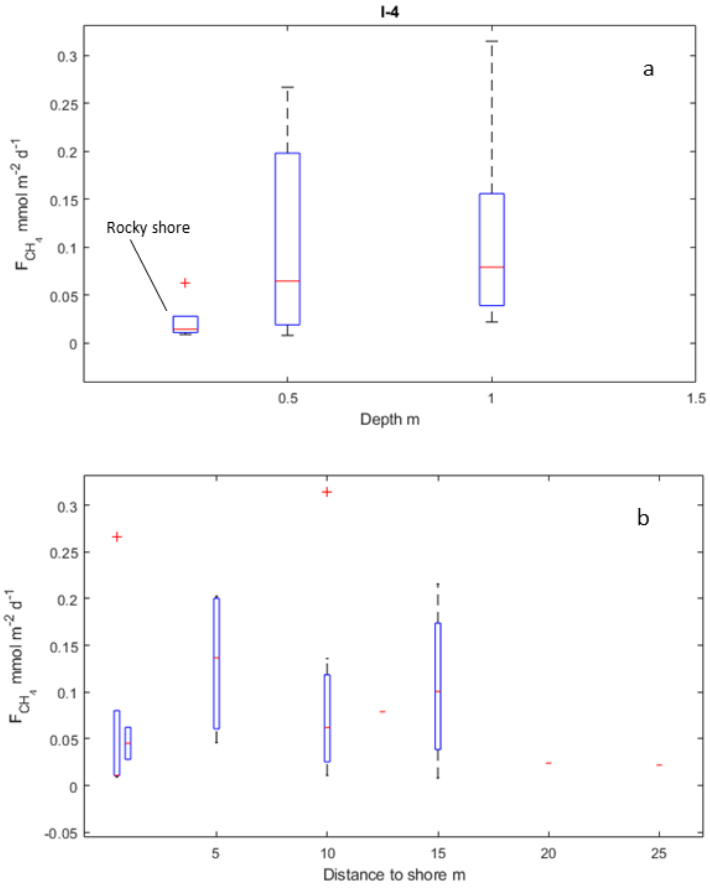

FIGURE 23: Boxplot of F_{CH4} for a) different water depths and b) distance to shore for I-4. The red lines are the medians, the blue boxes are the 25th and 25th percentiles, the black dashed lines reaches the most extreme values not considered outliers and the red crosses are outliers. 3 m includes all measurements that reached 3 m and deeper. The sample sizes for a, starting from the left, are: n = 9, 10 and 11. For b, starting from the left, n = 5, 3, 9, 1, 6, 1 and 1.

Type 3:

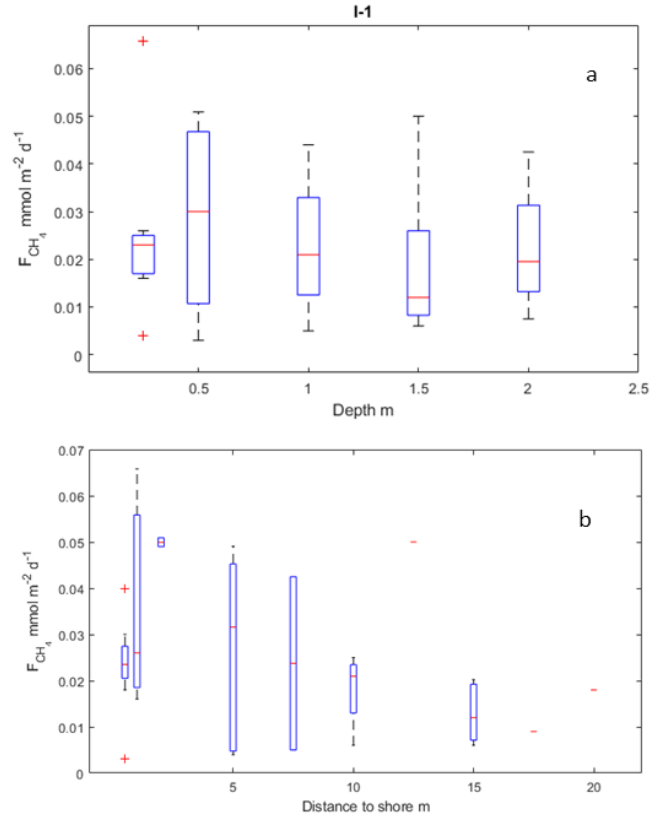

FIGURE 24: Boxplot of F_{CH4} for a) different water depths and b) distance to shore for I-1. The red lines are the medians, the blue boxes are the 25th and 25th percentiles, the black dashed lines reaches the most extreme values not considered outliers and the red crosses are outliers. 3 m includes all measurements that reached 3 m and deeper. The sample sizes for a, starting from the left, are: n = 8, 11, 5, 5 and 6. For b, starting from the left, n = 9, 3, 3, 5, 4, 4, 1, 5, 1 and 1.

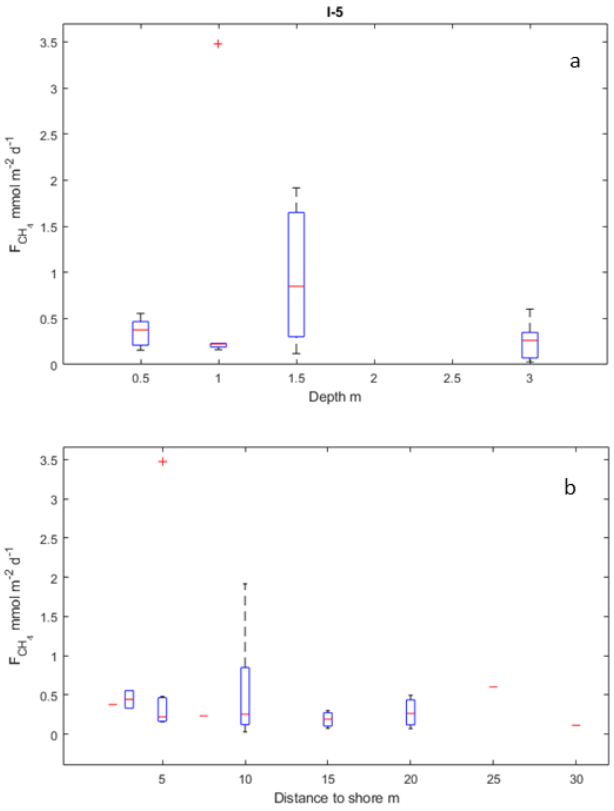

FIGURE 25: Boxplot of F_{CH4} for a) different water depths and b) distance to shore for I-5. The red lines are the medians, the blue boxes are the 25th and 25th percentiles, the black dashed lines reaches the most extreme values not considered outliers and the red crosses are outliers. 3 m includes all measurements that reached 3 m and deeper. The sample sizes for a, starting from the left, are: n = 7, 6, 4 and 10. For b, starting from the left, n = 1, 4, 8, 1, 7, 5 and 3.

Figure 24 and 25 visualizes the F_{CH4} measured in I-1 and I-5, respectively, at different depths and distances to shore. No significant differences between the water depths and F_{CH4} or distances to shore and F_{CH4} were found in either of the bays.

Type 4:

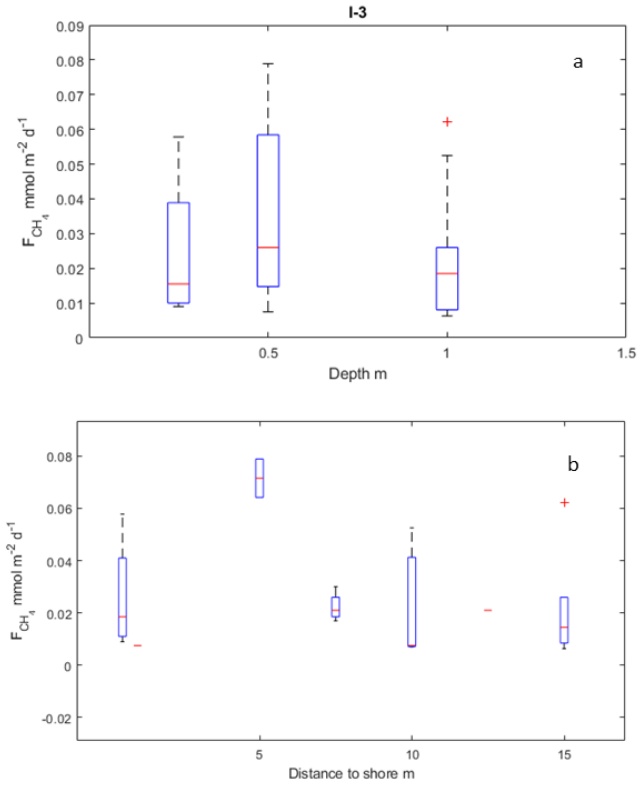

FIGURE 26: Boxplot of F_{CH4} for a) different water depths and b) distance to shore for I-3. The red lines are the medians, the blue boxes are the 25th and 25th percentiles, the black dashed lines reaches the most extreme values not considered outliers and the red crosses are outliers. 3 m includes all measurements that reached 3 m and deeper. The sample sizes for a, starting from the left, are: n = 7, 7 and 12. For b, starting from the left, n = 6, 1, 3, 5, 4 and 1.

Figure 26 visualizes the F_{CH4} measured in I-3 at different depths and distances to shore. No significant differences between the water depths or the distances to shore were found.

In summary, only in I-4, and only between measurements done above rocks, and measurements done in proximity to reed beds were there a difference found between water depths. The other bays did not show a dependence on water depth. However, the highest F_{CH4} in A-1 occurred in shallow waters, close to vegetated shore lines. No significant difference was found in any of the bays between the F_{CH4} measurements done in different distances to shore.

3.3.2 Time of day

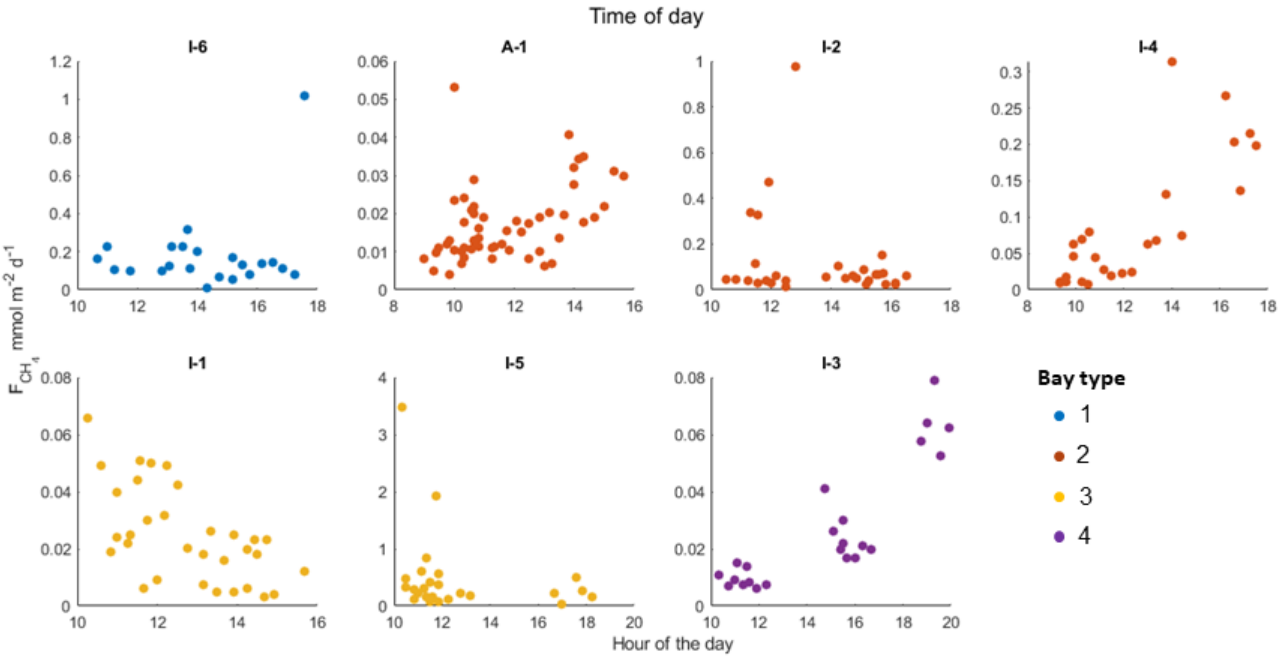

FIGURE 27: *F_{CH4} plotted against hour of the day. For clarity purposes; the standard deviations of the measurements are not included, but they are on average 25%.*

Regression data:	**A-1:**	**I-4:**	**I-1:**	**I-3:**
Time of day:	Slope = 0.002, p = 0.002	Slope = 0.027, p = 2e-06	Slope = -0.007, p = 2e-04	Slope = 0.006, p = 1e-07
U_{10} (m s^{-1}):	p > 0.05	p > 0.05	p = 0.002, VIF = 1.10	p = 0.002, VIF = 1.60
Water temp (°C):	p = 0.001, VIF = 1.17	p > 4e-04, VIF = 1.10	p > 0.05	p > 0.05

TABLE 7: *Regression data for Figure 27. The table also shows other factors that potentially could explain the behavior of F_{CH4} as well as the results of the VIF analysis performed on those statistically significant factors together with time of day. VIF = 1 = No collinearity. VIF > 1 but < 5 = modest collinearity. VIF > 10 = high collinearity.*

Figure 27 visualizes the relationship between the F_{CH4} and time of day. For A-1, I-1, I-3 and I-4, a statistically reliable relationship was found ($p < 0.05$). For all these bays, except for I-1, the F_{CH4} increased towards the afternoon/evening. In Table 7, regression data for Figure 27 is shown. Further, the table shows the result of an analysis to see if other parameters, including wind speed and water temperature, could explain the behavior of F_{CH4}. When one of these parameters proved to have a significant influence on F_{CH4}, a VIF test was performed to see if there was multicollinearity between that parameter and time of day. For all four bays, the analysis showed that, even when an alternative parameter had a significant relationship with F_{CH4}, there was only a modest collinearity between that parameter and time of day. This indicates that the alternative parameter cannot explain the correlation between F_{CH4} and time of day.

3.4 BL and FC method comparison

This section will show the gas transfer velocity calculated, as well as compare the fluxes obtained from the BL and FC methods, respectively.

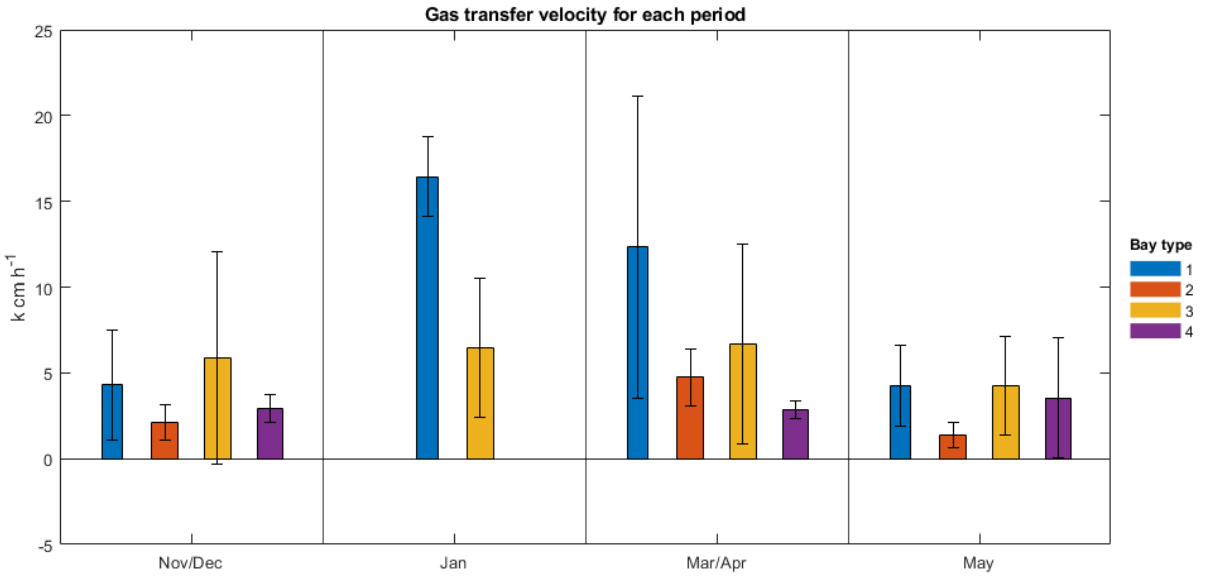

FIGURE 28: *Gas transfer velocity k, calculated from the chamber measurements, for each period and each type. The whiskers represent the standard deviation.*

Figure 28 shows the gas transfer velocities, k, calculated from the chamber measurements, divided into the different bay types. Bay type 1, I-6, had the highest calculated k of all types. Type 1 had a generally low k, while type 3 and 4 had large standard deviations indicating varying k values.

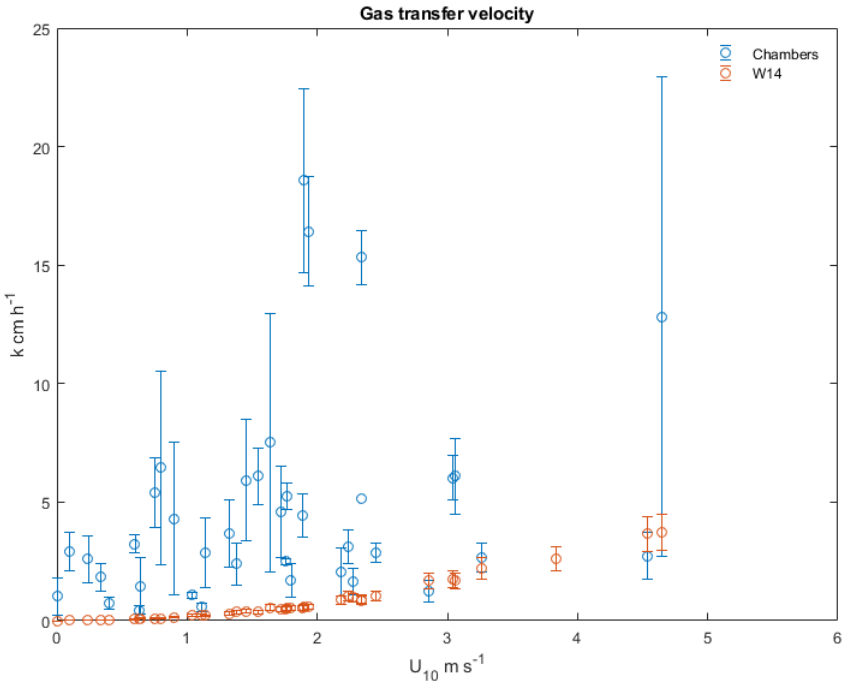

FIGURE 29: *Gas transfer velocity, k, plotted against U_{10}. The plot shows both chamber calculated k as well as k calculated based on W14. The whiskers represent the standard deviation for chamber derived k, and the 20% uncertainty connected to the W14 k.*

Figure 29 visualizes k derived from the chamber measurements, k_c, as well as W14, k_{w14}. k_c was up to a magnitude larger than k_{w14}. Only a few measurements gave k_c that were lower, or in the range of k_{w14}. Both k_c and k_{w14} did increase with U_{10}, but k_c showed more scatter for the same wind speeds.

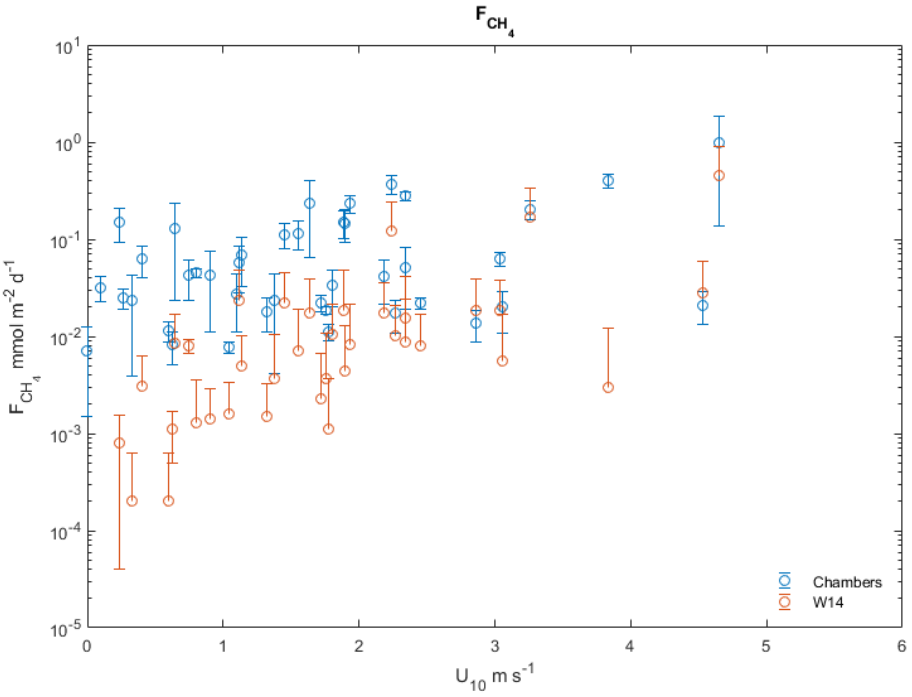

FIGURE 30: *F_{CH4} plotted against U_{10}. The plot shows both F_{CH4} from the FC as well as the BL method. The whiskers represent the standard deviations.*

Figure 30 plots F_{CH4} from the FC as well as the BL method against U_{10}. As with k, the general trend was higher FC F_{CH4} than BL F_{CH4}, for the same U_{10}. This pattern was more pronounced for lower U_{10}, for $U_{10} < 1$ m s^{-1} it was up to 2 magnitudes of difference, while $U_{10} > 2$ m s^{-1} showed better correlation between the F_{CH4} calculated from the two methods. There were less data points for higher winds, so the correlation might have been misleading since it was not showing the same range of distribution as for lower winds.

3.5 Possible CH_4 ebullition events

During a few of the measurements with the FC system, a sudden and large increase was seen in the CH_4 mole fractions that was deviating from the background increase and lasting for about a minute. This increase was repeated a few times. The increase was sometimes accompanied by an increase or decrease in CO_2 and H_2O, but not consistently. These events were interpreted as CH_4 ebullition, and occurred three times during the field measurement campaigns. Two of the events occurred at location I-1 (3rd of December and 22nd), and one at location I-5 (20th of Mars).

3rd of December, 2020

Figure 31, left, shows the first spotting of these events at location I-1. Location I-1 usually had a relatively low F_{CH4}, and therefore the background increase of CH_4 mole fractions in Fig. 31a (left) appears to be very small, or no increase at all. However, the very small increase during the unmarked times (Fig. 31a, left) is representing the interpreted diffusive F_{CH4}. The marked areas are the interpreted ebullition events. Table 8 shows the calculated CH_4 emissions from the ebullition. The first event at I-1 had the lowest release of CH_4, compared to the other dates. No reaction in CO_2 was seen during the events, but H_2O was a bit unstable.

22nd of Mars, 2021

Figure 31, middle, shows the second spotting of the interpreted ebullition events at location I-1. These events were 4 to 10 times larger than the ones in December. Unlike those in December, the H_2O mixing ratio showed the same general trend as CH_4. However, CO_2 was again relatively unaffected by the events. Unlike the first spotting of the event, the CH_4 mole fractions were decreasing after the initial increase, this decrease was included in the calculations of the emission rate and total release (Table 8), since it was interpreted as the system equilibrating. This goes for all events showing this decrease.

20th of May, 2021

Figure 31, right, shows the first and only spotting of the ebullition events in location I-5. In I-5, the events were in another scale than in I-1, the CH_4 mole fractions were, at one time, above 1000 ppm_m. Here, CO_2 and H_2O showed some correlating reactions as well, where both of their mole fractions were decreasing during the events. When the CH_4 mole fractions were increasing in such scale as they were here, the other gases would decrease when reported in mole fractions, since it is a relative unit.

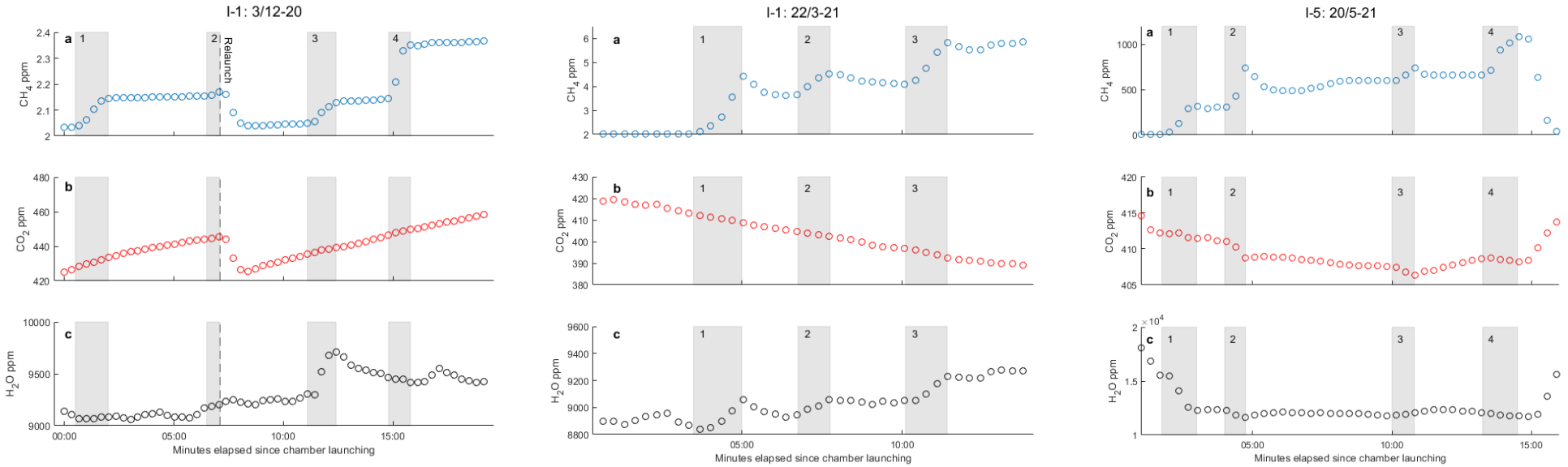

FIGURE 31: *Location I-1 the 3rd of December, 2020 and the 22nd of Mars, 2021 as well as I-5 the 20th of May, 2021. The plots show raw data from the LGR-1: The hollow circles are spaced with 20 seconds gaps, the frequency that the LGR-1 sampled at, blue: CH_4, red: CO_2 and black: H_2O. The black dotted line marks the time of a relaunch of the chamber at the 3rd of December. The shaded areas mark the interpreted ebullition events.*

Day:	**I-1 [3/12/20]:**			**I-1 [22/3/21]:**			**I-5 [20/5/21]:**			
Event:	**1**	**2**	**3**	**1**	**2**	**3**	**1**	**2**	**3**	**4**
Increase (ppm_m):	0.1	8.6e-02	0.2	1.6	0.6	1.7	285.7	191.7	73.7	-
Time (sec):	101	101	60	101	60	81	81	41	40	-
CH_4 emission (nmol s^{-1}):	3.2e-02	2.8e-02	0.1	0.5	0.3	0.3	113.2	147.7	58.4	-
CH_4 total released (nmol):	3.3	2.8	6.0	52.2	18.1	24.6	9169.2	6055.7	2336.0	-

TABLE 8: *Emission rate per ebullition event as well as total released CH_4 per event. Calculations used are the same as in section 2.4.1.*

3.6 Eddy covariance data

The following sections will show the results for the EC data.

3.6.1 Determining the flux contribution through the land surface

An analysis trying to determine the best way to exclude or separate F_{land} from F_{water} was performed on the data from August to October 2020, since this was a period with detectable F_{CH4} (above the noise level of 0.233 mmol m^{-2} d^{-1}) as well as varying owf. This section contains the results from that analysis, laying the ground for how the rest of the results from the EC data have been handled in regards to F_{land}.

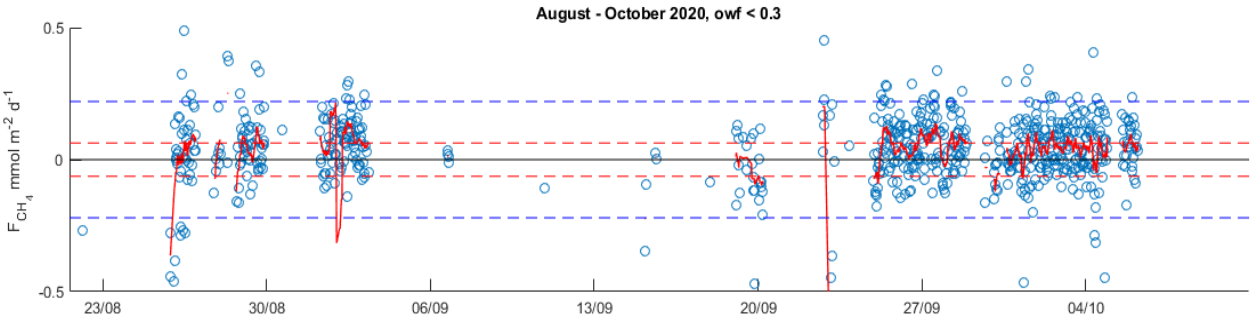

FIGURE 32: *F_{CH4} from August to October, 2020, meeting owf < 0.3. The blue circles are 30-minute flux periods, the blue dashed lines are the detection limit for one 30-minute flux period, the red full line is the 6RM and the dashed red lines are ±2SEM, of the 6RM, from zero.*

Figure 32 shows the data meeting owf < 0.3 from the period August to October, 2020. Owf < 0.3 indicates that over 70 % of the footprint of the measured F_{CH4} was over land. The 30-minute flux periods, meeting this criterion, were mainly within the detection limit of the system, but the 6RM was not centered on zero and was at multiple places reaching above, and below, the detection limit of the 6RM. The 30-minute flux periods with an owf < 0.3 had a mean of 0.025 ± 0.009_{2SEM} mmol m^{-2} d^{-1} and could, therefore, not be regarded as zero. F_{CH4} data with an owf of between 0.3 and 0.7 had a mean of 0.006 ± 0.007_{2SEM} mmol m^{-2} d^{-1} and data with and owf > 0.7 had a mean of 0.060 ± 0.003_{2SEM} mmol m^{-2} d^{-1}. There was no gradual increase of F_{CH4} with increasing owf which one might expect if $F_{CH4, land}$ was close to zero; rather the increase occurred at owf > 0.7.

a

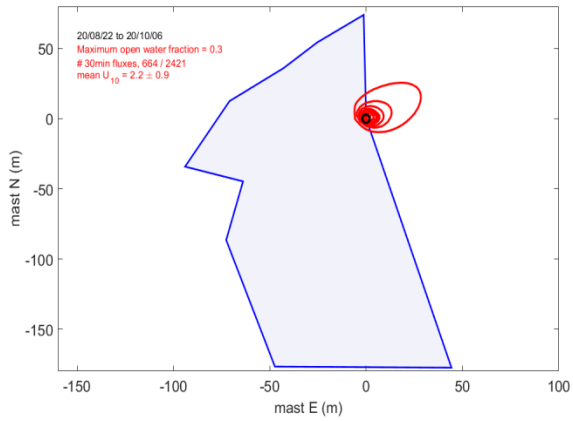

b

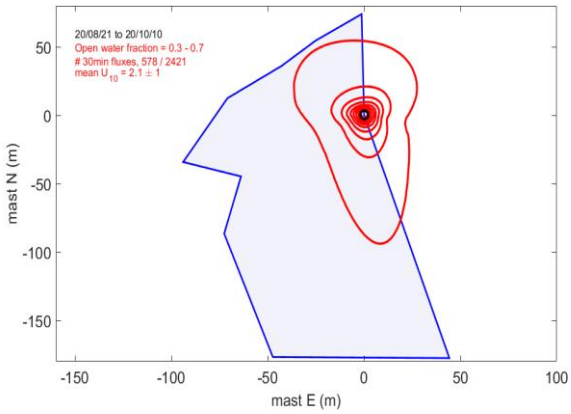

c

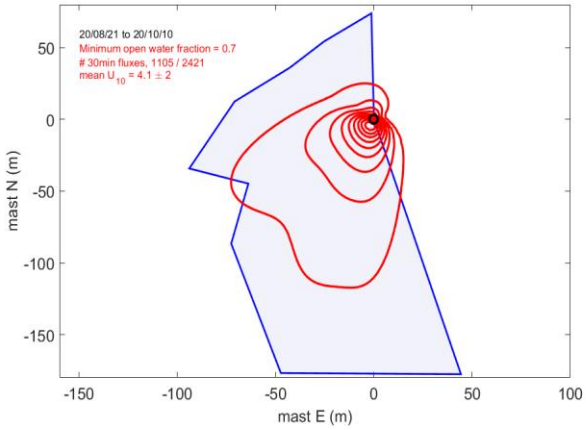

FIGURE 33: *Footprints for the three owf groups. Mean U_{10} is also displayed. A: owf < 0.3, b: 0.3 < owf < 0.7 and c: owf > 0.7.*

FIGURE 34: *The bay dimensions used in the footprint model for the EC data plotted above a satellite image of A-1 (Google Maps, 2021).*

Figure 33 shows the footprints for the different owf-groups, while Figure 34 shows the bay dimensions plotted on a satellite picture. The bay dimensions are a simplified version of the real dimensions in A-1 (Fig. 33). In the footprint for the owf < 0.3 as well as owf between 0.3 and 0.7, there is a part of the bay that was not included in the dimensions. It is therefore possible that the F_{CH4} from these wind directions were affected by the water in that part of the bay and in reality had a higher owf than the footprint analysis suggested. Due to the

uncertainties the footprint induced, the separation of F_{land} from F_{water} proved to be a difficult task. Determining F_{land} as either a constant or varying with a known variable did not seem possible since the lowest owf might in fact have represented a larger water fraction than the estimated owf indicated.

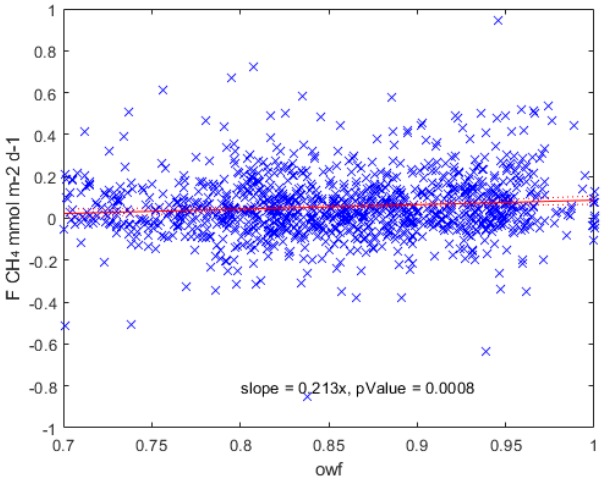

FIGURE 35: *F_{CH4} for owf > 0.7 plotted against owf. The blue crosses are 30-minute flux periods, the red full line is a least squares linear regression, the dotted red lines are the confidence bounds for that regression. Slope and belonging pValue are also displayed.*

F_{land} could not successfully be determined and quantified, but F_{CH4} for owf > 0.7 showed a significant positive relationship with owf ($p < 0.05$) (Fig. 35). If there was any F_{land} influencing the measured F_{CH4}, meeting the owf criterion set, it did not appear to be larger than F_{water}; in which case, the relationship would not have been positive.

Based on these results, the best way to handle F_{land} appeared to be by a simple scaling, where measured F_{CH4} was scaled by owf in an attempt for it to be representative of F_{water}. In the following sections for the EC results, the reported F_{CH4} has been handled this way. The owf limit was set to 0.7, this was determined by weighting the importance of including as much data as possible against the risk of including too large land fraction.

3.6.2 Meteorology and fluxes

The following section contains meteorological and EC F_{CH4} data from the periods when the EC tower was in operation. 3013 30-minute flux periods, that passed the quality control and owf-limit, are presented.

When the average F_{CH4} is given it was calculated from the 30-minute flux periods and the uncertainty is reported as the 2SEM. The other parameters are, if nothing else is stated, reported in the 30 min flux periods and when an average is given, the uncertainty is reported as the standard deviation.

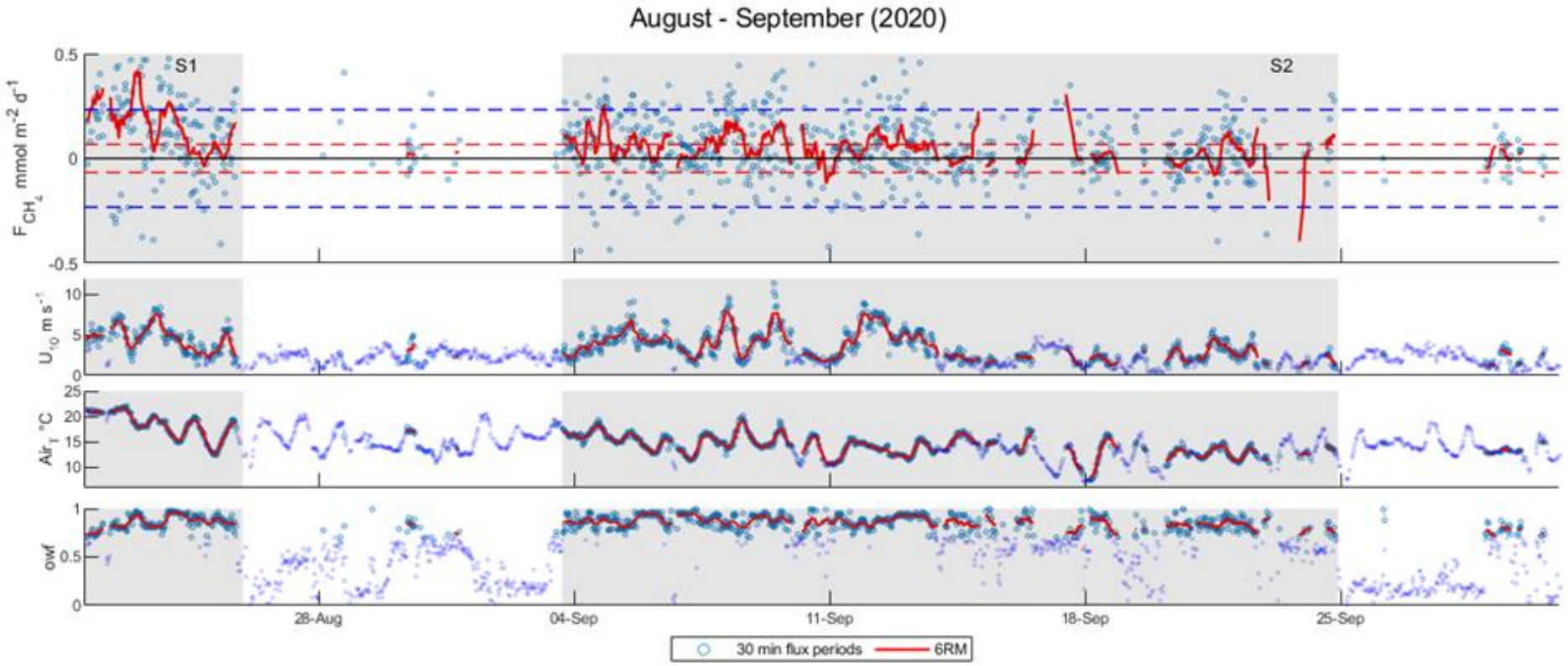

FIGURE 36: *Meteorological and EC F_{CH4} data from 21st of August to 30th of September 2020. The owf limit is 0.7, only F_{CH4} meeting this criteria is show. The U_{10}, air temperature, and owf is displayed so that only the data meeting the owf limit have a 6RM, represented by the red line. The blue markers are 30-minute flux periods. 30-minute flux periods with less than 6 hours gaps in between are connected with the 6RM, otherwise the 6RM is disconnected. In the F_{CH4} plot, the detection limit for the system for one 30-minute flux period is marked as a dashed blue line (±0.233 mmol m^{-2} d^{-1}) and the detection limit for the 6RM (2SEM) is marked as a red dashed line (±0.067 mmol m^{-2} d^{-1}). Sections are marked out for the purpose of making the result more clear.*

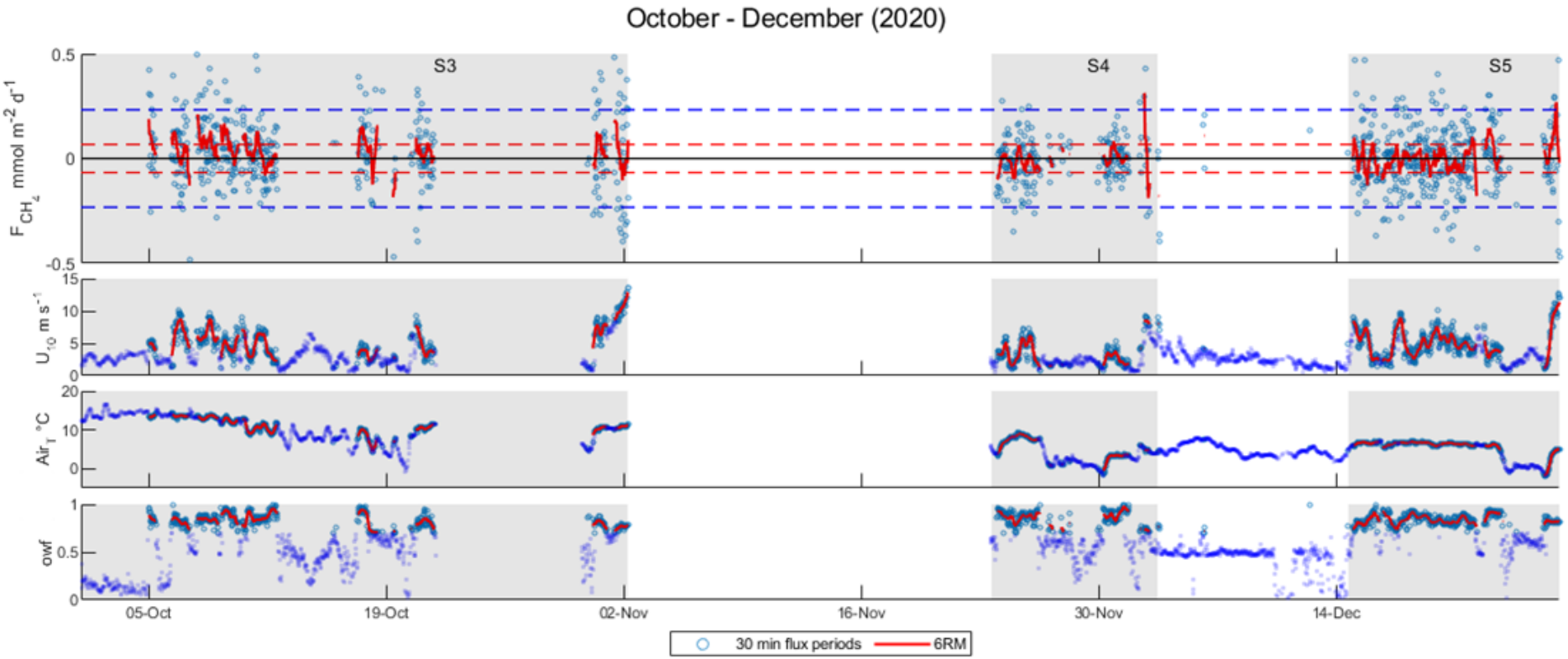

FIGURE 37: *Meteorological and EC F_{CH4} data from the 1^{zt} of October and the 27th of December, 2020. The figure is built up the same way as Figure 36.*

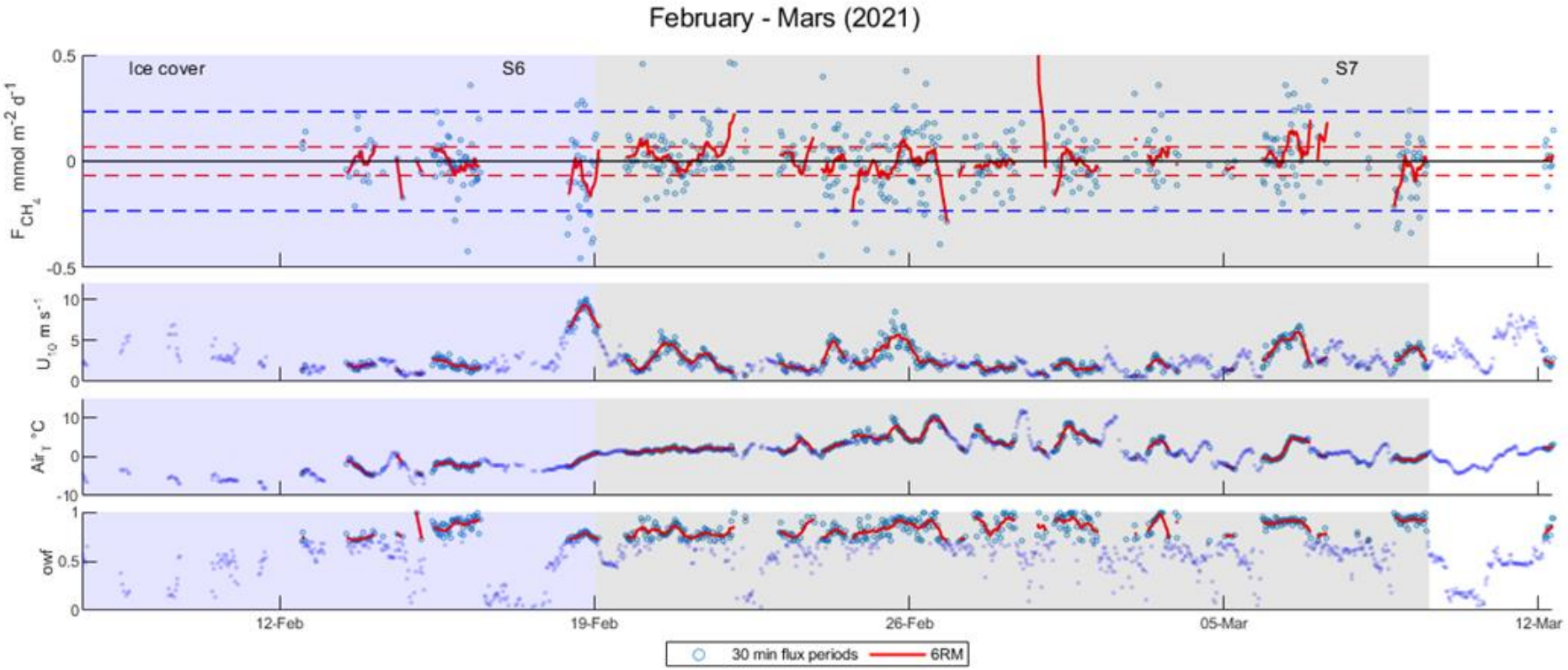

FIGURE 38: *Meteorological and EC F_{CH4} data from the 7th of February to the 12th of March, 2021. The figure is built up the same way as Figure 36, but with blue shading for ice-cover.*

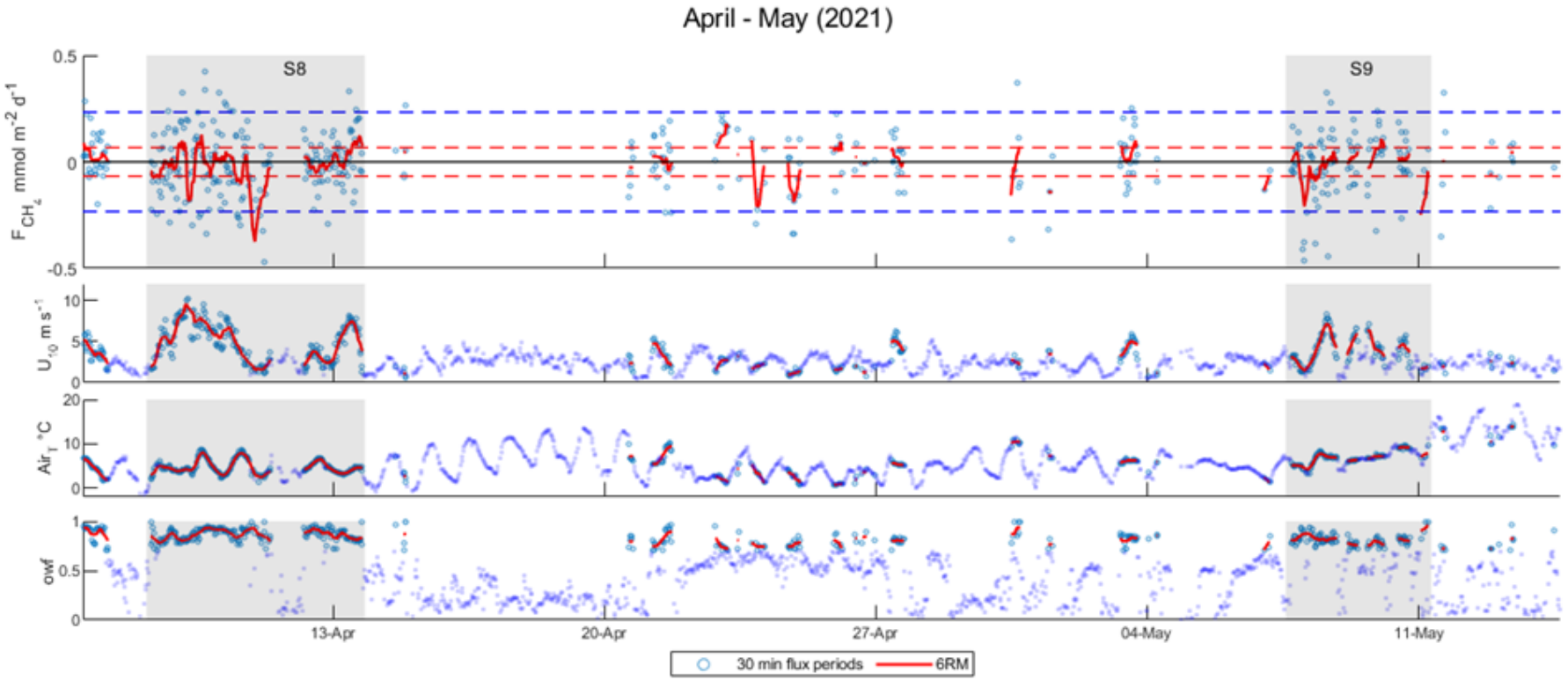

Figure 39: *Meteorological and EC F_{CH4} data from the 6th of April to the 14th of May, 2021. The figure is built up the same way as Figure 36.*

August – September, 2020

Figure 36 shows U_{10}, air temperature, and F_{CH4}, measured by the EC tower for the period: 21st of August to the 30th of September. S1, from the 21st to the 25th of August, as well as S2, from the 3rd to the 24th of September, were the two periods where the owf limit was met for a more continuous duration. For these two periods, the average U_{10} was 3.8 ± 1.8 m s^{-1} and average air temperature was 15 ± 2.6 °C. The F_{CH4} had three high peaks during S1, where the 6RM reached up to 0.403 mmol m^{-2} d^{-1} at the maximum. The average F_{CH4} was 0.137 ± 0.018_{2SEM} mmol m^{-2} d^{-1} for S1. In S2 the F_{CH4} was generally lower than S1, with an average F_{CH4} of 0.048 ± 0.010_{2SEM} mmol m^{-2} d^{-1}. Both S1 and S2 had F_{CH4} that could be said to differ from zero. The generally higher F_{CH4} during S1 correlated with a higher air temperature.

October – November – December, 2020

Figure 37 shows the data for the period between the 1st of October and the 27th of December. Unfortunately, the data set contained some gaps since either the owf limit was not met or the system did not record data. The periods that do contain some data have been marked as S3 (1st of October – 2nd of November), S4 (24th of November – 3rd of December) and S5 (15th to 27th of December). For these periods, U_{10} had an average value of 5.2 ± 2.5 m s^{-1}. Air temperature had an average of 8.1 ± 3.1 °C. In S3, the F_{CH4} was still detectable, and had a mean of 0.041 ± 0.011_{2SEM} mmol m^{-2} d^{-1}. However, in both S4 and S5 the F_{CH4} decrease to under the detection limit of the system. S4 and S5 had -0.008 ± 0.016_{2SEM} and 0.007 ± 0.011_{2SEM} mmol m^{-2} d^{-1} as their respective means, and could not be said to differ significantly from zero.

February – March, 2021

Figure 38 includes data from the 7th of February to the 12th of Mars. S6, from the 7th to the 19th of February, marks the period when the bay was ice-covered. S7, from the 19th of February to the 9th of March, contained some varying wind directions, but mainly above the owf limit. The believed date for ice break-up is the 19th of February, which coincided with a high wind event (10 m s^{-1}) and air temperature reaching above 0 °C. The 19th was represented by a negative F_{CH4} with the 6RM reaching down to -0.167 mmol m^{-2} d^{-1}. In S7, the average U_{10} was 2.9 ± 1.5 m s^{-1}, and average air temperature was 3.2 ± 2.6 °. Similar to S4 and S5, the F_{CH4} could not be said to differ significantly from zero with a mean of 0.009 ± 0.012_{2SEM}.

April – May, 2021

The period from the 6th of April to the 14th of May, shown in Figure 39, unfortunately had very unfavorable wind directions and the majority of the data did not meet the owf criterion. Two periods during this time contained data that was relatively continuous: S8, from the 8th to the 13th of April, and S9, from the 7th to the 11th of May. These two periods

corresponded to days with higher U_{10}, with 4.9 ± 2.4 m s^{-1} and 3.4 ± 1.4 m s^{-1} as averages. Air temperature had 5.5 ± 2.5 ° as mean over both periods. Similar to earlier periods, S8 and S9, contained F_{CH4} that did not reach above the detection limit, with averages of -0.009 ± 0.015_{2SEM} mmol m^{-2} d^{-1} and -0.014 ± 0.022_{2SEM} mmol m^{-2} d^{-1}.

3.6.3 Factors influencing F_{CH4}

Time of day

Two-sample t-tests/U-tests for determining differences between daytime and nighttime F_{CH4}:

Month:	Daytime F_{CH4} mean [mmol m^{-2} d^{-1}]:	Sample size (daytime):	Nighttime F_{CH4} mean [mmol m^{-2} d^{-1}]:	Sample size (nighttime):	*p*-value:
August	**0.098 ± 0.023**	**106**	**0.203 ± 0.025**	**87**	**0.001**
September	**0.048 ± 0.012**	**397**	**0.043 ± 0.013**	**333**	**0.660**
October	**0.064 ± 0.016**	**211**	**0.023 ± 0.016**	**201**	**0.014**
November	**0.023 ± 0.021**	**119**	-0.020 ± 0.020	119	0.230
December	-0.003 ± 0.015	253	**0.017 ± 0.015**	**259**	0.098
February	0.004 ± 0.020	135	0.013 ± 0.021	124	0.848
Mars	0.022 ± 0.025	89	0.001 ± 0.023	101	0.239
April	0.003 ± 0.017	182	-0.019 ± 0.019	149	0.421
May	-0.003 ± 0.023	94	0.013 ± 0.024	98	0.325

TABLE 9*: EC F_{CH4} for the different months divided into daytime mean F_{CH4} and nighttime mean F_{CH4}, the means have been tested, with a two sample t-test (when the distribution proved to be parametric) and with a Wilcoxon-Mann-Whitney U-test (for non-parametric months), to see if there was a significant difference between them. P-Values for the tests are shown, where significant difference was found, the p-value is underlined. Uncertainties in the F_{CH4} averages are displayed as 2SEM. For reference: A whole month (30.5 days) would contain a total of 1464 (732 day/night) 30 min flux periods if they all met the owf limit and quality criteria. The averages that could be said to significantly differ from zero are in bold.*

August and November showed significant differences ($p < 0.05$) between daytime F_{CH4} and nighttime F_{CH4} (Table 9). The data available for August (21^{st} – 31^{st}) had two times larger F_{CH4} during nighttime than during daytime. October had larger F_{CH4} during daytime.

U_{10}

Looking at Table 9, EC F_{CH4} data showed a significant relationship ($p < 0.05$) with U_{10} for August (nighttime) (Fig. 40a2), September (Fig. 40b), October (daytime) (Fig. 4o0c1).. The relationship was the strongest for August (nighttime) and September with $p < 0.01$. The slopes were not consistent throughout the months.

There were relationships between U_{10} and April (Fig. 40h), and May (Fig. 40i). However, as these months did not have F_{CH4} above the detection limit the chance of a random correlation becomes very high.

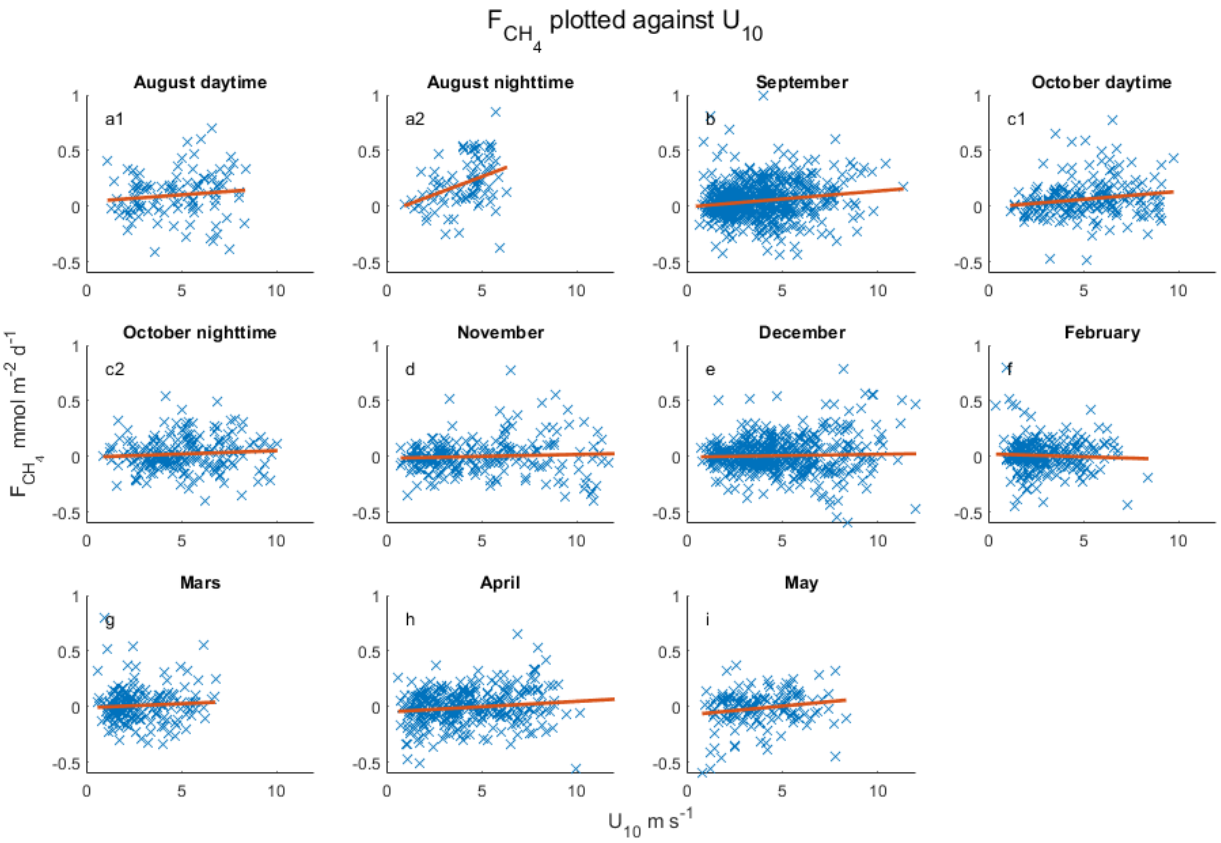

FIGURE 40*: EC F_{CH4} data plotted against U_{10} for all months. The months where F_{CH4} showed differences between daytime and nighttime have been divided into two plots. The blue markers are 30 min flux periods. The red lines represent a least squares regression (regression data shown in Table 8).*

Month:	Slope:	*p*-Value:	R^2:
August (daytime):	**0.008**	**0.409**	**0.01**
August (nighttime):	**0.064**	**0.0003**	**0.14**
September:	**0.016**	**0.00002**	**0.02**
October (daytime):	**0.014**	**0.012**	**0.03**
October (nighttime):	**0.001**	**0.252**	**0.01**
November:	0.003	0.297	<0.01
December:	0.003	0.394	<0.01
February:	-0.004	0.605	<0.01
Mars:	0.008	0.389	<0.01
April:	0.011	0.015	0.02
May:	0.019	0.049	0.03

TABLE 9: *Regression data for Figure 40. Where a significant relationship was found; the p-value is underlined. The months that were found to have an average F_{CH4} above the detection limit for both day- and nighttime are in bold.*

Air temperature

Of the months that could be considered to contain detectable F_{CH4}, the F_{CH4} data showed a linear relationship ($p < 0.05$, see Table 10) with air temperature in August (nighttime) (Fig. 41a2) and September (Fig. 41b). Similar to U_{10}, the slopes were not consistent between the months that showed a relationship with temperature.

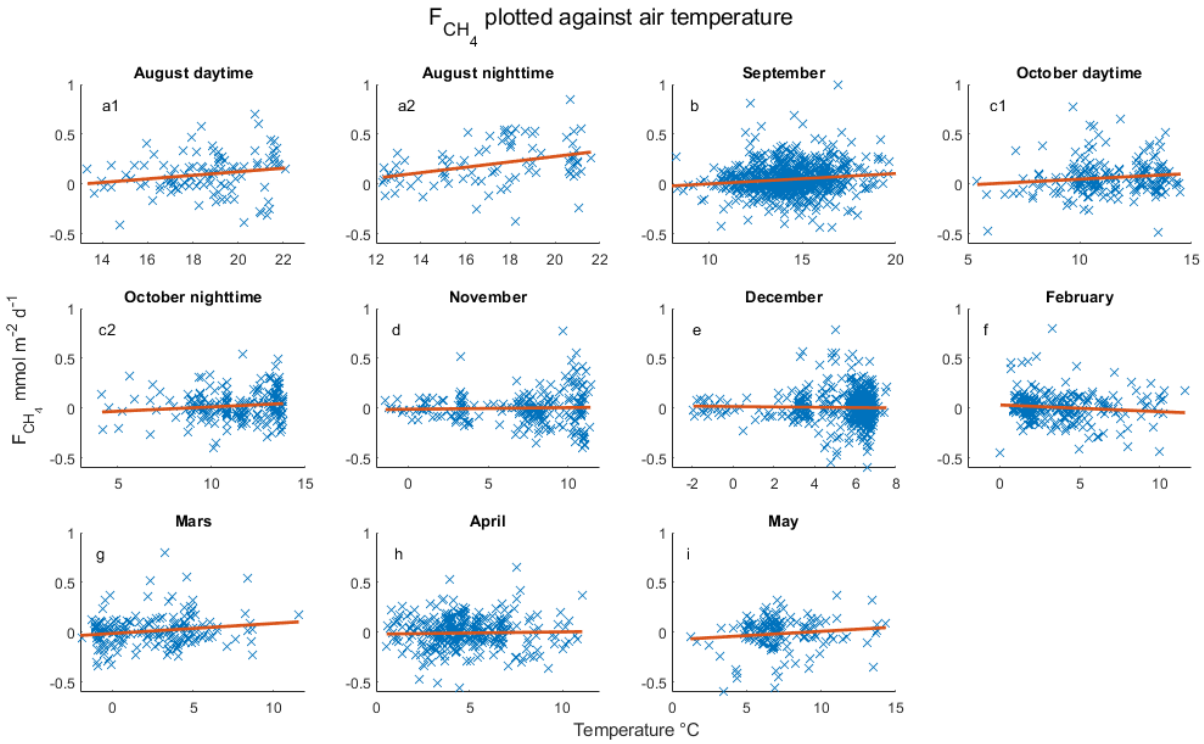

FIGURE 41*: EC F_{CH4} plotted against air temperature for all months. The months where F_{CH4} showed differences between daytime and nighttime have been divided into two plots. The blue markers are 30 min flux periods. The red lines represent a least squares regression (regression data shown in Table 9).*

Month:	Slope:	*p*-Value:	R^2:
August (daytime):	**0.018**	**0.055**	**0.03**
August (nighttime):	**0.027**	**0.0006**	**0.13**
September:	**0.010**	**0.0004**	**0.02**
October (daytime):	**0.012**	**0.053**	**0.02**
October (nighttime):	**0.009**	**0.068**	**0.02**
November:	0.002	0.594	<0.01
December:	-0.002	0.648	<0.01
February:	-0.007	0.087	0.01
Mars:	0.010	0.022	0.03
April:	0.002	0.621	<0.01
May:	0.008	0.131	0.02

TABLE 10: *Regression data for Figure 41. Where a significant relationship was found; the p-value is underlined. The months that were found to have an average F_{CH4} above the detection limit for both day- and nighttime are in bold.*

A multiple linear regression was performed on the months where two predictors were found. A multiple regression analysis showed a better fit for the august nighttime data when both temperature and U_{10} were used as predictors, than when they were analyzed separately, the model gave a *p*-value of 7.1e-05 and a R^2 of 0.2. The same was true for September that, when analyzed for both temperature and U_{10}, generated a *p*-value of 1.5e-06 and a R^2 0f 0.04.

Checking for dependence of F_{CH4} on owf

Month:	Slope:	*p*-Value:	R^2:
August (daytime):	**-0.368**	**0.246**	**0.01**
August (nighttime):	**0.410**	**0.140**	**0.02**
September:	**0.140**	**0.080**	**<0.01**
October (daytime):	**0.282**	**0.075**	**0.02**
October (nighttime):	**0.067**	**0.678**	**<0.01**
November:	-0.348	0.122	0.02
December:	0.008	0.943	<0.01
February:	0.256	0.020	0.02
Mars:	0.062	0.673	<0.01
April:	-0.129	0.305	<0.01
May:	0.087	0.676	<0.01

TABLE 11: *Regression data for least squares linear regression for F_{CH4}' dependence on owf. Where a significant relationship was found, the p-value is underlined. The months that were found to have an average F_{CH4} above the detection limit for both day- and nighttime are in bold.*

The EC F_{CH4} data was checked against owf (Table 11) to see if any affect from the scaling could be interpreted. Only in February was a significant relationship found, $p = 0.02$.

3.7 Comparison of EC, FC and bulk model F_{CH4} for A-1

Period:	Date:	FC:	EC:	BL:	U_{10}	Temperature
September:	15-16 Sep	0.029 ± 0.011/0.009	0.027 ± 0.125/0.026	NaN	< 1	16.5 ± 1
Nov/Dec:	25-27 Nov (25-26 Nov)	0.014 ± 0.009/0.004 *0.015 ± 0.010/0.005*	-0.008 ± 0.093/0.017	0.015 ± 0.019/0.013	2.5 ± 2	6.7 ± 2.5
Mar/Apr:	30-31 Mar (1-7 Apr)	0.017 ± 0.009/0.004	0.009 ± 0.141/0.020	0.003 ± 0.003/0.001	2 ± 0.8	10.8 ± 3
May:	11-12 May (7-10 May)	0.016 ± 0.006/0.003	-0.012 ± 0.126/0.023	0.003 ± 0.003/0.001	2.5 ± 0.6	15.2 ± 1.3

TABLE 12*: FC, EC and BL model F_{CH4} for the four periods that the FC measurements were carried out in A-1. Dates, U_{10} and temperature are also shown. F_{CH4} is reported in mmol m^{-2} d^{-1} with* ± standard deviation/2SEM. U_{10} is reported in m s^{-1} and temperature in °C. For Nov/Dec, EC and bulk F_{CH4} was only available for the 25th to the 26th of November, a second FC F_{CH4} is therefore reported for only those two days. For Mar/Apr, the F_{CH4} from the EC did not pass the quality control so EC F_{CH4} from the 1st to the 7th of April was used instead. For May, the owf criterion was not met for the EC F_{CH4} so the 7th to the 10th of May was used instead. For the EC data taken from other dates, only F_{CH4} corresponding to similar U_{10} and temperature was used.

Table 12 shows the comparison of FC, EC and BL F_{CH4} for A-1. The different methods were coinciding quite well in magnitude. September only had FC and EC data, both the methods were measuring very similar F_{CH4}, only a difference of 0.002 mmol m^{-2} d^{-1} was found between the means. For Nov - Dec the FC and BL methods were again measuring very similar F_{CH4}, while the EC method reported slightly smaller F_{CH4}. For Mar – Apr and May, there were no EC data for the days that the FC and BL measurements were carried out, which may have caused an offset in the F_{CH4} between the methods. FC data, for these periods, measured the highest F_{CH4} (as for all periods), the EC and bulk BL cannot be said to differ significantly from zero.

4. DISCUSSION

4.1 Are the classification to any help in predicting the F_{CH4}?

Availability of organic carbon, its quantity and quality, is one of the dominant factors controlling the rate of methanogenesis, and hence the sediment to water flux (Schmiedeskamp *et al.,* 2021; Megonigal *et al.,* 2014). The classification of the bays was therefore performed based on how densely they were vegetated, as well as the character of the sediment. There are uncertainties in this way of classifying; the sediment has not been analyzed for total organic C-content, which leads to a lack of knowledge in how much carbon is actually available for methanogenesis (Schmiedeskamp *et al.,* 2021). However, there are perks with this type of classification when it comes to, for example, upscaling. It is not defendable to classify the bays based on sediment organic content, since it would defeat the purpose of time efficiency in an upscaling model; if you have to collect sediment samples you might as well measure the actual flux.

The statistical analysis preformed in this study showed that the classification, at least for the winter season, was a week predictor for the F_{CH4}; where greater deviance was found within the types than between them. The hypothesis that denser vegetation in a bay would create higher F_{CH4} was supported by most of the bays. However, A-1 and I-5 showed patterns that were not in agreement with this hypothesis. A-1, that was relatively densely vegetated, showed much lower F_{CH4} than the other two bays categorized as the same type (I-2 and I-4). This was especially true in May, when I-2 and I-4 had almost one magnitude higher F_{CH4} than A-1. The pattern of F_{CH4} was mirrored in the CH_4 surface water concentrations. Lundevall-Zara *et al.* (2021) categorized parts of A-1 as their 'habitat A', which was the habitat with the highest F_{CH4}, with all categories located on Askö. The diffusive F_{CH4} they reported were in the order of 0.5 – 1.5 mmol m^{-2} d^{-1} in July – September, and below 0.1 mmol m^{-2} d^{-1} in October. This study's FC F_{CH4} was constantly below 0.1 mmol m^{-2} d^{-1}, including September, and the EC tower measured the highest F_{CH4} in August, reaching up to 0.5 mmol m^{-2} d^{-1}. The generally lower F_{CH4} in this study is most likely a result of chamber placement and footprint of the EC tower. Lundevall-Zara *et al.* (2021) placed their chambers in the reed beds, while this study has FC measurements from the whole bay and EC measurements from only the more open fraction of A-1. Further, the different seasons have most likely influenced the offset in the results between the studies as well. The low F_{CH4} in A-1 is supported in both methods used here, and it is within a reasonable range when compared to F_{CH4} reported by Lundevall-Zara *et al.* (2021). It has been suggested that the coastal regions elevated CH_4 concentrations are in part due to riverine and terrestrial inputs of organic matter, pollutants and excess nutrients (Borges and Abril, 2011; Walsh *et al.,* 2005). As a relatively small island with few residences, the shallow bights around Askö might not be as exposed to this as the more inner parts of the archipelago. The lower F_{CH4} in A-1 could therefore be a consequence of a lower degree of eutrophication, as less carbon would be produced, in combination with more oxygen in the water column for the oxidation of methane (Megonigal *et al.,* 2014; Borges & Abril, 2011; Chanton & Dacey, 1991). Increased F_{CH4} due to eutrophication has been observed in both lakes (Zhang *et al.,* 2021; Beaulieu *et al.,* 2019; DelSontro *et al.,* 2018) and coastal environments (Wallenius *et al.,* 2021).

The other bay that deviated from the hypothesis was I-5, a wind exposed sand beach with some seaweed growing in it. I-5 proved to have very high F_{CH4} during all sampling periods. Since the CH_4 concentrations correlated with the F_{CH4} and were high as well, the elevated F_{CH4} could not solely be explained by wind induced turbulence, and accompanying increase in gas transfer velocity. Either the CH_4 had been produced *in situ* or the concentrations originated from another source and had only been transported to I-5. Transport could be in the form of riverine runoff (Bussmann, 2013), horizontal transport (Martens & Klump, 1980) or submarine groundwater discharge (SGD) (Bugna *et al.,* 1996). One aspect supporting an allochthounus source is a narrow stream draining into the bay that during heavy rainfall transported a lot of runoff into the catchment. On the other hand, an allochthonous source of the dissolved CH_4 would not explain the magnitude of the interpreted ebullition events, since CH_4 ebullition is the result of the total partial pressure of all gases, in the pore water, reaching above the hydrostatic and atmospheric pressures and forming gas bubbles (Chanton & Dacey, 1991). The magnitude of the ebullition events would therefore have required high CH_4 production in the sediment. The freshwater runoff into the bay, even if not a source of already produced CH_4, could bring organic matter to be degraded and stimulate the methanogenesis in the sediment (Grinham *et al.,* 2017). The elevated methanogenesis could then generate the high CH_4 concentrations in comparison to other bays with similar autochthonous vegetation content like I-1. However, the decomposition of allochthonous carbon has been shown to be more difficult than autochthonous carbon (Grasset *et al.,* 2018), which would make it unlikely that allochthonous carbon could explain the elevated CH_4 concentrations in I-5. It might be that I-5 was actually more productive than the vegetation density indicated during the winter season. It has been suggested that wastewater, or wastewater treatment discharge can elevate CH_4 concentrations in marine environments (Castro-Morales *et al.,* 2014; Liu *et al.,* 2014). There is a wastewater treatment plant on Ingarö (Blaab, 2021), but it is not adjacent to I-5. However, the bay is quite densely surrounded by residences and they could potentially have individual sewage disposal system. Regardless if there was wastewater discharge into the bay, the dense residences could be a source of other contaminants to the water, stimulating primary production and eutrophication (Wang *et al.,* 2021).

Apart from the two bays that deviated from the hypothesized outcome, it was also difficult to distinguish between the other bays in order to analyze the effect from the classification. On occasions, the bays had F_{CH4} whose variance was in the same range within the bay as between them. In the multiple comparison analysis, the Bonferroni correction decreases the chance of a type I error occurring, that is: a significant difference is found by chance, but in doing so it also stimulates a drop in power of the factors analyzed, risking the opposite where it oversees a true effect (Francis & Thunell, 2021). The statistical test therefore needs to be interpreted with caution. A larger sample size might indicate a better correlation between the classification and the bays.

Our results do underline the complexity of the factors controlling the production and consumption of CH_4 in inshore marine waters (Rosentreter *et al.,* 2021), which is highlighting the importance of continuing to collect these types of data for deeper understanding of the spatial variation of dissolved CH_4 in coastal regions (Gutiérrez-Loza *et al.,* 2019). The majority of the bays did show F_{CH4} values that agreed relatively well with the hypothesis behind the classification, especially in May when the denser vegetated bays showed a quite large

increase in F_{CH4}. The increase in May indicates that the classification might be of better use during the more productive months of the year when F_{CH4} increase overall (Yasui *et al.,* 2016). With the results from the winter season, the range of F_{CH4} cannot be predicted solely based on autochthonous vegetation and sediment type. Based on the lower F_{CH4} measured on Askö and the surprisingly high F_{CH4} measured in I-5, it might be effective to include a predictor in the classification that describes the anthropogenic influence on the bay.

4.2 U_{10} and temperature as predictors for an inshore environment

The majority of the BL models used to quantify CH_4 emissions are dependent on U_{10} as their sole factor affecting turbulence (Wanninkhof, 2014, 1992; Ho *et al.,* 2011, 2006; Nightingale *et al.,* 2000; Wanninkhof & McGillis, 1999; Liss & Merlivat, 1986; Liss & Slater, 1974). However, the models were developed for the open ocean, and limited fetch have proven to weaken the relationship between gas transfer and wind velocity. Prytherch & Yelland (2021) found that gas transfer had a relationship with lead dimensions, in their study on gas transfer velocity in Arctic sea-ice leads. They discussed the result as a consequence of decreasing fetch with decreasing size of the lead. Our results do support the fetch dependence of the relationship between U_{10} and F_{CH4}, where the most exposed bays had the strongest dependence on U_{10}, and onshore winds affected the F_{CH4} the most. For the more sheltered bays, the relationship between F_{CH4} and U_{10} was not as clear, and when a relationship was found, U_{10} did not have as much of an effect on F_{CH4} as it did for the more exposed bays.

Our FC F_{CH4} data did not show a dependence on U_{10} in A-1 (Openness 2), contradicting the EC F_{CH4} data, that for the majority of the months, containing detectable F_{CH4}, showed a relationship with U_{10}. The disagreeing results could be an effect from the variance of the measurement location of the chamber, while the EC footprint was more or less constant in a specific part of the bay. Large spatial variation in F_{CH4} has been found in lakes, where heterogeneous SOC in the underlying sediment influenced the local CH_4 concentrations (Schmiedeskamp *et al.,* 2021; Grinham *et al*, 2017). Our measured F_{CH4} showed some variance in the spatial distribution in A-1, however, not statistically reliable differences. The relationship with U_{10} for the EC F_{CH4} data ranged from a 0.014 to 0.064 increase in mmol m^{-2} d^{-1} per m s^{-1} increase in wind speed, in the measurement periods of August, September and October. Potentially, the dependence on U_{10} was too weak to become statistically significant, when the influence from spatial variance was present in the FC measurements. Another explanation for why a week relationship with U_{10} could be missed by the FC method is the interference of the chamber with the boundary layer. The chamber could artificially enhance the gas transfer during launching, or when anchored, while the water is moving (Mannich *et al.,* 2019). The launching could induce higher gas transfer velocity at low wind speeds, weakening the relationship between F_{CH4} and U_{10}. The test performed in this study, to see the influence from anchored versus not anchored, was carried out in low wind speeds (1.3 m s^{-1}). It was performed to see if sediment resuspension, when the anchor hit the bottom, would affect the F_{CH4} by releasing CH_4 (Bussmann, 2005), which it did not. However, at such low wind speeds it is possible that the effect discussed by Mannich *et al*. (2019), when the water is moving and the chamber is static, was not detected. This effect would,

however, increase the dependence on U_{10}, rather than decrease it, and could not explain the weak relationship. Another factor that will influence the relationship between F_{CH4} and U_{10} is the dissolved CH_4 concentrations (Jähne *et al*., 1987). It is possible that the difference in concentrations between the sampling periods induced differences in F_{CH4} that do not allow the linear regression to find a true relationship between U_{10} and F_{CH4}. However, the concentration differences in A-1 were relatively small. The stronger correlation between U_{10} and F_{CH4} for the more exposed bays does still, independent on the factors which might affect the relationship, support a higher dependence on U_{10} with larger fetch.

Temperature has been found to be one of the most important factors controlling methanogenesis (Yvon-Durocher *et al.,* 2014; Heyer and Berger, 2000). However, the results of this study did not show any correlation between F_{CH4} and temperature when analyzed over all bays. A-1 and I-4 showed a correlation between F_{CH4} and water temperature when analyzed separately. Many non-quantifiable factors can play a role in the generally low correlation between F_{CH4} and temperature; like the difference between water surface temperature and sediment temperature, and presence or absence of other electron acceptors, as well as oxidants in the water column (Barker Jørgensen & Kasten, 2006). Since we have not analyzed these properties they cannot be quantified, which makes it difficult to say if the vague, only occasionally existing, relationship between F_{CH4} and temperature can be explained by them. However, the effect of temperature on F_{CH4}, rather than CH_4 production itself, is a complex question. Temperature does not only increase methanogenesis, but it also increase the oxidation rates (King & Adamsen, 1992), having a reducing effect on the water surface CH_4 concentrations. Further, the temperature fluctuations on the depth of methanogenesis are usually not in the same range as water surface temperature fluctuations, and it has been shown that if organic carbon is limited, the temperature effect is lowered (Van der Nat & Middleburg, 2000; Kelley *et al.,* 1995). Even if temperature is a factor increasing gas transfer velocity, independent of the concentration gradient (Wanninkhof, 1992), it is not seen in the gas transfers calculated for A-1 and I-4, where March had a higher gas transfer than May.

It can be questioned if A-1 and I-4 showed a true relationship with water surface temperature or if it was an effect from seasonality. Van der Nat & Middleburg (2000) found that plant physiology in a tidal marsh had a higher effect on the F_{CH4} than temperature or oxidants, and that seasonality played a role through the vegetation, as well as its density, rather than through the temperature. The environments in our bays are not comparable to the amount of vegetation in a marshland, except perhaps for I-6, but the presence of reeds are common in many of the bays and vague evidence for the theory could be found in our results as well. May did have significantly higher F_{CH4} than Nov – Dec, while temperature did not have a significant effect on F_{CH4} in that scale. This suggests that seasonality played a role in F_{CH4}, independent of water temperature, and that the availability of labile organic carbon due to increased production was the underlying driver (Yasui *et al.,* 2016). Even if no direct plant-mediated F_{CH4} can be proved to be contributing, an overall increase in burial of labile organic carbon in the later spring would enhance methanogenesis and indirect F_{CH4} (Lundevall-Zara *et al.,* 2021; Schmiedeskamp *et al.,* 2021; Grinham *et al*, 2017).

4.3 Spatial and temporal variation in the bays

Depth and distance to shore has been suggested to affect the F_{CH4} in lakes (Zhang *et al.,* 2021; Schmeideskamp *et al.,* 2021), as well as coastal waters (Zhou *et al.,* 2009). However, the statistical analysis did not show any reliable variations in F_{CH4}, based on depth or distance to shore, in this study. One exception was present, I-4 showed a difference, where the deepest measurements were found to be higher than those measured at 50 cm depth, closest to shore. The difference found was most likely caused by the rock outcrop that reached into the water where the measurements for the shallower depths were carried out, while the measurements for the deeper parts were done above more muddy sediment, in close proximity to the reed beds. Similar results were found in A-1, where the shallowest measurements, done close to a rockier shoreline, had lower values, while measurements done on the same depths, but in approximation to reed-covered shorelines, reached higher F_{CH4}. However, the statistical analysis did not differentiate between these two groups in A-1, indicating that the high F_{CH4} measured close to reed beds were not consistent and that the distribution could not be distinguished from the measurements done close to rocky shorelines. Lundevall-Zara *et al*. (2021) found that habitats with dense reed beds and algal mats represented the highest F_{CH4} during the summer months and assigned it to possible contributions from plant-mediated F_{CH4}. Van der Nat & Middleburg (2000) also emphasized the importance of plant-mediated F_{CH4}, but discussed seasonality as an important factor enhancing the plant-mediated F_{CH4} during summer. As this study was carried out during the winter months, the effect from plant-mediated F_{CH4} might not appear as strong as it did in the two earlier mentioned studies. The month that could perhaps have shown a stronger deviation between the different habitats in the bays was May, and perhaps a more extensive sampling campaign would have had to be carried out solely in May to see a statistically reliable difference.

Gülzow *et al.* (2013) discussed ice break-up in spring as a potential time for high CH_4 emissions due to the accumulated, under the ice, CH_4 being released. F_{CH4} in I-2 did show significantly higher values for the day when the bay was partly ice-covered, which agrees with Gülzow *et al.* (2013), and the effect seen in the depth and distance to shore plot is most likely an effect of the ice break-up. However, the effect of ice break-up was not as visible in the EC data, where only a slightly negative peak was seen.

Overall, the depth or distance to shore did not have large enough of an effect on the F_{CH4}, measured in this study, to be considered statistically significant. Considering that the majority of the measurements in the bays were carried out in the littoral zone, if using the definition of the littoral zone as the nearshore habitats to where photosynthetically active radiation penetrates (Peters & Lodge*,* 2009), the homogeneity of the F_{CH4} is perhaps not surprising. Neither the larger oxidation potential of deeper waters (Reeburgh, 2007) did appear to influence F_{CH4} to the extent that it showed in the results. The results suggests that the enhancement of the F_{CH4} in coastal waters, as opposed to the open ocean (Bange *et al.,* 1994), extends further out and to deeper waters than the range of this study's sampling areas.

Time of day showed an effect on F_{CH4} in A-1, I-1, I-3 and I-4. A-1, I-3 and I-4 all showed an increase from morning to afternoon, while I-1 showed the opposite. Diurnal variations in

F_{CH4} have been reported for lakes (Erkilää *et al.,* 2018; Podgrajsek *et al.,* 2014; Bastviken *et al.,* 2010), as well as for coastal environments (Heyer & Berger, 2000). Both temperature (Heyer & Berger, 2000) and wind speed (Bastviken *et al.,* 2010) patterns have been proposed to explain these variations. However, while some of the bays showed correlations between F_{CH4} and temperature (or seasonality as discussed above) or U_{10}, these factors only showed a modest collinearity (VIF < 5) with time of day, suggesting that they cannot explain the relationship. Solar radiation has been brought forward as an explanation for higher CH_4 emissions during daytime, since it reduces oxidation in the water column (Mitchell *et al.,* 2005), which could explain the increase during the day in A-1, I-3 and I-4. However, it would not explain why the highest F_{CH4} was measured later in the evening (8 pm) in I-3. Why I-1 would decrease over the day cannot be explained by solar radiation either, nor can the non-existent relationship between the F_{CH4} in I-2, I-5 and I-6, and time of day. Temperature driven convection (Podgrajsek *et al.,* 2014) and upwelling from deeper layers (Erkilää *et al.,* 2018) have also been used in an attempt to explain the diurnal variations in lakes. Both of them are possible to imagine here as well, but the inconsistency in the results makes it difficult to find evidence for them, like with solar radiation.

The EC F_{CH4} data also showed indications that there could be correlations between F_{CH4} and time of day. The measurement period in August showed higher F_{CH4} during nighttime, this could not be explained by temperature or wind, since both these predictors were slightly higher during daytime. However, in October, higher F_{CH4} were found during the day, with the same independence from U_{10} and temperature. Again, the inconsistency hinders a conclusion of the causes behind the pattern. Further, the patterns found with the chambers can be questioned on the basis that the measurements were not performed continuously. They expand over 9 months and are carried out for 2-3 hours each sampling day, twice every period. It is not impossible to consider a coincidental relationship with time of day, when actually other factors influenced the F_{CH4}. However, the occasional correlation between F_{CH4} and time of day implies that timing of the sampling should be taken into account when planning field work for these types of studies, especially when using short time-intervals with the chambers.

4.4 The EC system's functionality in A-1

Unfortunately, the EC system in A-1 had a rather high, noise induced detection limit, when put in relation to the F_{CH4} that were measured at the location. Considering that the highest measured F_{CH4}, with the FC method, was 0.053 ± 0.029 mmol m^{-2} d^{-1} in A-1, a detection limit of just over ± 0.2 mmol m^{-2} d^{-1} makes it difficult to analyze the data, produced by the EC tower, at a high temporal resolution. Uncertainty in EC measurements are usually due to variability in the ambient mixing ratios or noise produced by the instruments (Blomquist, 2012, 2010). No analysis to determine the origin of the noise has been done in this study so the reason for the high detection limit is uncertain. Thornton *et al*. (2020) reported noise levels of ± 0.062 mmol m^{-2} d^{-1} (1σ) on their shipborne eddy covariance system. Yang *et al*. (2016) reported an even lower noise level of 0.020 mmol m^{-2} d^{-1}, for their system located in an inshore environment. The noise level for our system was 10 times larger than Yang *et al*.

(2016) and doubles that of Thornton *et al*. (2020). Either the instruments, like the LGR-2, had a large uncertainty or the very heterogeneous surroundings in A-1 induced large variations in the mixing ratios. Considering that the corresponding LGR-1, used for the FC measurements, did not show the same noise level; the LGR-2 should not be the source of the noise, if the instrument is well-maintained. However, it cannot be said with certainty that the LGR-2, other parts of the system or the data processing caused the noise. Therefore, it is possible to consider that there is a large variability in the ambient mixing ratios causing the high noise level. Yang *et al.* (2019, 2016) used 10 min flux periods, instead of 30 min flux periods, in an attempt to reduce the noise cause by a heterogeneous environment. This was argued as a way to decrease the influence from, for example, horizontal mixing on the F_{CH4} calculated sea-air flux. In the future, this could be worth trying on the data from A-1.

Additional uncertainties come from the land and water contributions. In this study, no successful separation of the land fraction from the water fraction was possible, like the one in Prytherch *et al.* (2021), so only a simple scaling was performed. The owf limit allowed for wind directions from 175 – 250 °N. Setting wind direction conditions that need to be met for the F_{CH4} is often used in inshore environments or lakes (Erkkilä *et al.*, 2018; Yang *et al.*, 2016), to ensure water-only contributions, and it is perhaps the best way for this study as well. But in A-1, the owf criterion potentially induced a bias version of the bay footprint when including mostly deeper waters and excluding the shallower, more organic rich parts of the bay. The FC data showed that the highest F_{CH4} in A-1 was measured in, or very close to, the reed beds. This was supported by Lundevall-Zara *et al.* (2021). The EC F_{CH4} measurements did not include this part of the bay, so it most likely underestimated the total water-F_{CH4} from A-1. As the tower is placed now, it would be difficult to include the more organic rich parts of A-1 since the small peninsula, which the tower is placed on, blocks that part of the bay. The air masses coming from north to northeast of the tower, that would include the organic rich part, would at the same time risk terrestrial pollution (Yang *et al.,* 2016) effecting the measured F_{CH4}. In the light of this, A-1 might not be the most suitable location for EC measurements. A location, where the tower could be placed so that the main wind sector better included all the parts of the bay, would make the analysis easier. Further, if the noise level remains the same, a location with higher CH_4 emissions is necessary. Of the bays included in this study, I-2, I-4 or I-5 could all be suitable locations.

Due to instrumental problems with the KT-15 thermometer that brought large uncertainties in the water surface temperatures, it was not possible to investigate the stability of the atmospheric boundary layer (ABL). Since near-neutral conditions are expected over water surfaces (Pal Araya, 1988), U_{10} was calculated based on this assumption. However, if the air and water temperatures deviate from each other, they can create a stable (air warmer than water), or unstable (water warmer than air) ABL which affects the wind profile. A stable ABL would mean that our U_{10} calculations underestimated the true wind speed at 10 meters height, while an unstable ABL would have done the opposite. However, the deviation would be in the range of ± 1 m s^{-1} (Floors *et al.,* 2011) and considering that our EC F_{CH4} data already had a very small signal to noise ratio the uncertainty of U_{10} was not considered to influence the results significantly.

4.5 Correlation between the methods, and implications for interpolation of the FC data

Overall, the FC, EC and BL methods used in this study did show a good agreement in F_{CH4}, but FC data showed slightly higher values. This relationship was found by Erkkilä *et al.* (2018) as well, in their study focusing on the three, above mentioned, methods in a lake environment. Our FC and BL results showed that, in relation to the FC method, the BL method underestimated the F_{CH4} at low wind speeds, an effect that was already predicted by Wanninkhof (2014). Our results do support that, at lower wind speeds, the turbulence is enhanced by other factors like: microbubbles, temperature driven convection or currents, which determines the gas transfer (McGinnis *et al.,* 2015; Podgrajsek *et al.,* 2014; Zappa *et al.,* 2003) in the shallow bays of this study. Currents were most likely the cause behind the high gas transfers in I-6. Based on the results, the BL method, at least W14, is not suitable to measure the F_{CH4} in inshore marine environments that, in many cases, have a small fetch, and are generally very sheltered. However, for the bays that are more exposed to wind and waves, the FC method is unsuitable to capture the full variation in F_{CH4}. As the wind speed increases, the shallow coastlines are subject to breaking waves. This almost makes it impossible to sample with the chamber, partly due to it being carried by the waves, but also due to the moisture-sensitivity of the LGR and the risk of water entering the tubes. In these conditions, a manual chamber method, where air is sampled with certain time intervals, like the one used by Lundevall-Zara *et al.* (2021), rather than measured continuously like in this study, would be a safer option since it does not risk expensive instrumentation. However, as the wind increases and the sea state gets rough, even the manual chambers risk being lifted from the water surface by a wave or wind, which would interrupt the experiment. For this reason, the FC method potentially gives a bias representation of the total CH_4 emission from a bay.

The EC measuring periods in August, September, and October all had F_{CH4} that were above the detection limit, indicating that late summer, and early autumn have higher F_{CH4} than the winter season. However, since the measurements from late spring, 2021, had unfavorable wind directions, it is difficult to say with certainty that they represented lower F_{CH4} than August, September and October, since there was only limited amounts of data. The results from the EC in August, September, and October are in agreement with Lundevall-Zara *et al.* (2021), Heyer & Berger (2000), Bange *et al.* (1994), whose results indicated higher emissions during summer months. Our FC results do also support this increase in F_{CH4} in the warmer, more productive months.

An EC system could be of help in extrapolating FC F_{CH4} data to higher wind speeds, or generally fill in gaps between sampling periods. However, even though the EC F_{CH4} data showed correlations to time of day, temperature, and U_{10}, the inconsistency in these relationships makes it difficult to use them as predictors. The relationships between EC F_{CH4} and the environmental factors showed statistical significance, but the varying slope coefficients and generally low R^2 values induce problems when using the relationships to create a model. As it is now, the EC method would not be of help in interpolating the FC data. However, the good correlation between the two methods does give some hope for future use of EC and FC data in this way. The FC method is reliable, but the extent of labor required is not sustainable for the amount of data that needs to be collected in order to

expand the knowledge on the subject (Guriérrez-Loza *et al.,* 2019; Gülzow *et al.,* 2013). Therefore, it is necessary to find a method that is more efficient. Further, sampling at higher wind speeds is very difficult with the FC method, which eventually gives a bias estimate of the F_{CH4}, only representing lower wind speeds. Adding to these uncertainties is the chambers interference with the boundary layer (Mannich *et al.,* 2019). There are clearly reasons for why an EC system with a lower detection limit would be of great interest, especially since the W14 method unfortunately underestimated the CH_4 emissions in this study, and was concluded not to be suitable.

4.6 Ebullition

Out of 214 FC measurements, 3 managed to catch ebullition events, whereas 2 of them were in the same location, I-1. Ebullition occurs when the partial pressures, of all dissolved gases in the pore water combined, exceed that of atmospheric, plus hydrostatic, pressures (Miyake, 1951). Interestingly I-1 is one of the bays that contained the lowest dissolved CH_4 so either the ebullition indicates that a lot of oxidation takes place before the CH_4 reaches the surface waters or that other gases, such as N_2, had a large influence on the overall pressure (Langenegger *et al.,* 2019; Walter *et al.,* 2008). However, the fact that we managed to catch ebullition events in I-1, does not indicate that they are more common in this bay. It is very likely that they occurred in all bays just that we did not manage to catch them there (Langenegger *et al.,* 2019), since the chamber only covers a small percentage of the total area.

In I-5 the ebullition event released up to 4 magnitudes more CH_4 than the events did in I-2, supporting what has already been observed by the F_{CH4} measurements; that I-5 was a much bigger source of CH_4 to the atmosphere than I-1 was.

An estimate of how much of the F_{CH4} was ebullition and how much was diffusion is difficult to do since the spatial and temporal variability of ebullition cannot be determined from these few occasions. However, based on how much CH_4 was released during the ebullition events compared to the measurements on diffusive F_{CH4}, the results do support that ebullition contribute with substantial amounts of CH_4 (Wang *et al.,* 2021).

4.7 Implications for upscaling

Bange *et al.* (1994) discussed the coastal environments as contributing up to 75% of the total oceanic CH_4 emissions to the atmosphere, and, therefore, to have a larger F_{CH4} than the open oceans. Our measured FC F_{CH4} was generally higher than F_{CH4} reported for the more open waters in the Baltic Sea. Gülzow *et al.* (2013) measured values between 0.003 and 0.019 mmol m^{-2} d^{-1}, both summer and winter seasons included. These are in the lower range of our measurements. Bange *et al.* (1994) reported similar values for the winter season, but for the summer months their measured F_{CH4} ranged between 0.100 and 1.20 mmol m^{-2} d^{-1}. The summer values are generally higher than our F_{CH4}, but we did have values in that range

even during the winter period. In comparison to these studies, the coastal environments in our study appear to be larger sources of CH_4 than the open waters. However, Gutiérrez-Loza *et al.* (2019) reported monthly averages of up to 3.11 mmol m^{-2} d^{-1} for the Gotland Basin, which is at least one order of magnitude higher than our monthly F_{CH4}. Coastal summer emissions in the Baltic are generally higher than our results, as well as varying a lot between the types of environments studied. Reported F_{CH4} ranges from 0.006 up to 156.3 mmol m^{-2} d^{-1} (Lundevall-Zara *et al.,* 2021; Humberg *et al.,* 2019; Heyer & Berger, 2000). The literature available on CH_4 emissions in the Baltic is varying in study sites, time of year, duration, and methods, so specific comparisons are difficult to make. However, the general trend appears to be lower emissions for the open waters, and for the colder seasons. There are generally more studies carried out during summer (Lundevall-Zara *et al.,* 2021; Humberg *et al.,* 2019; Heyer & Berger, 2000), most likely due to the increased emissions during the more productive months. Our results indicate that high F_{CH4} can be measured during the winter period as well, and that a large spatial variability is present, which raises the need for more studies to include these months, to be able to represent the total F_{CH4} more accurately.

Another question one would have to consider for an upscaling model is the statistical handling of the data. Rosentreter *et al.* (2021) highlighted the tendency of overestimating the global CH_4 budget from aquatic environments to the atmosphere, since the majority of the empirical data is positively skewed, and upscaling is usually preformed on the mean. Our measured, diffusive, F_{CH4} had a positively skewed distribution. Differences between this study's means and medians, for the different periods, were up to 0.160 mmol m^{-2} d^{-1}, a very large offset considering the scale, which supports the statement by Rosentreter *et al.* (2021).

Further, our results indicate that habitats in the inner archipelago potentially emit more CH_4 than similar habitats in the outer archipelago do. This statement is, so far, premature and would need more data. However, a bay that has stronger anthropogenic influence and higher degree of eutrophication has been shown to inhibit elevated methanogenic processes (Wallenius *et al.*, 2021). Since Askö was our sole location in the outer archipelago, and our bays on Ingarö were also relatively closely located, it might be an effect caused by site specific properties on Askö and Ingarö. Further, the locations on Ingarö could be bias since they are partly chosen based on the possibility to reach them by car. Infrastructure usually indicates residencies or other sorts of anthropogenic activities, and, therefore, the bays in this study might represent a part of Ingarö that is particularly exposed to alteration. However, independent of the uncertainties it might be worth considering the effect from eutrophication when extrapolating F_{CH4} data to various places.

Lundevall-Zara *et al.* (2021) used an area extending 10 meters from shore in an attempt to extrapolate their data to the whole island of Askö. Our results indicate that the elevated F_{CH4} for the coastal habitats might extend further than that. However, Lundevall-Zara *et al.* (2021) measured in close proximity to shore, so to extend their results further might be misleading. While our results did not show strong enough correlations, to depth and distance to shore, to be concluded statistically reliable, there were some indications, in the more vegetated bays, that a chamber placement in proximity to reed beds might generate elevated F_{CH4}. The reed beds are generally closer to shore and if measurements were done dominantly within the beds, the result could represent a bias version of the bay. However,

with the sampling methods used in this study, a median value could be considered to at least represent the bay extending 20-30 meters.

While our data is not extensive enough to use for an upscaling model, the above mentioned considerations are helpful in the gathering of knowledge on the dynamics of the sea-to-air F_{CH4} and can potentially be used to base future studies on.

5. CONCLUSIONS

This study has produced CH_4 flux estimates of 7 shallow marine bays, both by the floating chamber method and through bulk model estimates during the winter season in Stockholm, Sweden, 2020-2021. Further, 3013 30-minute flux eddy covariance measurements for one of the bays were presented. We conclude the following:

- No clear relationship between vegetation density and F_{CH4} was found during the winter season, the classification based on vegetation and sediment type in the bays did not prove to be of any help in predicting F_{CH4}. This was mainly due to two bays deviating from the classification. The results support an increase in F_{CH4} towards the warmer months. It is possible that an increased production of CH_4 in the summer months would make the relationship between F_{CH4} and vegetation density stronger, but cannot be concluded based on the results in this study. The results indicate higher emissions from more densely populated areas, and we suggest including a factor for anthropogenic influence in the classification.

- U_{10} showed the strongest relationship with the most exposed bays, where onshore winds had the highest influence. The more protected bays are not as influenced by wind speed, indicating that models based on U_{10} as the turbulence predictor is not suitable in these environments. Air and water temperature proved to be a poor predictor of F_{CH4} in the shallow bays, for the sampled periods.

- Depth and distance to shore did not show a statistically significant relationship to F_{CH4}, for the depths (3 meter) and distances (30-40 meters) used in this study. However, the results showed variations with time of day, indicating that timing should be taken under consideration when planning the field work for a similar study.

- The EC system had a noise level of just above 0.2 mmol m^{-2} d^{-1}, resulting in the majority of the F_{CH4} data being below the detection limit. Further, the wind sector chosen to avoid including F_{CH4} from land, potentially showed a bias version of the bay since it excluded the shallower, more densely vegetated part of the bay. We conclude that the bay chosen for the tower was not optimal, and it may be beneficial to choose another location where the full bay can be included in the footprint.

- The FC, EC and BL methods show an acceptable level of agreements in these environments. However, in this study, the FC method represents the best choice, since the BL model potentially underestimates the F_{CH4} when the gas transfer is stimulated by other factors than wind. The EC system used proved to have a too large detection limit. On the other hand, the FC method becomes too labor intensive and is difficult to sample with in high wind speeds, so an alternative method is needed. With a decrease in the noise level or a location with higher F_{CH4}, the EC method still represents a good option.

Acknowledgements

First and foremost, I want to thank my supervisors. Volker, for being an indefatigable enthusiast and really seeing, and helping me see, the possibilities with this project, your approach have taught me to not put limits on what can be done. John, for all the patience, never ending support, and for fully following up on a statement in an early conversation that 'there are no stupid questions', god knows I have been taken advantage of that. You have helped me through a project that for sure was a bit out of my league in the beginning. Secondly, I want to thank all the people around me who has in one or another way contributed to this project; Emily, for being my go to person when I needed to complain about everything from broken instruments to difficult statistics; Julia, for all the help in the lab; The staff at Askö, for always lending a hand with all sorts of stuff; My family, for letting me store all the equipment in their garage without complaining (too much) and for all the help carrying the LGR and batteries in and out of the car; an extra thank you to my brother, for the step-in-help in the field. Last but not least, I want to thank my partner, Max, for being the best possible field assistant/technical support one could hope for. Truly, this project wouldn't have been possible to do without you and I am forever grateful for everything you have done!

5. References

Amorocho, J. and DeVries, J.J. (1980). *A new evaluation of the wind stress coefficient over water surfaces.* Journal of Geophysical Research: Oceans, v. 85, Issues C1: 433-442.

Andersen, J.H., Carstensen, J., Conley, D.J., Dromph, K., Fleming-Lehtinen, V., Gustafsson, B.G., Josefson, A.B., Norkko, A., Villnas, A. and Murray, C. (2017). *Long-term temporal and spatial trends in eutrophication status of the Baltic Sea*. Biology Reviews, v. 92: 135–149.

Araujo, J., Pratihary, A., Naik, R., Naik. H. And Naqvi, S.W.A. (2018). *Benthic fluxes of methane along the salinity gradient of a tropical monsoonal estaury: Implications for CH_4 supersatureation and emission.* Marine Chemistry, v. 202: 73-85.

Bakker, D. C. E., Bange, H. W., Gruber, N., Johannessen, T., Upstill-Goddard, R. C., Borges, A. V., Belille, B., Löscher, C. R., Naqvi, S. W. A, Omar, A. M. and Santana-Casiano, M. (2014). *Air-sea interactions of natural long-lived greenhouse gases (CO_2, N_2O, CH_4) in a changing climate.* In Liss, P. S. and Johnson, M. T. (eds.): Ocean-atmosphere interactions of gases and particles. Springer Earth System Sciences: 113-169.

Bange, H.W., Bartell, U.H., Rapsomanikis, S. and Andreae, M.O. (1994). *Methane in the Baltic and North Seas and a reassessment of the marine emissions of methane.* Global Biogeochemical Cycles, v. 8, no. 4: 465-480.

Beaulieu, J.J., DelSontro, T. and Dowing, J.A. (2019). *Eutrophication will increase methane emissions from lakes and impoundments during the 21st century.* Nature Communications, v. 10: 1375.

Bariteau, L., Helmig, D., Fairwall, C.W., Hare, J.E., Hueber, J. and Lang, E.K. (2010). *Determination of oceanic ozone deposition by ship-borne eddy covariance flux measurements.* Atmospheric Measurement Technics, v. 3: 441-455.

Barker Jørgensen, B. and Kastern, S. (2006). *Sulfur cycling and methane oxidation.* In Schulz, H.D. and Zabel, M. Marine Geochemistry 2nd edition. Springer-Verlag Berlin Heidelberg. 270–302.

Bastviken, D., Santoro, A.L., Marotta, H., Pinho, L.Q., Calheiros, D.F., Crill, P. and Enrich-Prast, A. (2010). *Methane emissions from Pantanal, South America, during low water season: Toward more comprehensive sampling.* Environmental Science and Technology, v. 44: 5450-5455.

Bastviken, D., Cole, J., Pace, M. and Tranvik, L. (2004). *Methane emissions from lakes: Dependence of lake characteristics, two regional assessments, and a global estimate.* Global Biogeochemical Cycles, v. 18, GB4009.

Battino, R. (1984). *The Ostwald coefficient of gas solubility.* Fluid Phase Equilibria, v. 15: 231-240.

BenSaïda, A. (2021). *Shapiro-Wilk and Shapiro-Francia normality tests.* (https://se.mathworks.com/matlabcentral/fileexchange/13964-shapiro-wilk-and-shapiro-francia-normality-tests), MATLAB Central File Exchange. Retrieved [21-08-23].

Belsley, D.A., Kuh, E. and Welsch, R.E. (1980). *Regression Diagnostics.* Hoboken, NJ: John Wiley & Sons.

Bianchi, T.S. (2007). *Biogeochemistry of estuaries.* New York: Oxford University Press, Inc.

Blaab: Björnö-Långviks Avlopps AB (publ). *Själva verket. (https://blaab.com/web/hem/info/sjalva-verket/) Retrieved [21-08-27].*

Blomquist, B.W., Fairall, C.W., Huebert, B.J. and Wilson, S. T. (2012). *Direct measurement of the oceanic carbon monoxide flux by eddy correlation.* Atmospheric Measurement Techniques, v. 5: 3069-3075.

Blomquist, B.W., Huebert, B.J., Fairall, C.W. and Faloona, I.C. (2010). *Determining the sea-air flux of dimethylsulfide by eddy correlation using mass spectrometry.* Atmospheric Measurement Techniques, v. 3: 1-20.

Borges, A.V., Champenois, W., Gypens, N., Delille, B. and Harlay, J. (2016). *Massive marine methane emissions from near-shore shallow coastal areas.* Scientific Report: 6:27908.

Borges, A.V. and Abril, G. (2011). *Carbon dioxide and methane dynamics in estuaries.* Treatise on Estuarine and Coastal Sciences, v. 5: 119-161.

Bugna, G.C., Chanton, J.P., Cable, J.E., Burnett, W.C. and Cable, P.H. (1996). *The importance of groundwater discharge to the methane budgets of nearshore and continental shelf waters of the northeastern Gulf of Mexico.* Geochimica et Cosmochimica Acta, v. 50, no. 23: 4735-4746.

Bussmann, I. (2013). *Distribution of methane in the Lena Delta and Buor-Khaya Bay, Russia.* Biogeosciences, v. 10: 4641-4652.

Bussmann, I. (2005). *Methane release through resuspension of littoral sediment.* Biogeochemistry, v. 74: 283-302.

Castro-Morales, K., Macías-Zamora, J.V., Canino-Herrera, S.R. and Burke, R.A. (2014). *Dissolved methane concentration and flux in the coastal zone of the Southern California Bight-Mexican sector: Possible influence of wastewater.* Eustarine, Coastal and Shelf Science, v. 144: 65-74.

Carmichael, M.J., Bernhardt, E.S., Bräuer, S.L. and Smith, W.K. (2014). *The role of vegetation in methane flux to the atmosphere: should vegetation be included as a distinct category in the global methane budget?* Biogeochemistry, v. 119: 1-24.

Chanton, J.P. and Dacey, J.W.H. (1991). *Effects of vegetation on methane flux, reservoirs, and carbon isotopic composition.* Edited by Sharkey, T.D., Holland, E.A. and Mooney, H.A. in Trace Gas Emissions by Plants. Elsevier Inc. 65-92.

Cicerone, R.J. and Oremland, R.S. (1988). *Biogeochemical aspects of atmospheric methane.* Global Biogeochemical Cycles, v. 2, no. 4: 299-327.

Conley, D.J., Carstensen, J. and Aigars. J. (2011). *Hypoxia is increasing in the coastal zone of the Baltic Sea.* Environmental Science & Technology, v. 4: 6777–6783.

Dargahi, B., Kolluru, V. and Cvetkovic, V. (2017). *Multi-layered stratification in the Baltic Sea: Insight from a modeling study with reference to environmental conditions.* Journal of Marine Science and Engineering, v. 5, no. 2: 1-26.

De Angelies, M.A. and Lee, C. (1994). *Methane production during zooplankton grazing on marine phytoplankton.* Limnology and Oceanography, v. 39, no. 6: 1298-1308.

DelSontro, T., Beaulieu, J.J. and Downing, J.A. (2018). *Greenhouse gas emissions from lakes and impoundments: upscaling in the face of global change.* Limnology and Oceanography Letters, v. 3: 64-75.

Dlugokencky, E. (2020). *Trends in atmospheric methane.* NOAA/GML. (www.esrl.noaa.gov/gmd/ccgg/trends_ch4/) Collected: 12/10/20.

Duchemin, E., Lucotte, M. and Canuel, R. (1999). *Comparison of static chamber and thin boundary layer equation methods for measuring greenhouse gas emissions from large water bodies.* Environmental Science Technology, v. 33: 350-357.

Elder, C., Hanke, P., Anthony, K.W., Thompson, D.R., Miller, C.E and Thorpe, A.K. (2020). *AboVE: Methane flux across two thermokarst lake ecosystems, interior Alaksa, 2018.* ORNL DAAC, Oak Ridge, Tennesse, USA.

Erkkilä, K.M, Ojala, A., Bastviken, D., Biermann, T., Heiskanen, J.J., Lindroth, A., Peltola, O., Rantakari, M., Vesala, T. and Mammarella, I. (2018). *Methane and carbon dioxide fluxes over a lake: comparison between eddy covariance, floating chambers and boundary layer method.* Biogeosciences, v. 15: 429-445.

Fay, M.P. and Proschan, M.A. (2010). *Wilcoxon-Mann-Whitney or t-test? On assumptions for hypothesis tests and multiple interpretations of decision rules.* Statistic Surveys, v. 4: 1-39.

Feistel, R., Nausch, G. and Wasmund, N. (2008). *State and evolution of the Baltic Sea, 1952-2005: A detailed 50-year survey of meteorology and climate, physics, chemistry, biology and marine environment.* John Wiley and Sons, Inc., Hoboken, New Jersey.

Fendinger, N.J., Adams, D.D. and Glotfelty, D.E. (1992). *The role of gas ebullition in the transport of organic contaminants from sediments.* Science Total Environment, v. 112:189-201.

Floors, R., Batchvarova, E., Gryning, S.-E., Hahmann, A. N., Peña, A. and Mikkelsen, T. (2011). *Atmospheric boundary layer wind profile at a flat coastal site – wind speed lidar measurements and mesoscale modeling results.* Advances in Science and Research, v. 6: 155-159.

Francis, G. and Thunell, E. (2021). *Revising Bonferroni.* Psychonomic Bulletin & Review, v. 28: 788-794.

Garbe, C.S., Rutgersson, A., Boutin, J., Nightingale, P.D., Pettersson, H., Piskozub, J., Sahlée, E., Tsai, W., Ward, B., Woolf, D.K. and Zappa, C.J. (2014). *Transfer across the air-sea interface.* In Ocean-Atmosphere Interactions of Gases and Particles, edited by Liss, P.S. and Johnson, M.T.: 55-112. Springer.

Gentz, T., Damm, E., Schneider von Deimling, J., Mau, S., McGinnis, D.F. and Schlüter, M. (2014). *A water column study of methane around gas flares located at the West Spitsbergen continental margin.* Continental Shelf Research, v. 72: 107-118.

Google Maps. (2021). *Askö.* Google Maps [Online]: https://www.google.com/maps/search/ask%C3%B6/@58.8233028,17.6329536,438m/data=!3m1!1e3?hl=sv (Collected 6/7/21).

Google Maps. (2021). *Askö.* Google Maps [Online]: Ingarö – Google Maps (Collected 1/9/21).

Grasset, C., Mendonça, R., Villamor Saucedo, G., Bastviken, D., Roland, F. and Sobek, S. (2018). *Large but variable methane production in anoxic freshwater sediment upon addition of allochthonous and autochthonous organic matter.* Limnology and Oceanography, v. 63: 1488-1501.

Green, S.B. and Salkind, N.J. (2008). *Using SPSS for Windows and Macintosh: Analyzing and understanding data (5th edition).* Upper Saddle River, NJ: Pearson Prentice Hall.

Grinham, A., Dunbabin, M. and Albert, S. (2017). *Importance of sediment organic matter to methane ebullition in a sub-tropical freshwater reservoir.* Science of the Total Environment, v. 621: 1199-1207.

Grunwald, M., Dellwig, O., Beck, M., Dippner, J. W., Freund, J.A., Kohlmeier, C., Schnetger, B. and Brumsack, H. J. (2009). *Methane in the southern North Sea: sources, spatial distribution and budgets.* Estuarine, Coastal and Shelf Science, v. 81: 445-456.

Gutiérrez-Loza, L., Wallin, M.B., Sahlée, E., Nilsson, E., Bange, H.W., Kock, A. and Rutgersson, A. (2019). *Measurement of air-sea methane fluxes in the Baltic Sea using the eddy covariance method.* Frontiers in Earth Science, v. 7: 1-13.

Gülzow, W., Rehder, G., Schneider, v. Deimling J., Seifert, T. and Tóth, Z. (2013). *One year of continuous measurements constraining methane emissions from the Baltic Sea to the atmosphere using a ship of opportunity.* Biogeosciences, v. 10: 81-99.

Herlina and Jirka, G.H. (2008). *Experiments on gas transfer at the air–water interface induced by oscillating grid turbulence*. Journal of Fluid Mechanics, v. 594: 183–208.

Heyer, J. and Berger, U. (2000). *Methane emission from the coastal area in the southern Baltic Sea.* Estuarine, Coastal and Shelf Science, v. 51: 13-30.

Ho, D.T., Wanninkhof, R., Schlosser, P., Ullman, D.S., Hebert, D. and Sullivan, K.F. (2011). *Toward a universal relationship between wind speed and gas exchange: Gas transfer velocities measured with $^{3}He/SF_6$ during the Southern Ocean Gas Exchange Experiment.* Journal of Geophysical Research, v. 116: C00F04.

Ho, D.T., Law, C.S., Smith, M.J., Schlosser, P., Harvey, M. and Hill, P. (2006). *Measurements of air-sea gas exchange at high wind speeds in the Southern Ocean: Implications for global parameterizations.* Geophysical Research Letters, v. 33: L16611.

Holland, P.W. and Welsch, R.E. (1977). *Robust regression using iteratively reweighted least-squares.* Communications in Statistics: Theory and Methods, A6: 813-827.

Humborg, C., Geibel, M.C., Sun, X., McCrackin, M., Mörth, C.M., Stanne, C., Jakobsson, M., Gustafsson, B., Sokolov, A., Norkko, A. and Norkko, J. (2019). *High emissions of carbon dioxide and methane from the coastal Baltic Sea at the end of a summer heat wave.* Frontiers in Marine Science, v.6: 493.

Jeffrey, L.C., Maher, D.T., Johnston, S.G., Kelaher, B.P., Steven, A. and Tait, D.R. (2019). *Wetland emissions dominated by plant-mediated fluxes: contrasting emissions pathways and seasons within a shallow freshwater subtropical wetland.* Limnology and Oceanography, v. 64: 1895-1912.

Jähne, B., Münnich, K.O., Bösinger, R., Dutzi, A., Huber, W. and Libner, P. (1987). *On the parameters influencing air–water gas exchange.* Journal of Geophysical Research, C: Oceans, v. 92: 1937–1949.

Karl, D.M., Beversdorf, L., Björkman, K.M., Church, M.J., Martinez, A. and Delong, E.F. (2008). *Aerobic production of methane in the sea.* Nature Geoscience, v. 1: 473-478.

Karl, D.M. and Tilbrook, B.D. (1994). *Production and transport of methane in oceanic particulate organic matter.* Nature, v. 368: 732–734.

Kelley, C.A., Martens, C.S. and Ussler, III W. (1995). *Methane dynamics across a tidally flooded riverbank margin.* Limnology and Oceanography, v. 40: 1112-1129.

Kelley, C.A., Martens, C.S. and Chanton, J.P. (1990). *Variations in sedimentary carbon remineralization rates in the White Oak River estuary, North Carolina.* Limnology and Oceanography, v. 35: 372-383.

King, G.M. and Ademsen, A.P.S. (1992). *Effects of temperature on methane consumption in a forest soil and in pure cultures of the methanotroph Methylomonas rubra.* Applied Environmental Microbiology, v. 58: 2758-2673.

Kljun, N., Calanca, P., Rotach, M.W. and Schmid, H.P. (2015). *A simple two-dimensional parameterization for Flux Footprint Prediction (FFP).* Geoscience Model Development, v. 8, i. 11: 3695-3713.

Kummu, M., de Moel, H., Salvucci, G., Viviroli, D., Ward, P.J. and Varis, O. (2016). *Over the hills and further away from the coast: Global geospatial patterns of human and environment over the 20^{th}-21^{st} centuries.* Environmental Monitoring and Assessment, v. 87, no. 4: 187.

Langenegger, T., Vachon, D., Donis, D. and McGinnis, D.F. (2019). *What the bubble knows: Lake methane dynamics revealed by sediment gas bubble composition.* Limnology and Oceanography, v. 64, I. 4: 1526-1544.

Lecher, A.L., Kessler, J., Sparrow, K., Garcia-Tigreros Kodovska, F., Dimova, N., Murray, J, Tulaxzyk, S. and Paytan, A. (2015). *Methane transport through submarine groundwater discharge to the North Pacific and Arctic Ocean at two Alaskan sites.* Limnology and Oceanography, v. 61, I. S1: S344-S355.

Liss, P.S. and Merlivat, L. (1986). *Air-Sea gas exchange rates: Introduction and synthesis* in: The Role of Air-Sea Gas Exchange in Geochemical Cycling, edited by Baut-Ménard, P.: 113-127. D. Riedel Publishing Company, Holland.

Liss, P.S. (1983). *Gas transfer: Experiments and geochemical implications.* In Air-sea Exchange of Gases and Particles, edited by Liss, P.S. and Slinn, W.: 241-298. Springer.

Liss, P.S. and Martinelli, F. (1978). *The effect of oil films on the transfer of oxygen and water vapor across an air-water interface.* Thalass. Jugosl., v. 14: 215-220.

Liss, P.S. and Slater, P.G. (1974). *Flux of gases across the air-sea interface.* Nature, v. 247: 181-184.

Liu, Z.H., Yin H., Dang, Z. and Liu, Y. (2014). *Dissolved methane: a hurdle for anaerobic treatment of municipal wastewater.* Environmental Science Technology, v. 48: 889-890.

Loose, B., McGillis, W.R., Perovich, D., Zappa, C.J. and Schlosser, P. (2014). *A parameter model of gas exchange for the seasonal sea ice zone.* Ocean Science, v. 10: 17-28.

Lundevall-Zara, M., Lundevall-Zara, E. and Brüchert, V. (2021). *Sea-air exchange of methane in shallow inshore areas of the Baltic Sea.* Frontiers in Marine Science, v. 8: 657459.

Magen, C., Bosman, S., Chanton, J.P. Lapham, L.L., Marshall, K., Pohlman, J.W. and Casso, M. (2014). *A simple headspace equilibration method for measuring dissolved methane.* Limnology and Oceanography: Methods, v. 12: 637-650.

Mannich, M., Fernandes, C.V.S. and Bleninger, T.B. (2019). *Uncertainty analysis of gas flux measurements at air-water interface using floating chambers.* Ecohydrology & Hydrobiology, v. 19: 475-486.

Martens, C.S. and Klump, J.V. (1980). *Biogeochemical cycling in an organic-rich coastal marine – J. Methane sediment-water exchange processes.* Geochimica Cosmochimica Acta, v. 44: 471-490.

McGinnis, D.F., Kirillin, G., Tang, K.W., Flury, S., Bodmer, P., Engelhardt, C., Casper, P. and Grossart, H. (2015). *Enhancing surface methane fluxes from an oligotrophic lake: Exploring the microbubble hypothesis.* Environmental Science Technology, v. 49: 873-880.

Megonigal, J.P., Hines, M.E. and Visscher, P.T. (2014). *Anaerobic Metabolism: Linkages to Trace Gases and Aerobic Processes.* Treatise on Geochemistry (Second Edition), v. 10: 273-359.

Mitchell, B.G., Broody, E.A., Holm-Hansen, O. and McClain, C. (2005). *Inhibitory effect of light on methane oxidation in the pelagic water column of mesotrophic lake (Lake Biwa, Japan).* Limnology and Oceanography, v. 36: 1662-1677.

Miyake, Y. (1951). *The possibility and the allowable limit of formation of air bubbles in the sea.* Papers in Meteorology and Geophysics, v. 2: 95-101.

Naturvårdsverket. (2009). *Naturtyper på havets botten, baserat på art- och habitatmodellering.* Naturvårdsverket, rapport 5987.

Naqvi, S.W.A., Bange, H.W., Farías, L., Monteiro, P.M.S., Scranton, M.I. and Zhang, J. (2010). *Marine hypoxia/anoxia as a source of CH_4 and N_2O.* Biogeosciences, v.7: 2159-2190.

Nightingale, P.D., Gill, M., Law, C.S., Watson, A.J., Liss, P.S., Liddicoat, M.L., Boutin, J. and Upstill-Goddard, C. (2000). *In situ evaluation of air-sea gas exchange parameterizations using novel conservative and volatile tracers.* Global Biogeochemical Cycles, v. 14, no. 1: 373-387.

Nisbet, E.G., Manning, M.R., Dlugokencky, E.J., Fisher, R.E., Lowry, D., Michel, S.E., Lund Myhre, C., Platt, S.M., Allen, G., Bousquet, P., Brownlow, R., Cain, M., France, J.L., Hermansen, O., Hossaini, R., Jones, A.E., Levin, I., Manning, A.C., Myhre, G., Pyle, J.A., Vaughn, B.H., Warwick, N.J. and White, J.W.C. (2019). *Very strong atmospheric methane growth in the 4 years 2014 – 2017: Implications for the Paris agreement.* Global Biogeochemical Cycles, v. 22, I. 3: 317-342.

Nisbet, E.G. and Weiss, R. (2010). *Top-down versus bottom-up.* Science, v. 328: 1241-1243.

NOAA Research. *Carbon Cycle Gases data.* NOAA/ESRL/GML/CCGG. (https://www.esrl.noaa.gov/gmd/dv/iadv/graph.php?code=PAL&program=ccgg&type=ts) Collected 17/02/21, 25/5/21.

Pal Arya, S. (1988). *Marine Atmospheric Boundary Layer.* In Introduction to Micrometeorology, v. 43. Academic Press, Inc. San Diego, California.

Persson, P.O.G., Hare, J.E., Fairall, C.W. and Otto, W.D. (2005). *Air-sea interaction processes in warm and cold sectors of extratropical cyclonic storms observed during FASTEX.* Quaternary Journal of the Royal Meteorological Society, v. 131, no. 607: 877-912.

Peters, J.A. and Lodge, D.M. (2009). *Littoral Zone.* Lake Ecosystems. Elsevier Inc. https://www.climate-policy-watcher.org/lake-ecosystems/littoral-zone.html [Collected 01-10-21].

Podgrajsek, E. Sahlée, E. and Rutgersson, A. (2014). *Diurnal cycle of lake methane flux.* Journal of Geophysical Research: Biogeosciences, v. 119: 236-248.

Prytherch, J. and Yelland, M.J. (2021). *Wind, convection and fetch dependence of gas transfer velocity in an Arctic sea-ice lead determined from eddy covariance CO_2 flux measurements.* Global Biogeochemical Cycles, v. 32, i. 2: 1-32.

Prytherch, J., Brooks, I.M., Crill., P.M., Thornton, B.F., Salisbury, D.J., Tjernström, M., Anderson, L.G., Geibel, M.C. and Humborg, C. (2017). *Direct determination of the air-sea CO_2 gas transfer velocity in Arctic sea ice regions.* Geophysical Research Letters, v. 44: 3770-3778.

Reeburgh, W.S. (2007). *Oceanic methane biogeochemistry.* Chemical Reviews, v. 107: 486-513.

Rosentreter, J.A., Borges, A.V., Deemer, B.R., Holgerson, M.A., Liu, S., Song, C., Melack, J., Raymond, P.A., Duarte, C.M., Allen, G.H., Olefeldt, D., Poulter, B., Battin, T.I. and Eyre, B.D. (2021). *Half of global methane emissions come from highly variable aquatic ecosystem sources.* Nature Geoscience, v. 14: 225-230.

Schaefer, H., Mikaloff Fletcher, S.E., Veidt, C., Lassey, K.R., Brailsford, G.W., Bromley, T.M., Dlugokencky, J., Michel, S.E., Miller, J.B., Levin, I., Lowe, D.C., Martin, R.J., Vaughn, B.H. and White, J.W.C. (2016). *A 21^{st}-century shift from fossil-fuel to biogenic methane emissions indicated by $^{13}CH_4$.* Science, v. 352, I. 6281.

Schiermeier, Q. (2020). *Global methane levels soar to record high.* Nature. doi: 10.1038/d41586-020-02116-8

Schmiedeskamp, M., Praetzel, L.S.E., Bastviken, D. and Knorr, K.H. (2021). *Whole-lake methane emissions from two temperate shallow lakes with fluctuating water levels: Relevance of spatiotemporal patterns.* Limnology and Oceanography, v. 66, I. 6: 2455-2469.

Smith, S. (1988). *Coefficients for sea surface wind stress, heat flux, and wind profiles as a function of wind speed and temperature.* Journal of Geophysical Research, v. 93: 15467-15472.

Sveriges Geologiska Undersökningar. (2021). *Kartvisaren: Baskarta.* SGU. https://www.sgu.se/produkter/kartor/kartvisaren/ (Collected: 1/9/2021).

Şahintürk, L. and Özcan, B. (2017). *The comparison of hypothesis tests determining normality and similarity of samples.* Journal of Naval Science and Engineering, v. 13, I. 2: 21-36.

Thießen, O., Schmidt, M., Theilen, F., Schmitt, M. and Klein, G. (2006). *Methane formation and distribution of acoustic turbidity in organic-rich surface sediments in Arkona Basin, Baltic sea.* Continental Shelf Research, v. 26: 2469-2483.

Thornton, B.F., Prytherch, J., Andersson, K., Brooks, I.M., Salisbury, D. Tjernström, M. and Crill, P.M. (2020). *Shipborne eddy covariance observations of methane fluxes constrain Arctic sea emissions.* Science Advances, v. 9, no. 5, eaay7934.

Upstill-Goddard, R.C., Barnes, J., Frost, T., Punshon, S. and Owens, N.J.P. (2000). *Methane in the southern North Sea: Low salinity inputs, estuarine removal, and atmospheric flux.* Global Biogeochemical Cycles, v. 14: 1205-1217.

Van der Nat, F.J. and Middleburg, J.J. (2000). *Methane emission from tidal freshwater marshes.* Biogeochemistry, v. 49: 103-121.

Van Dijk, A., Moene, A.F. and Debruin, H.A.R. (2004). *The principles of surface flux physics: theory, practice and description of the ECPACK library.* Meteorology and Air Quality (MAQ) (Internal Report 2004/1).

Vickers, D. and Mahrt, L. (1997). *Quality control and flux sampling problems for tower and aircraft data.* Journal of Atmospheric and Oceanographic Technology, v. 14: 512-526.

Wallenius, A.J., Dalcin Martins, P., Slomp, C.P. and Jetten, M.S.M. (2021). *Constraints on the microbial methane cycle in coastal sediments*. Frontiers in Microbiology, v. 12: 631621.

Walsh, C.J., Roy, A.H., Feminella, J.W., Cottingham, P.D., Groffman, P.M. and Morgan, R.P. (2005). *The urban stream syndrome: Current knowledge and the search for a cure.* Journal of the North American Benthological Society, v. 24, no. 3: 706-723.

Walter, K.M., Chanton, J.P., Chapin, F.S., Schuur, A.G. and Zimov, S.A. (2008). *Methane production and bubble emissions from arctic lakes: Isotopic implications for source pathways and ages.* Journal of Geophysical Research, v. 113: G00A08.

Wang, G., Xia, X., Liu, S., Zhang, L., Zhang, S., Wang, J., Xi, N. and Zhang, Q. (2021). *Intense methane ebullition from urban inland waters and its significant contribution to greenhouse gas emissions.* Water Research, v. 189: 116654.

Wanninkhof, R. (2014). *Relationship between wind speed and gas exchange over the ocean revisited.* Limnology and Oceanography: Methods, v. 12: 351-362.

Wanninkhof, R. and McGillis, W.R. (1999). *A cubic relationship between air-sea CO_2 exchange and wind speed.* Geophysical Research Letters, v. 26, no. 13: 1889-1892.

Wanninkhof, R. (1992). *Relationship between wind speed and gas exchange over the ocean.* Journal of Geophysical Research, v. 97, no. C5: 7373-7382.

Weber, T., Wiseman, N.A. and Kock, A. (2019). *Global oceanic methane emissions dominated by shallow coastal waters.* Nature Communications, 10:4584.

Wiesenburg, D.A. and Guinasso, Jr.N.L. (1979). *Equilibrium solubilities of methane, carbon monoxide, and hydrogen in water and sea water.* Journal of Chemical and Engineering Data, v. 24, no. 356-360.

Wilczak, J.M., Oncley, S.P. and Stage, S.A. (2001). *Sonic anemometer tilt correction algorithms.* Boundary-Layer Meteorology, v. 99: 127-150.

Winn, E.B. (1950). *The temperature dependence of the self-diffusion coefficients of Argon, Neon, Nitrogen, Oxygen, Carbon Dioxide, and Methane.* Physical Review, v. 80: 1024-1027.

Yang, M., Bell, T.G., Brown, I.J., Fishwick, J.R., Kitidis, V., Nightingale, P.D., Rees, A.P. and Smyth, T.J. (2019). *Insights from year-long measurements of air-water CH_4 and CO_2 exchange in coastal environment.* Biogeosciences, v. 16: 961-978.

Yang, M., Bell, T.G., Hopkins, F.E., Kitidis, V., Cazenave, P.W., Nightingale, P.D., Yellands, M.J., Pascal, R.W., Prytherch, J., Brooks, I.M. and Smyth, T.J. (2016). *Air-sea fluxes of CO_2 and CH_4 from the Penlee Point Atmospheric Observatory on the south-west coast of the UK.* Atmospheric Chemistry and Physics, v. 16: 5745-5761.

Yasui, S., Kanda, J., Usui, T. and Ogawa, H. (2016). *Seasonal variations of dissolved organic matter and nutrients in sediment pore water in the inner part of Tokyo Bay.* Journal of Oceanography, v. 72: 851-866.

Yvon-Durocher, G., Allen, A.P., Bastviken, D., Conrad, R., Gudasz, C., St-Pierre, A., Thanh-Duc, N. and A. del Giorgio, P. (2014). *Methane fluxes show consistent temperature dependence across microbial to ecosystem scales.* Nature, v. 507(7493): 488-491.

Zappa, C., Raymond, P., Terray, E. and McGillis, W. (2003). *Variation in surface turbulence and the gas transfer velocity over tidal cycle in a macrotidal estuary.* Estuaries, v. 26: 1401-1415.

Zehnder, A.J. (1978). *Ecology of methane formation.* Edited by Mitchell, R. in Water Pollution Microbiology, v. 2: 349-376. Wiley, New York.

Zhang, L., Liao, Q., Gao, R., Luo, R., Liu, C., Zhong, J. and Wang, Z. (2021). *Spatial variations in diffusive methane fluxes and the role of eutrophication in subtropical shallow lake.* Science of the Total Environment, v. 759: 143495.

Zhou, H., Yin, X., Yang, Q., Wang, H., Wu, Z. and Bao, S., (2009). *Distribution, source and flux of methane in the western Pearl River Estuary and northern South China Sea.* Marine Chemistry, v. 117: 21-31.